UNIVERSIDADE D
COIMBRA

Juan Emanuel Aguiar Baptista

COMPORTAMENTO DA ALMA DA COLUNA AO CORTE

Dissertação de Mestrado em Engenharia Civil, na área de Especialização Mecânica Estrutural, orientada pelo Professor Doutor Filip Ljubinkovic e pelo Professor Doutor João Pedro Simões Cândido Martins apresentada ao Departamento de Engenharia Civil da Faculdade de Ciências e Tecnologia da Universidade de Coimbra.

Setembro de 2023

Faculdade de Ciências e Tecnologia da Universidade de Coimbra
Departamento de Engenharia Civil

Juan Emanuel Aguiar Baptista

COMPORTAMENTO DA ALMA DA COLUNA AO CORTE

COLUMN WEB PANEL IN SHEAR

Dissertação de Mestrado em Engenharia Civil, na área de Especialização em Mecânica Estrutural, orientada pelo Professor Doutor Filip Ljubinkovic. e pelo Professor Doutor João Pedro Simões Cândido Martins

Setembro de 2023

UNIVERSIDADE D
COIMBRA

AGRADECIMENTOS

Em agradecimento especial aos meus orientadores pelo seu apoio, paciência e dedicação e por acreditarem em mim para o desenvolvimento deste trabalho.

Aos meus professores do início ao fim do meu percurso académico, que sempre procurara me transmitir os seus conhecimentos com a maior dedicação e disponibilidade. Nas suas aulas a aprendi não apenas conhecimentos técnicos, também me foi transmitida a voz da sua experiência de indubitável valor para o meu futuro profissional e pessoal.

A todos os meus entes queridos, por estarem sempre presentes, pela sua inestimável e incondicional ajuda, motivação e apoio e por me encorajarem a continuar o meu percurso mesmo nas situações mais difíceis.

A todas as pessoas que em algum ponto da minha vida estenderam a sua mão para me ajudar com a maior humildade e desinteresse.

A todos eles, é dedicada esta dissertação.

RESUMO

O método das componentes constitui uma potente ferramenta de análise para o cálculo da resistência e a rigidez das ligações metálicas e encontra-se integrado na norma europeia EN 1993-1-8 e na norma de europeia de segunda geração FprEN 1993-1-8.

No entanto, o método das componentes encontra-se limitado a casos padrão pelo que alguns problemas e situações não estão, atualmente, completamente formulados ou estudados. Daí a importância crescente nos últimos anos de métodos de análise alternativos tais como a modelação numérica por elementos finitos ou ainda o aparecimento dos Métodos dos Elementos Finitos Baseados em Componentes (Component-Based Finite Element Method, «CBFEM»), como uma ferramenta que procura conjugar as potencialidades de ambas abordagens.

A formulação referida baseia-se na adoção de elementos do tipo casca e lineares para a modelação de placas, parafusos e soldaduras e pretende ultrapassar as restrições, em termos computacionais, de tempo e memória associadas à utilização de elementos finitos sólidos 3D, tal é o caso do software comercial IDEA StatiCa®.

Dadas a limitada quantidade de dados experimentais e a ausência de regras de segurança para determinados casos a norma atual prevê a implementação de restrições adicionais, sendo esse o caso do comportamento da alma da coluna ao corte numa ligação viga-coluna de secções abertas, componente fortemente dependente da razão dos momentos atuantes em ambos lados de uma ligação de resistência total o que conduz, normalmente, ao reforço da alma da coluna com considerável impacto económico no dimensionamento e fabrico da ligação.

Pretende-se desta forma estudar se a utilização de modelos de elementos finitos do tipo casca com recurso ao software comercial Abaqus® e modelos CBFEM com recurso ao software IDEA StatiCa® para o caso da análise do comportamento da alma da coluna ao corte permite o relaxamento das referidas restrições, comparando os resultados fornecidos pelo software com os resultados de um modelo de elementos finitos tradicional e ainda com o Método das Componentes previsto no Eurocódigo atual para um conjunto de ligações com perfis considerados representativos das soluções comumente adotadas.

Ainda nesse contexto, pretende-se comparar diversas alternativas para a modelação das ligações através de modelos de casca com o intuito de ter uma melhor perceção de qual pode ser a metodologia mais adequada em termos geométricos para a referida análise.

O estudo mostrou que para a amostra de juntas escolhidas, o método das componentes implementado nas normas EN 1993-1-8 e FprEN 1993-1-8 parecem fornecer resultados mais conservativos para o momento resistente e a rigidez inicial em juntas com apenas uma viga e não reforçadas. No entanto, na presença de esforço axial e para alguns casos mais específicos o método das componentes poderá fornecer resultados menos conservativos que os modelos de elementos finitos. Adicionalmente, o presente estudo conclui que os modelos CBFEM parecem conduzir a resultados de momento resistente consideravelmente próximos aos modelos de elementos finitos quando uma malha o suficientemente refinada é escolhida.

Finalmente, o uso de elementos finitos de casca para modelar juntas viga-coluna internas com apenas uma viga e perfis abertos laminados a quente parece ser aceitável, permitindo reproduzir razoavelmente o comportamento verificado para essas juntas em ensaios experimentais. Também, a consideração da influência do raio de concordância da coluna nos modelos de elementos finitos de casca parece ter efeitos quer na rigidez inicial da junta quer no momento resistente da mesma levando a valores inferiores para ambas grandezas se for negligenciado.

ABSTRACT

The component method constitutes a powerful tool to analyse and calculate the resistance and stiffness of steel joints and due to this, is the basis of the European codes EN 1993-1-8 and the new generation FprEN 1993-1-8.

However, the component method is limited to standard cases and therefore, some problems and situations are not yet completely formulated and studied. Due to this, the importance of alternative methods of analysis has been growing during the last years. Among those are the numerical modelling based on finite elements and the Component-Based Finite Element Method, "CBFEM", that seeks to combine the potentialities finite elements with the component method.

CBFEM is based on the adoption of shell and linear finite elements to model plates, bolts, and welds. The objective of such an approach is to overtake the restrictions in computational terms such as storage capacity and running time associated with the use of 3D solid finite element models. Among the commercial software available using CBFEM is IDEA StatiCa®.

Due to the limitations in the amount of experimental data, the inexistence of safety rules for some specific cases the actual European code foresees the use of additional restrictions. That happens with the study of the Column Web Panel (CWP) in shear (in a beam-to-column joint with open-sections. The CWP in shear component has been proven to be highly dependent on the ratio between the applied moments at both sides of a moment-resistant joint. This situation usually leads to the reinforcement of the joint resulting in a significative increase in fabrication costs.

This study is going to analyse the use of shell finite element models using the commercial software Abaqus® and CBFEM using IDEA StatiCa® to model the behaviour of CWP in shear. The objective is to compare the results of these alternative methods with the codes component method to estimate if it is possible to have a more accurate value of the joint moment-resistance and its stiffness leading to a decrease in production costs. Therefore, those methods are going to be applied to a set of joints considered as being representative of the most adopted solutions.

Still in that context, different alternatives are going to be used to modelling the shell finite element models seeking a better understanding of which geometrical configuration may be considered adequate for that type of analysis.

The study shows that for the studied set of joints, EN 1993-1-8 (CEN, 2005b) and FprEN 1993-1-8 (CEN, 2023) may lead to more conservative results for moment resistance in one-sided-unstiffened joints without axial force. Nevertheless, in the presence of axial force for some specific cases the CM may lead to less conservative results than FEM. It also shows that CBFEM may lead to moment-resistance values considerably closer to shell FEM if a sufficiently refined mesh is used.

Finally, the use of shell finite elements to model on-sided internal beam-to-column joints with hot-rolled open sections may be acceptable, allowing a reasonable reproduction of the overall behaviour of such joints shown on experimental tests. Also, the consideration of the column radius in shell FEM seems to have significant effects on the joint initial stiffness and moment resistance and may lead to lower values for both magnitudes when neglected.

TABLE OF CONTENTS

LIST OF FIGURES

LIST OF TABLES

SYMBOLOGY

Latin Uppercase

A - Cross-section area A = $2 \cdot A_{fl} + A_w$

A_{CWS} - Area of the column web in shear component

A_d - Area of the flat part of the web panel

A_{fl} - Area of one flange

A_{vz} - Shear area as defined in EN 1993-1-1:2005 (strong axis bending)

A_w - Area of the web (total area minus flange area)

E - Elastic modulus of steel

G - Shear modulus of steel

I - Second moment of inertia of the cross-section

L_c - Total length of column between supported points

W - Plastic modulus of the cross-section

Latin Lowercase

a - Geometrical distance between external face of beam flange and column support.

b - Flange width

b_b - Beam flange width

b_c - Column flange width

b_{eff} - Effective width

d - Width of the flat part of an I section ($h - 2 \cdot tf - 2 \cdot r$)

d_c - Width of the flat part of the column

h - Height of the cross-section

h_b - Beam height

h_c - Column height

t - Thickness

t_{fb} - Beam flange thickness

t_{fc} - Column flange thickness

t_{wb} - Beam web thickness

t_{wc} - Column web thickness

z_b - Beam lever arm (distance between centroids of flanges)

Greek Symbols

λ - Mechanical slenderness

λ_{wp} - Mechanical slenderness of the web panel

v - Poisson's ratio

ABBREVIATIONS

BFC - Beam Flange and Web in Compression

BWT - Beam Web in Tension

CBFEM - Component-Based Finite Element Method

CM - Component Method

CWC - Column Web in Compression

CWC - Column Web in Compression

CWP - Column Web Panel

CWS - Column Web in Shear

CWT - Column Web in Tension

FE - Finite Elements

FEM - Finite Element Model

IS - Idea StatiCa®

WP - Web Panel

SUBSCRIPTS AND SUPERSCRIPTS

c – column

b – beam

1 INTRODUCTION

1.1 Overview

On steel construction the design philosophy based on porticade structures constituted by linear elements such as beams and columns is widespread. Therefore, the use of connection points between linear elements leads to the use of connections points by joints. Due to this, steel joints are fundamental for resistance, stiffness, reliability, economy, and other important topics related to steel construction. In addition, joints are complex objects, constituted by multiple elements that interact with each other. Because of those two factors (the importance and complexity of the joints) the study of their behaviour is an important research field. Among the diverse types of joints that may be used on porticade structures are beam-to-column joints that can be welded, bolted or a combination of both.

The component method (CM) is a powerful and simple tool of analysis that is already implemented on the European codes EN 1993-1-8 (CEN, 2005b) and FprEN 1993-1-8 (CEN, 2023). Therefore, its use is well-established and has been validated by experimental work. Nevertheless, the main weakness of the CM as analysis tool is its limitation to standard cases. The necessity to analyse non-standard cases lead to the development of alternative methods such as numerical finite element models (FEM) and even a combination of both known as component based finite element models (CBFEM).

For the moment resisting beam-to-column joints the column web panel (CWP) in shear is one of the possible conditioning components that determines the overall behaviour of the joint including its resistance and stiffness. As referred by Corman (2022) the study of this specific component has been gaining attention since the late 60's and beginning of the 70's due to a change in the design philosophy used on the United States of America from rigid to semi-rigid joints in addition to the impossibility to achieve perfectly rigid behaviour with bolted joints (more common in Europe). A better understanding of that component may avoid the use of heavy reinforcement leading to more economical solutions.

1.2 Motivation and thesis objectives

The main objective of this study is to compare the results provided using shell FEM using the commercial software Abaqus®, CBFEM using the commercial software IDEA StatiCa® and the CM implemented in the European codes. That comparison seeks to evaluate the applicability

of these methods to the study of internal beam-to-column joints due to their advantages when compared to more sophisticated methods of analysis such as solid FEM.

Aiming that, three shell FEM are going to be defined considering or neglecting the effect of the column radius and then validated against two experimental tests. After that a set of joints is going to be chosen attempting it to be reasonably statistically representative. Then, through python scripting, that set of joints is going to be modelized and analysed with FEM and CBFEM for moment resistance. As moment resistance criteria the development of a 5% plastic strain at any point of the column is going to be established.

The results provided by the numerical models are going to be compared with the ones provided by the CM according to the European codes.

In addition, the initial stiffness and moment rotation curves are going to be obtained for shell FEM and its results compared with the initial stiffness prediction of the CM provided by the European codes.

All results for moment resistance and initial stiffness are going to be statistically analysed and some results discussion about them is going to be developed.

Finally, the main conclusions and findings are going to be presented and future work is going to be defined.

1.3 Contents of the thesis

Chapter 1 – Introduction

On this chapter a brief overview of CWP in shear on beam-to-column joints is provided, including the problems related to the analysis of its behaviour and historical context. The main motivations for this study and the main objectives are also presented in this chapter.

Chapter 2 – State of the Art

This chapter may be divided into 10 parts. Namely, an overview of the historical context of the study of the CWP including the motivations for the increased interest on that research topic, a distinction between joint and connection, an explanation of the system of internal forces that act on the CWP including a mention to the transformation parameter, a brief explanation of the deformability of a joint, the analytical multilinear model proposed by Jaspart (1990) for load introduction, the analytical multilinear models proposed by Jaspart (1990) and Krawinkler (1978) and an explanation of the statics of the joint.

Chapter 3 – Methods

On this chapter the approach used by the CM adopted by the European codes EN 1993-1-8 and FprEN 1993-1-8 are presented. In addition, a description of CBFEM models including material and geometrical characteristics, mesh size, joints configuration, types of analysis and python scripts used is presented.

Finally, the approach used for shell FEM is presented including creation using Python scripts, geometry, material properties, the consideration of initial imperfections, loading support conditions, finite element type and size, and validation of the proposed models against experimental data.

Chapter 4 -Parametric Study

The scope of the study is presented in this chapter, including the columns chosen for analysis, and the joints configuration and geometrical characteristics to be analysed. A brief explanation of the way results is presented is provided followed by the detailed results constituted by tables that include the joints moment-resistances and initial stiffness obtained with each method.

Chapter 5 – Results discussion

On this chapter the main results are discussed, highlighting mean tendencies the results dispersion. The differences in behaviour from different shell models are identified, referring if the moment resistance or initial stiffness provided by each of them is higher or lower between them. The general tendencies that seem to exist for each method and the comparison between them is also referred.

Chapter 6 – Conclusions

On this chapter, the main conclusions and finding for every method used are presented, evaluating is the are more/less conservative, potential problems or limitations detected are also highlighted on this chapter and future work is proposed.

2 STATE OF THE ART

2.1 Overview

Corman (2022) noticed that the study of the column web panel (CWP) in shear has experienced an increment in the attention given by the scientific community after the 60s and the beginning of the 70s. He also points out a reason for this increase in attention, referring that before the 60s the design philosophy in the United States of America for steel joints was based on rigid behaviour. A rigid behaviour in a still joint was achieved by using heavy reinforcement including horizontal and vertical stiffeners leading to an uneconomical design. According to Corman (2022), perfectly rigid joint behaviour is only achievable by welding, and unlike in the United States of America, welding in steel construction is not so common in Europe where designs using bolted joints are usually adopted.

As a result of those problems, semi-rigid welded joints started to be considered for the structural design of buildings, allowing the dispense of stiffeners and the use of improved bolted joints leading to more economic design.

Therefore, from the 70s until the 90's authors such as Popov & Stephen (1972) and Bose et al. (1972a) (1972b), developed several experimental and analytical studies to better understand the CWP behaviour. Popov & Stephen (1972) established a relation between the increment in the capacity of CWP in shear and the material strain-hardening, and, later, the work by Popov (1987) identified the shortcomings of the Rigid-Joint philosophy when seismic behaviour was considered and pointed to the need of more refined analytical models as wells as improvements in design practices.

Based on those studies and in the works about beams in elastic foundations developed by Hetenyi (1952), the theory of elastic stability by Timoshenko & Gere (1963), and early studies of the behaviour of welded steel joints by Graham et al. (1960) new analytical models were proposed to predict the behaviour of the CWP in shear and compression. The main Analytical models that stand out are the ones proposed by Krawinkler (1971) and (1978) (adopted by the American standard ASCI 360-16 (American Institute of Steel Construction, 2016)) and by Atamaz & Jaspart (1989) and Jaspart (1990) (adopted by the European standard EN 1993-1-8).

Finally, as pointed out by Corman (2022), to extend the range of cases covered by analytical models and increase, at the same time, their accuracy, the behaviour of the CWP is still an

important topic in steel construction research. Several studies have been carried out in the late 2000s as are the cases of Jordão (2008) and Girão Coelho (2009). While the work of Jordão (2008) attempted to predict the behaviour of two-sided joints with unequal depth beams, the work by Girão Coelho et al. (2009) provided an experimental database where the behaviour of high-strength steel joints is compared to the design behaviour as idealized by EN1993-1-8. Recently, the works by Skiadopoulos (2021), who proposed an analytical model that was derived using results from a numerical model calibrated with experimental data have gained attention.

2.2 Distinction between joint and connection

It is important to make the distinction between some terms and definitions before going deeper into the characterization of the CWP in shear.

At first, a clear distinction between joint and connection must be made. A joint between a column and one or two beams comprises a web panel zone and one or two connections, see Figure 2.1, defined as follows:

- ***The web panel zone*** corresponds to the web and flanges of the column for the height of the connected beam profiles.
- ***Connection*** represents all the elements that fasten the beam and the column such as bolts, welds, end plates, etc.

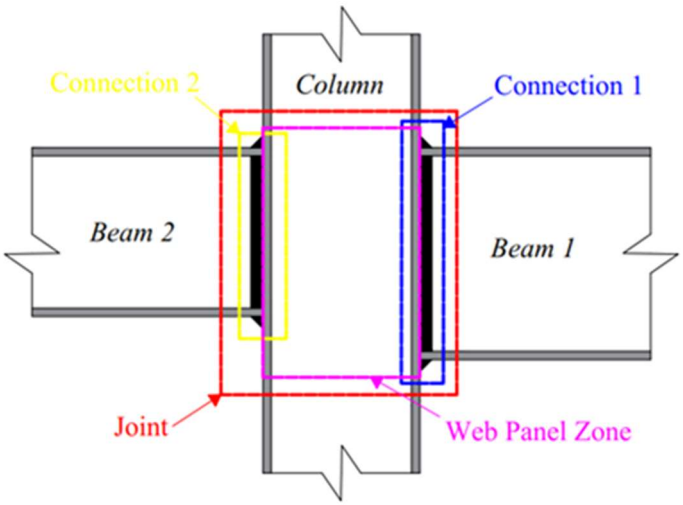

Figure 2.1 Distinctions between joint and Connection. (Girão Coelho A. M., 2001)

2.3 System of internal forces acting on the column web panel.

The system of internal forces acting in the CWP consists of the shear force applied on the top and bottom of the column and the bending moments in the beams and column (see Figure 2.2).

(Note: the sign convention for the internal forces adopted throughout the document follows EN 1993-1-8).

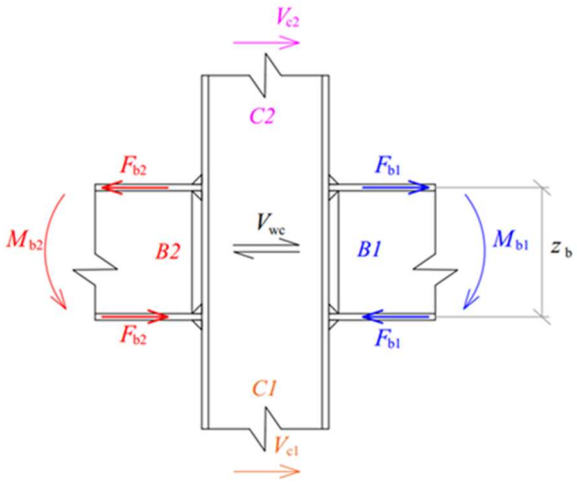

Figure 2.2 Sign convention adopted in EN 1993-1-8 (CEN, 2005b)

According to Figure 2.2 and the formulation based on the equilibrium on the contour of the CWP proposed by Atamaz and Jaspart (1990) the real shear acting on the CWP is given by:

$$V_{wc} = \frac{M_{b1} - M_{b2}}{z_b} - \frac{V_{c1} - V_{c2}}{2} \tag{1}$$

EN 1993-1-8 (CEN, 2005) adopts this expression. The given formulation is valid for a two-sided joint only if both beams have the same lever arm of the resultant tensile and compressive forces z_b.

2.4 Transformation Parameter *β*

The transformation parameter β relates the tensile and compressive forces F_b to the shear force on the column web panel (CWP). Since those forces are statically equivalent to the bending moment acting on the beam, the transformation parameter relates that bending moment with the shear force:

$$V_{wc} = \frac{M_{b1,i}}{z_b}\beta_i \tag{2}$$

The subscription *i* indicates the connection side (1 or 2). Considering Eq. (1) and Eq. (2) Atamaz & Jaspart, 1990 obtained Eq. for one-sided joints and Eq. (3) for two-sided joints (it may be

highlighted that Eq. (3) is equivalent to Eq. (4) considering the respective moments 1 or 2 equal to zero on each case respectively).

$$\beta = 1 - \frac{z_b}{2M_b}(V_{c1} - V_{c2}) \tag{3}$$

$$\begin{aligned} \beta_1 &= 1 - \frac{M_{b1}}{M_{b2}} - \frac{z_b}{2M_{b2}}(V_{c1} - V_{c2}) \\ \beta_2 &= 1 - \frac{M_{b2}}{M_{b1}} - \frac{z_b}{2M_{b1}}(V_{c1} - V_{c2}) \end{aligned} \tag{4}$$

The second Eurocode generation FprEN 1993-1-8 (CEN, 2023) will give conservative values for the transformation parameter by neglecting the effect of the shear forces on the column's top and bottom (see Table 2.1).

Table 2.1 Conservative values for the transformation parameter according to FprEN 1993-1-8 (CEN, 2023)

Joint type	**Moments on beams relation**	β
Single-sided	$M_{b1}=0 \vee M_{b2}=0$	$=1$
Double-sided	$M_{b1}=M_{b2}$(Same value and balanced)	$=0$
	$M_{b1}=-M_{b2}$(Same value but unbalanced)	$=2$
	$M_{b1}/M_{b2} > 0$	≈ 1
	$M_{b1}/M_{b2} < 0$	≈ 2

2.5 Deformability of the joint

The deformability of the joint is the result of the deformation at the region of load-introduction in the CWP, the deformation of fastening elements, and the deformation of the CWP in shear.

The deformation at the region of load-introduction in the CWP and the deformation of the fastening elements lead to a differential rotation between the beam's axes and the column's axes, see Figure 2.3.

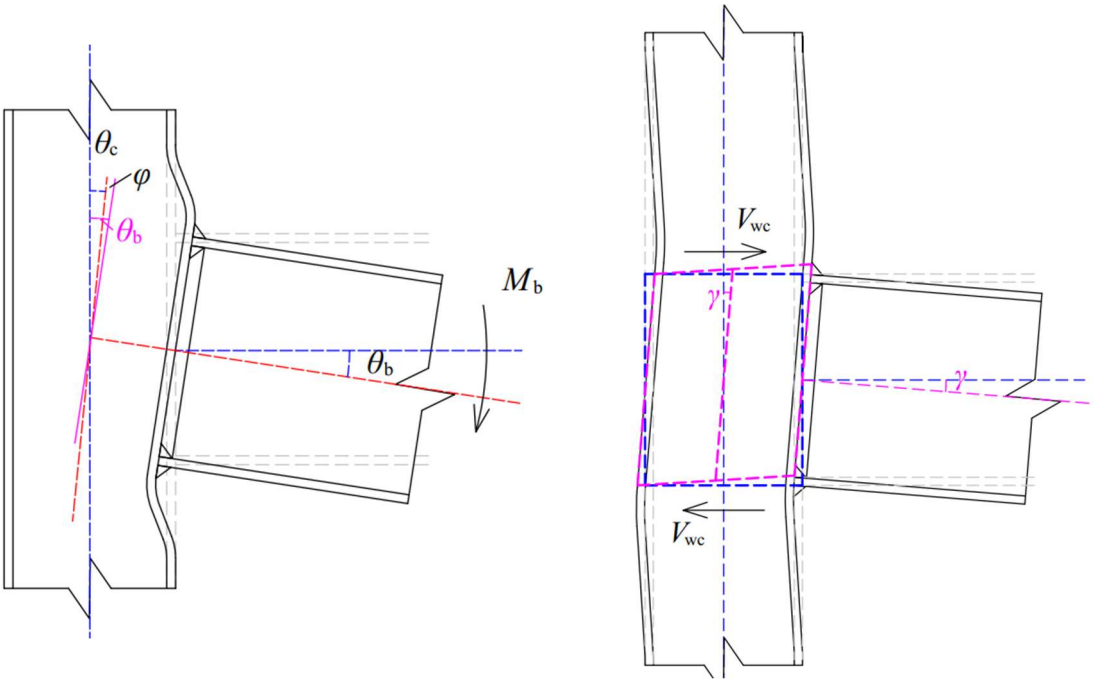

a) b)

Figure 2.3 Relative rotation between the beam and the column: a) due to load-introduction in web-panel and fastening elements deformation, b) due to column web panel in shear. Adapted from: (Jordão, 2008) and (Girão Coelho A. M., 2001).

As derived from Figure 2.3, the differential rotation between the beam and the column is the difference between the rotate \on of the beam and the rotation of the column, see Eq. (5)

$$\varphi = \theta_c - \theta_b \tag{5}$$

The shear force V_{wc} acting on the column web panel leads to the differential deformation γ see Figure 2.3 b).

2.6 Flexural deformability curves

Since the differential rotations of the joint depend on the applied bending moment by the beam (with the load-introduction in the CWP) and by the shear force (that can be related to the bending moment using the transformation parameter as previously explained), the flexural deformability of the joint is obtained by adding the two curves relating differential rotations and bending using the principle of superposition, see Figure 2.4.

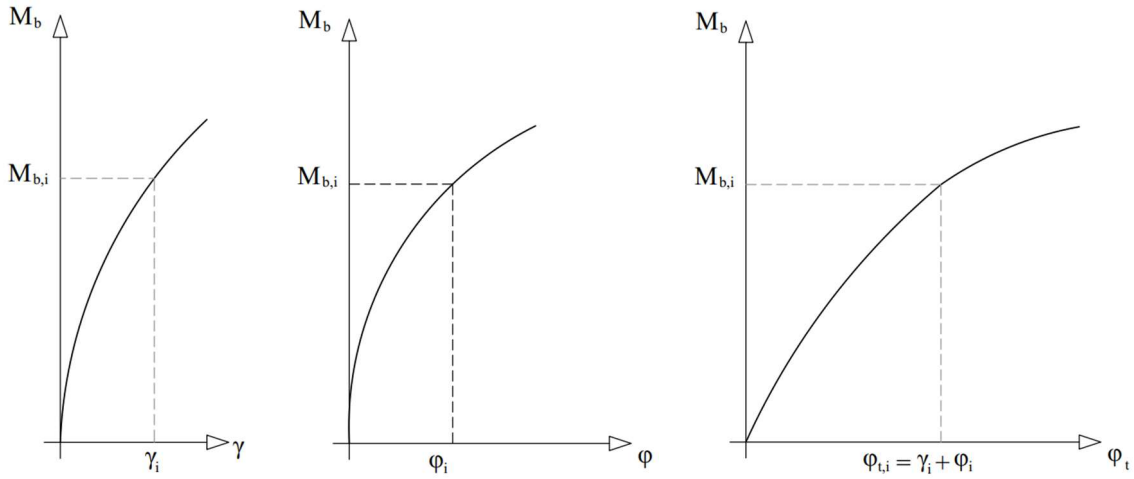

a) b) c)

Figure 2.4 Relative rotation - bending moment curves: a) for column web panel in shear, b) for load introduction and fastening elements deformation, c) global curve. (Jaspart & Weynand, 2016)

2.7 Analytical multilinear models to predict the behaviour of the column web panel due to load-introduction

To understand the behaviour of the CWP due to the load-introduction and to obtain the relative rotation-bending moment curve (M_b - γ) Atamaz & Jaspard (1989) and Jaspart (1990) proposed an analytical trilinear model, see Figure 2.5.

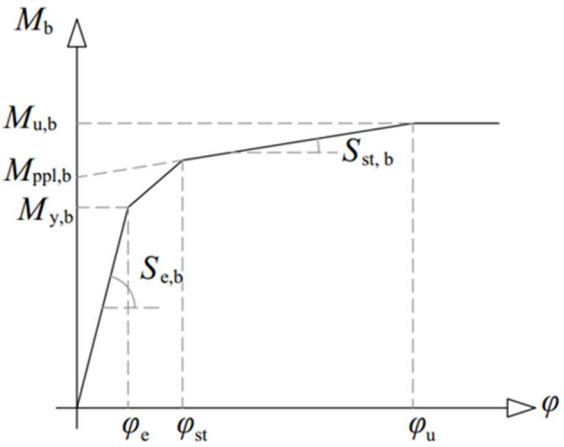

Figure 2.5 Jaspart (1990) load-introduction model, differential rotation - bending moment curve.

The initial stiffness $S_{e,\,b,}$ see Eqs. 6 to 8, is obtained considering an elastic beam (the flange of the column) in an elastic foundation (the web of the column) as described by Jaspart (1990) and Girão Coelho (2001).

$$S_{e,b} = k\frac{z_b^2}{2}\left[\frac{1}{\lambda}+\frac{2}{\lambda^2 z_b}\left(1+\frac{1}{\lambda z_b}\right)+\frac{z_b}{6}\right], \tag{6}$$

$$k = \frac{Et_{wc}}{h_{wc}}, \tag{7}$$

$$\lambda = \left(\frac{k}{4EI_{fc}}\right)^{0.25}, \tag{8}$$

Afterward, the maximum elastic bending moment of the web $M_{y,b}$ is achieved corresponding to the beginning of yielding in the column web, see Eqs. 9 and 10.

$$M_{y,b} = \frac{2t_{wc}S_{e,b}}{z_b k}\sigma_{h,max}, \tag{9}$$

$$\sigma_{h,max} = \omega f_{y,wc} \le f_{y,wc}. \tag{10}$$

The reduction coefficient ω is introduced to consider the stress interaction. That interaction can be considered by the Von Misses criterion, as described by Girão Coelho (2001), considering a small web element, see Figure 2.6, in equilibrium with normal vertical stress σ_v, normal horizontal stress $\sigma_{h,}$ and shear stress τ.

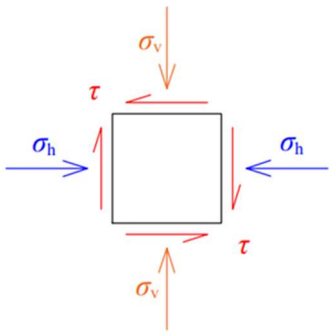

Figure 2.6 Stress state in a web panel element, adapted from Girão Coelho (2001)

Therefore, the Von Misses criterion including the effect of the vertical normal stress is given by Eq. (11).

$$\sigma_{\mathrm{h,max}}^2+\sigma_{\mathrm{v}}^2-\sigma_{\mathrm{h,max}}\sigma_{\mathrm{v}}+3\tau^2=f_{\mathrm{y,cw}}^2. \tag{11}$$

By neglecting the effect of the vertical normal stress, the reduction coefficient is given by Eq. 12.

$$\omega=\frac{1}{\sqrt{1+3\beta^2\xi^2\left(\frac{b_{\mathrm{eff}}t_{\mathrm{wc}}}{A_{\mathrm{wc}}}\right)}}. \tag{12}$$

The parameter ξ depends on the shear stress distribution on the CWP and the value of 0.2 for this parameter was suggested by Tsai & Popov (1990); b_{c} represents the effective width of the column web, according to Jaspart (1990) (as earlier proposed by Graham (1960)) and it is given by Eq. .

$$b_{\mathrm{eff}}=t_{\mathrm{fb}}+2\sqrt{2}a_{\mathrm{b}}+5(t_{\mathrm{fc}}+r_{\mathrm{c}}), \tag{13}$$

The strain-hardening begins for the rotation φ_{st} given by Eq. 14.

$$\varphi_{\mathrm{st}}=\frac{\varepsilon_{\mathrm{st,wc}}h_{\mathrm{wc}}}{z_{\mathrm{b}}}. \tag{14}$$

The pseudo-yielding bending moment $M_{\mathrm{ppl,b}}$ as noticed by Girão Coelho (2001) is associated with plastic flexural resistance to load-introduction and is given by Eq. 15.

$$M_{\mathrm{ppl,b}}=t_{\mathrm{wc}}b_{\mathrm{wc}}z_{\mathrm{b}}\sigma_{\mathrm{h,max}}. \tag{15}$$

During the hardening stage, the stiffness decreases with respect to the elastic stiffness. That decrease is given by the quotient between the elasticity modulus of the material E and the elasticity modulus when the steel is in the hardening stage E_{st} and corresponds, approximately, to 1/50 of the elastic value, see Eq. 16.

$$S_{\mathrm{st,b}}=\frac{E_{\mathrm{st}}}{E}S_{\mathrm{e,b}}=\frac{S_{\mathrm{e,b}}}{50}. \tag{16}$$

The ultimate flexural resistance $M_{\mathrm{u,b}}$ depends on the yielding of the CWP and the instability phenomenon as warping buckling and/or cripling. Therefore, it must be taken as the lower value given by the Eqs. 17 to 19.

$$M_{\mathrm{uy,b}} = t_{\mathrm{wc}} b_{\mathrm{wc}} z_{\mathrm{b}} \sigma_{\mathrm{hu,wc}}, \tag{17}$$

$$M_{\mathrm{uinst,b}} = \sqrt{M_{\mathrm{uy,b}} M_{\mathrm{cr,b}}} \geq M_{\mathrm{ppl,b}}, \tag{18}$$

$$M_{\mathrm{cr,b}} = (h_{\mathrm{c}} - 2t_{\mathrm{fc}}) t_{\mathrm{wc}} z_{\mathrm{b}} k \frac{\pi^2 E}{12(1-\nu^2)} \left(\frac{t_{\mathrm{wc}}}{h_{\mathrm{c}} - 2t_{fc}^2} \right) \tag{19}$$

The buckling factor *k* as given by Atamaz & Jaspart (1989) depends on the restrains of the plate: taken equal to 1 for double-sided joints and equal to 2 for single-sided joints for HE profiles columns.

2.8 Analytical multilinear models of Jaspard and Krawinkler

A group of analytical models to predict the CWP deformability and moment-rotation behaviour in shear have been proposed by different authors. Among those the ones developed by Jaspart (1990) and Krawinkler (1973) are highlighted due to the adoption of them by the European and American codes respectively (European standard EN 1993-1-8 (CEN, 2005b) and American standard ASCI 360-16 (American Institute of Steel Construction, 2016)).

Corman (2022) noticed that both Jaspart and Krawinkler models are trilinear and admitted that the CWP has the following behaviour:

- Elastic behaviour until the yield stress is achieved in the most stressed region.
- The first plastic stage considers the flanges of the columns, the root fillets, and the use or not of stiffeners.
- The second plastic stage is associated with the hardening of the material.

The model developed by Atamaz & Jaspart (1989) and refined by Jaspart (1990) can be seen in Figure 2.7. The stiffness during the elastic stage is given by Eq. (20).

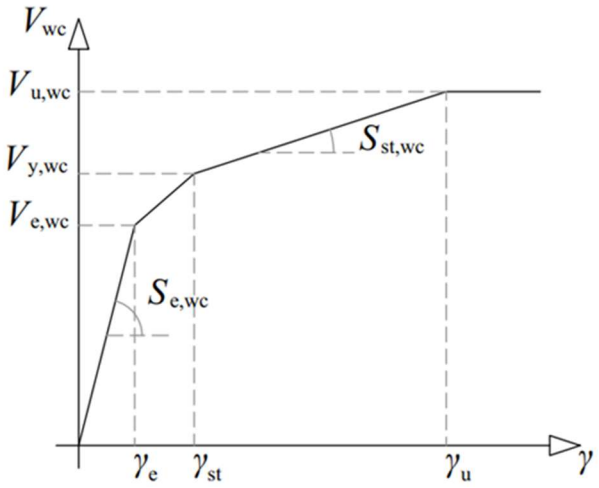

Figure 2.7 Multilinear model proposed by Jaspart (1990).

$$S_{e,wc} = \frac{E_{wc}}{2(1+\nu)} A_{wc} \tag{20}$$

The elastic shear resistance $V_{e,wc}$ can be obtained by Eq. (1), while the yielding shear force $V_{ppl,wc}$ (that gives the plastic capacity of the web) is given by (21).

$$V_{ppl,wc} = A_{wc} \sqrt{\frac{1}{3}\left(f_{y,wc}^2 - \sigma_v^2\right)} \tag{21}$$

The strain-hardening rotation γ_{st} as noticed by Girão Coelho (2001) is given by Eq. (22).

$$\gamma_{st} = \frac{1}{2}\left[\frac{2V_{y,wc}(1+\nu)}{EA_{wc}} + \sqrt{3}\left(\varepsilon_{st,wc} - \varepsilon_{y,wc}\right)\right] \tag{22}$$

The stiffness during hardening is given by the Eq. (23).

$$S_{st,wc} = \frac{E_{st}}{3} A_{wc}. \tag{23}$$

The ultimate shear resistance is no more than considering the ultimate stress along the entire area of the CWP (see Eq. (24))

$$V_{u,wc} = A_{wc} \tau_{u,wc}. \tag{24}$$

The model developed by Krawinkler (1973), see Figure 2.8, and referred to by Girão Coelho (2001) is one of the most popular models because of its simplicity. Within this model, the elastic shear force is given by Eq. (25).

$$V_{\mathrm{e,wc}} = \frac{f_{\mathrm{y,wc}}}{z_{\mathrm{b}}\sqrt{3}} \frac{t_{\mathrm{wc}} h_{\mathrm{c}} h_{\mathrm{b}}}{\beta}. \tag{25}$$

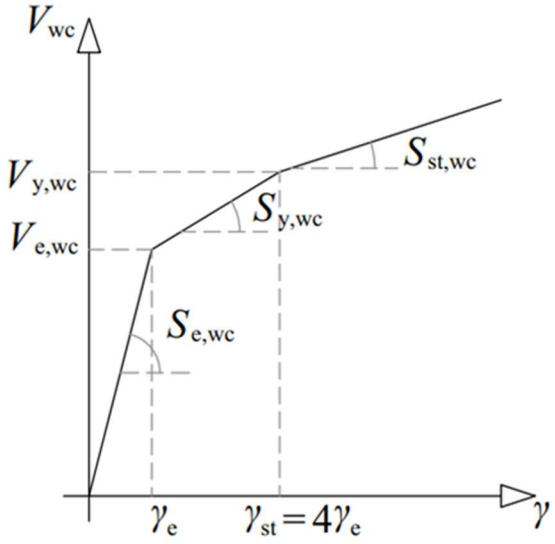

Figure 2.8 Krawinkler (1978) shear-deformation model, adapted from Girão Coelho (2001).

The rotation that belongs to the shear elastic force is given by Eq. (26).

$$\gamma_e = \frac{2 f_{\mathrm{y,wc}} (1+\nu)}{\sqrt{3} E}. \tag{26}$$

The stiffness during the elastic stage is given by Eq. (27).

$$S_{\mathrm{e,wc}} = \frac{E h_{\mathrm{c}} h_{\mathrm{b}} t_{\mathrm{wp}}}{2 z_{\mathrm{b}}^2 (1+\nu) \beta}. \tag{27}$$

Krawinkler set that the stiffness after the beginning of yielding is given by Eq. (28).

$$S_{\mathrm{y,wc}} = \frac{2}{5} \frac{E b_{\mathrm{c}} t_{\mathrm{fc}}^2}{z_{\mathrm{b}}^2 \beta}. \tag{28}$$

This post-yielding stage develops until the yielding stress on the column flanges is achieved, according to Krawinkler (1978) and as referred by Girão Coelho (2001) that occurs at a rotation of $4\gamma_e$.

The shear that corresponds to the beginning of the hardening of the material $V_{y,wc}$ is given by Eq. (29) and the hardening stiffness is given by Eq. (30).

$$V_{y,wc} = V_{e,wc}\left(1+\frac{3.12 b_c t_{fc}^2}{h_c h_b t_{wc}}\right), \tag{29}$$

$$S_{st,wc} = \frac{E_{st}}{E} S_{e,wc}. \tag{30}$$

2.9 Static of the Joints

The statics of the joints are going to be discussed in the following chapters for the one-sided internal story joint configuration adopted for the study cases presented in Chapter 4.

The basic case consists of a column of length Lc with a centred welded joint with support at the bottom and a simple support at the top, see Figure 2.9.

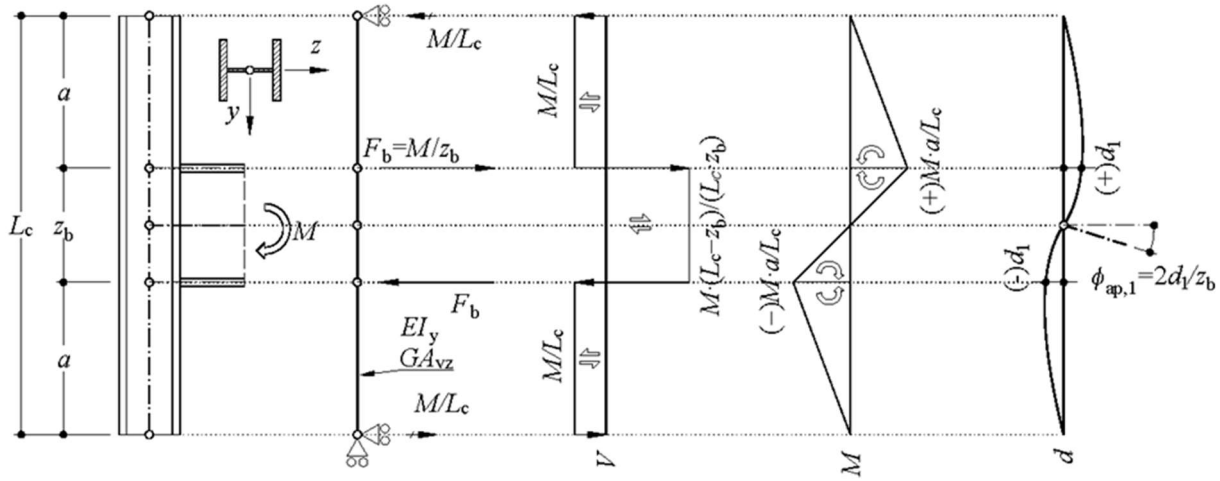

Figure 2.9 Statics of one-sided joint at internal story.

As may be seen in Figure 2.9, the bending moment M is applied on the beam stub and is statically equivalent to two forces according to Eq. (31) (considering z_b as the distance between centroids of beam flanges).

$$F_b = \frac{M}{z_b}, \tag{31}$$

$$z_{\mathrm{b}} = h_{\mathrm{b}} - t_{\mathrm{fb}}, \tag{32}$$

It should be highlighted that Eq. (32) is not exact because of the dependence of z_{b} on the level of plasticity of the beam cross-section. Considering a fully plastified beam the moment resistance is given by Eq. and the axial capacity of half section is given by 34.

$$M_{\mathrm{R}} = W_{\mathrm{pl,y}} f_{\mathrm{y}}, \tag{33}$$

$$N_{\mathrm{R}} / 2 = A f_{\mathrm{y}} / 2, \tag{34}$$

Considering simultaneously Eqs. (33) and (34) an exact expression for the lever arm z_{b} is obtained, see Eq.

$$z_{\mathrm{b,exact}} = 2W_{\mathrm{pl,y}} / A. \tag{35}$$

For IPE and HE sections in function of the high (h) Figure 2.10 shows the difference between the exact and approximate Eqs. (32) and (35). It may be seen that the approximate underestimates the lever arm systematically for I or H-shaped profiles however, in the following chapters is going to be adopted the approximate formulation due to the adoption of that formulation in most of the literature consulted.

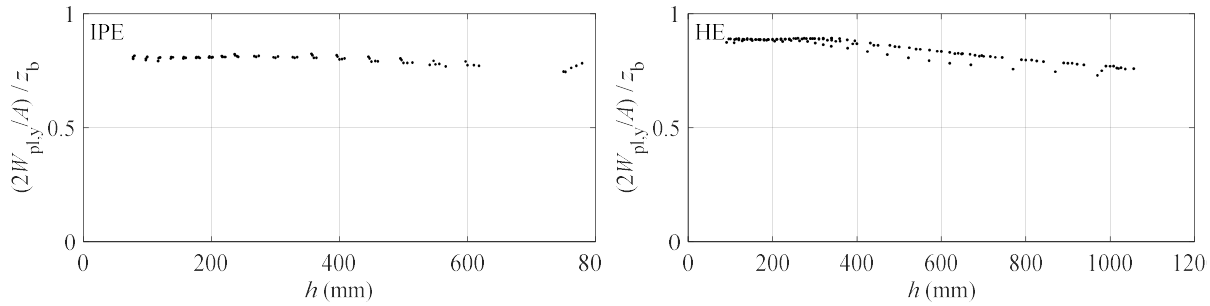

(a) (b)

Figure 2.10 Lever arm for plastic sections: (a) IPE; (b) HE.

The deformation of the joint is due to the application of the bending moment and the correspondent shear force in the CWP. However, the shear force V_{cw} acting on the joint's column web panel is not the total force F_{b}, but only a fraction as shown in Eq. (36)

$$V_{\mathrm{cw}} = M \frac{L_{\mathrm{c}} - z_{\mathrm{b}}}{L_{\mathrm{c}}\, z_{\mathrm{b}}} = \frac{M}{z_{\mathrm{b}}}\left(1 - \frac{z_{\mathrm{b}}}{L_{\mathrm{c}}}\right) = F_{\mathrm{b}}\left(1 - \frac{z_{\mathrm{b}}}{L_{\mathrm{c}}}\right). \tag{36}$$

The fraction of the bending moment that produces shear on the joint's column web panel is given by Eq. (37).

$$M_{cw} = M\left(1 - \frac{z_b}{L_c}\right). \tag{37}$$

Therefore, considering (36) and (37) and considering V_R as the shear resistance of the CWP the resisting bending moment of the CWP in shear is given by Eq. (38).

$$M_R = \frac{V_R z_b}{1 - \frac{z_b}{L_c}}, \tag{38}$$

Once the length of the beam is always bigger than the lever arm it may be noticed that the value of moment resistance for the CWP in shear given by Eq. 38 is always bigger than the usually adopted value of $V_R z_b$.

The value given by Eq. 38 is equivalent to the value considering shear on the verification established in EN 1993-1-8 and given by Eq. 39 where V_T and V_B are the shear force acting at the top and the bottom of the column respectively.

$$\frac{M}{z_b} - \frac{V_T + V_B}{2}, \tag{39}$$

2.10 Rotation of the joint when analysed using finite element models

The obtention of the moment-rotation curve using FEM for joints to study the behaviour of the CWP in shear requires the obtention of the displacements of the bottom and top of the beam. The displacements given because of a FEM analysis include the deformation of the column outside the joint and, therefore, that effect must be eliminated. Considering the static system shown in Figure 2.11 where infinite bending and shear stiffness are assumed for the joint region the corresponding displacements at the level of the beam flange can be found by applying the unit displacement theorem, see Eq. 40.

$$d_{FFRRFF} = M\frac{z_b a^3}{3L_c^2 EI_y} + M\frac{z_b a}{L_c^2 GA_{vz}}, \tag{40}$$

On Eq. 40 the first part on the right term is the bending deformation and the second part is the shear deformation. EI_y is the bending stiffness and GA_{vz} is the shear stiffness. The subscript for the displacement reads 'FFRRFF'; the first group of two letters refers to the bottom column bending stiffness and shear stiffness; the second group refers to the joint bending stiffness and shear stiffness; and the third group refers to the top column bending stiffness and shear stiffness; 'F' stands for flexible and 'R' for rigid.

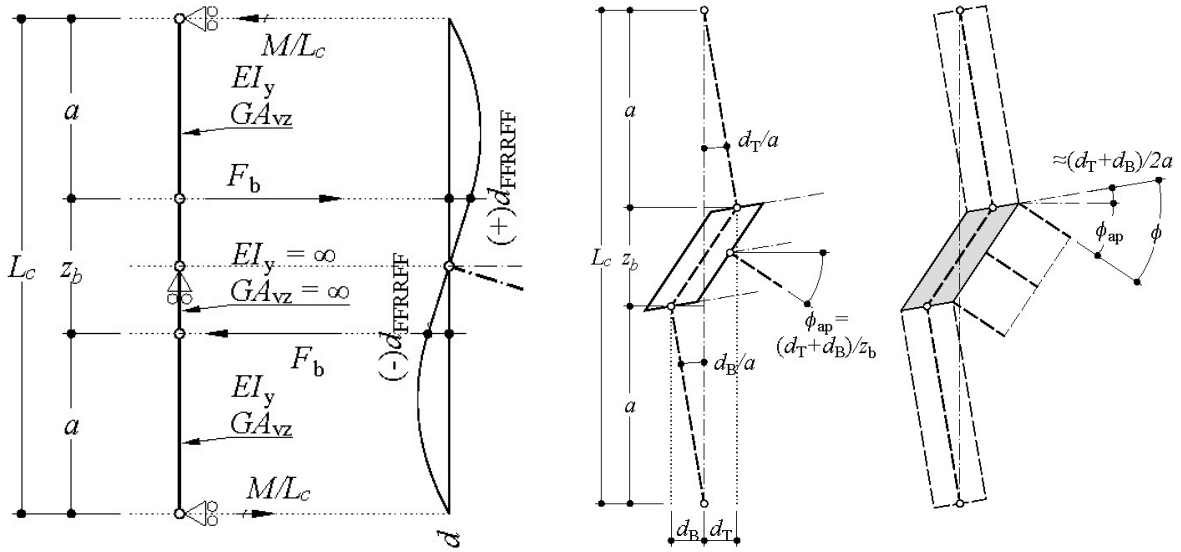

(a) (b)

Figure 2.11 Deformation of one-sided joint at internal story.

To exclude the column flexibility from the analysis the displacements given by the Eq. 40 must be subtracted from the displacements obtained by the FEM, see Eqs. 41 and 42.

$$d_{\mathrm{jT}} = d_{\mathrm{FEM,T}} - d_{\mathrm{FFRRFF}}, \tag{41}$$

$$d_{\mathrm{jB}} = d_{\mathrm{FEM,B}} + d_{\mathrm{FFRRFF}}, \tag{42}$$

where $d_{\mathrm{FEM,T}}$ (assumed positive) is the displacement at the top beam flange centroid level obtained from FEM, and bottom $d_{\mathrm{FEM,B}}$ (assumed negative) is the displacement at the bottom beam flange centroid level obtained from FEM. By adding the bending deformability to the central part Eq. 43 is obtained.

$$d_{\mathrm{FFFRFF}} = d_{\mathrm{FFRRFF}} + M\frac{z_{\mathrm{b}}^2 a^2}{6L_c^2 EI_y}, \tag{43}$$

The corresponding values of deformation at beam top and bottom centroids due only to the joint shear deformability are given by Eqs. 44 and 45.

$$d_{\mathrm{jVT}} = d_{\mathrm{FEM,T}} - d_{\mathrm{FFFRFF}}, \tag{44}$$

$$d_{\mathrm{jVB}} = d_{\mathrm{FEM,B}} + d_{\mathrm{FFFRFF}}. \tag{45}$$

If the shear deformability of the central part is added to Eq. 40 Eq. 46 is obtained.

$$d_{\mathrm{FFRFFF}} = d_{\mathrm{FFRRFF}} + M\frac{2a^2}{L_c^2 G A_v}, \tag{46}$$

Therefore, the corresponding values of deformation at beam top and bottom centroids due only to the joint bending deformability are given by Eqs. 47 and 48.

$$d_{\mathrm{jMT}} = d_{\mathrm{FEM,T}} - d_{\mathrm{FFRFFF}}, \tag{47}$$

$$d_{\mathrm{jMB}} = d_{\mathrm{FEM,B}} + d_{\mathrm{FFRFFF}}. \tag{48}$$

The apparent rotation ϕ_{ap} is defined as the rotation measured from the horizontal, see Figure 2.11 b), and is given by Eq. 49.

$$\phi_{\mathrm{j,ap}} \approx \frac{d_{\mathrm{jT}} - d_{\mathrm{jB}}}{z_{\mathrm{b}}}, \tag{49}$$

Assuming d_{jB} as negative. To characterize the joint rotation, it must also include the component due to the rotation of the column, as shown in Figure 2.11 b). See Eq. 50.

$$\phi_j \approx \frac{d_{\mathrm{jT}} + d_{\mathrm{jB}}}{z_{\mathrm{b}}} + \frac{d_{\mathrm{jT}} + d_{\mathrm{jB}}}{2a} = (d_{\mathrm{jT}} + d_{\mathrm{jB}})\left(\frac{1}{z_{\mathrm{b}}} + \frac{1}{2a}\right). \tag{50}$$

2.11 Limitations of the component method and alternatives

Based on the analytical models presented on previous sections, the component method has been implemented on the European EN 1993-1-8 and FprEN 1993.-1-8. However, recent research began to question the results provided by the CM as implemented in the European codes, pointing out that its predictions may be too conservative if the column web panel in compression (CWC) is the critical component (Golea, Jaspart, & Demonceau, 2022) or unconservative if the column web panel in shear (CWS) is the critical component (Corman, Jaspart, & Demonceau, 2019; Brandonisio, De Luca, & Mele, 2012). However, those studies have also highlighted the necessity to expand the sample of joints analysed.

Also, Golea et al refers that further studies must be carried out to evaluate the sensibility of the T-Stub model implemented on the European codes. He also highlights that work in that field is already been develop in the University of Liège.

Aiming to verify the accuracy of the results provided by the CM, the use of numerical finite element models (FEM) validated against experimental data, has been commonly employed to

characterize the behavior of beam-to-column joints. Among a variety of finite elements (FE) already implemented in commercial numerical finite element software, the use of solid FE has proven to be especially accurate when validated against experimental data (Corman, Jaspart, & Demonceau, 2019).

However, since the solid FE may require heavy computational resources and high processing times, the less computationally demanding shell FE has also been widely used as a good compromise. Naturally, the choice of the FE type usually depends on the level of accuracy claimed and the computational resources available. Some studies devoted to the analysis of beam-to-column steel compared the accuracy of the results of both solid and shell FEM and found almost no considerable differences in the overall behavior of the joint (Jordão, 2008) (El-Khoriby, Sakr, Khalifa, & Eladly, 2017). Nevertheless, those studies covered only some specific configurations of beam-to-column steel joints (4 configurations each).

2.12 CBFEM Overview

The component based finite element method assumes that the component method may be kept as main tool of analysis, once it may simplify the analysis of the joint compared to pure FEM. However, CBFEM points out that that weakness of the CM settles in the problems it may have to actually evaluate the stresses in the individual components (CBFEM Team, 2021).

Therefore, the CBFEM maintains the division in components of the CM but evaluates the stresses using finite element models aiming to combine the speed of analysis of the CM with the accuracy and detail provided by FEM.

Among the proposals existing, the commercial software IDEA StatiCa® points out. IS analyses the joint according to the following steps (StatiCa(R), 2016):

- Division of the joint into components.
- All steel plates are modeled by the finite element method assuming ideal elastic-plastic material (Usually shell elements).
- Bolts, welds, and concrete blocks are modeled as nonlinear springs.
- The finite element model is used for analyzing internal forces in each of the components.
- Plates are checked for limit plastic strain – 5% acc. to EC3.
- Each component is checked according to specific formulas defined by the national code, similarly as when using the component method.

The use of this methodology by the software allows it to provide results in a relatively short time and therefore becomes interesting for the industry. IS highlights a group of studies that seem to confirm their results (StatiCa(R)). However, further research may be needed to confirm its applicability to all failure modes.

3 METHODS

The purpose of this study is to perform a comparison of resistance predicted by different methods used in current practice, namely:

- The Component Method (CM) as implemented in European design codes (Eurocode 3, part 1-8); and
- the Component-Based Finite Element Method (CBFEM) as implemented in the software IDEA StatiCa.

The benchmark for comparison is the resistance predicted by sophisticated Finite Element Models (FEM), performed using Abaqus, and properly validated against lab experiments. A numerical study is designed to perform this comparison in a meaningful way for a large dataset of connections representative of current practice, under the scope of this work.

3.1 Component Method and Design Codes

3.1.1 The Component Method

The component method (CM) is a well-established general procedure to determine the main structural properties (resistance and stiffness) of a joint (Simões da Silva, 2008) The method is based on the identification of the joint active components, subsequent assessment of their individual structural properties, and creation of a joint model assembling the individual components using rigid links and springs. A detailed explanation of the CM is given in (Jaspart & Weynand, 2016) The most widespread application of the CM can be found in part 1-8 of Eurocode 3, hereinafter referred to as EC3-1-8 (CEN, 2005b), or its ongoing revision, hereinafter referred to as FprEC3-1-8 (CEN, 2023). The Component verification according to these codes is discussed in the next subsection.

3.1.2 Eurocode 3

EC3-1-8 presents CM-based expressions for strong–axis, open–section, welded, beam–column joints. According to the code, the joint resistance is limited by the most restrictive of the following individual components: column web panel in shear (CWS), column web in transverse compression (CWC), column web in transverse tension (CWT), column flange in transverse bending (CFB) or beam flange and web in compression (BFC). The joint stiffness is dependent on the individual stiffnesses of the CWS, CWT, and CWC. The CWC and CWT components

can be disregarded if a transverse stiffener is placed, aligned with the beam flange, in the compression or tension zone, respectively (actually, no rules are given regarding resistance for this case). The transverse stiffeners, together with the column flanges, increase the resistance of the CWS component. The joint is divided into a panel zone and either one (one-sided joint) or two (two-sided joint) connections. For a two-sided joint, the demand on the CWS component is dependent on the bending moments applied on both sides. This is considered using a transformation parameter β, applied to one connection, which is dependent on the bending moment ratio between both connections. FprEC3-1-8, currently under preparation, is based on a similar rationale, but includes some adjustments based on recent numerical studies (Jaspart, Corman, & Demonceau, 2022a; Corman, Adrien, 2022; Jaspart, Corman, & Demonceau, 2022b)

The EC3-1-8 and FprEC3-1-8 expressions are summarized and compared in Table 2 The main differences between both codes are i) the definition of the column shear area A_{CWS} (CWS); ii) the contribution of the column flange and transverse stiffeners (CWS); and iii) the definition of the web panel slenderness and buckling expressions (CWC).

EC3-1-8 (EN 1993-1-8:2005)

Using the expressions in the Table, the values of moment resistance limited by the joint components as per EC3-1-8 are $M_{CWS,R,EN}$, $M_{CWC,R,EN}$, $M_{CWT,R,EN}$, $M_{CFB,R,EN}$, where the subscript 'EN' is used to refer to the current version EC3-1-8. The moment resistance of the joint (referred to as the moment applied on side 1), is assessed as follows:

For internal story configuration (I):

$$M_{R,EN} = \min\left\{M_{CWS,R,EN}\left(\frac{1}{z_b}-\frac{1}{L_c}\right); M_{CWC,R,EN}; M_{CWT,R,EN}; M_{CFB,EN,R}\right\} \tag{51}$$

For roof configuration (R):

$$M_{R,EN} = \min\left\{M_{CWS,R,EN}; M_{CWC,R,EN}; M_{CWT,R,EN}; M_{CFB,EN,R}\right\}. \tag{52}$$

The value of $M_{CFB,EN,R}$ for unstiffened joints is obtained as:

$$M_{CFB,EN,R} = z_b b_{eff,CFB} t_{fb} \frac{f_{y,fb}}{\gamma_{M0}}, \tag{53}$$

Where:

$$b_{\text{eff,CFB}} = t_{\text{wc}} + 2r_{\text{c}} + 7kt_{\text{fc}}, \tag{54}$$

And:

$$k = \frac{t_{\text{fc}}}{t_{\text{fb}}} \frac{f_{\text{y,fc}}}{f_{\text{y,fb}}} \leq 1. \tag{55}$$

For stiffened joints, this component is assumed as not relevant. The criterion to avoid joint stiffening as per EC3-1-8 is:

$$b_{\text{eff,CFB}} = b_{\text{b}} \frac{f_{\text{yb}}}{f_{\text{ub}}}, \tag{56}$$

where f_{ub} is the ultimate strength of the beam flange.

The joint initial stiffness defined by EC3-1-8 and referred to as side 1 can be obtained from the stiffness components $k_{\text{CWS,EN}}$, $k_{\text{CWC,EN}}$, $k_{\text{CWT,EN}}$, as:

$$S_{\text{j,ini,EN}} = E\, z_{\text{b}}^2 \left(k_{\text{CWS,EN}}^{-1} + k_{\text{CWC,EN}}^{-1} + k_{\text{CWT,EN}}^{-1} \right)^{-1}, \tag{57}$$

and the secant stiffness $S_{\text{j,sec,EN}}$ is 1/3 of the previous value.

Table 3.1 Comparison of EC3-1-8 and FprEC3-1-8 component expressions for welded joints.

	EC3-1-8	**FprEC3-1-8**
Conditions in this study	One- or double-sided joints, hot-rolled open sections (H, I), strong-axis, welded. For double-sided joints, equal beam height. For stiffened joints, transverse stiffeners in both tension and compression zones, aligned with beam flanges, $f_{\text{y,st}} = f_{\text{y,b}}$; $t_{\text{st}} = t_{\text{fb}}$ $b_{\text{st}} = b_{\text{fb}}$.	
Limits	$d_{\text{c}} / t_{\text{wc}} \leq 69\sqrt{235\text{MPa} / f_{\text{y,c}}}$	$h_{\text{c}} / t_{\text{wc}} \leq 60\sqrt{235\text{MPa} / f_{\text{y,c}}}$
CWS	**Resistance**: $M_{\text{CWS,Rd}} = z_{\text{b}} \left(V_{\text{wp,Rd}} + V_{\text{wp,add,Rd}} \right) / \beta$, $V_{\text{wp,Rd}} = 0.9 A_{\text{CWS}} f_{\text{y,c}} / \gamma_{\text{M0}} \sqrt{3}$ $z_{\text{b}} = h_{\text{b}} - t_{\text{fb}}$, $\beta_1 = \left\lvert 1 - M_{\text{j,b2,Ed}} / M_{\text{j,b1,Ed}} \right\rvert \leq 2$, $\beta_2 = \left\lvert 1 - M_{\text{j,b1,Ed}} / M_{\text{j,b2,Ed}} \right\rvert \leq 2$	
	$A_{\text{CWS}} = A - 2bt_{\text{fc}} + (t_{\text{wc}} + 2r_{\text{c}})t_{\text{fc}}$	$A_{\text{CWS}} = h_{\text{c}} t_{\text{wc}}$
	Unstiffened joint: $V_{\text{wp,add,Rd}} = 0$ Stiffened joint: $V_{\text{wp,add,Rd}} = 4M_{\text{pl,fc,Rd}} / z_{\text{b}}$	Unstiffened joint: $V_{\text{wp,add,Rd}} = 4M_{\text{pl,fc,Rd}} / z_{\text{b}}$, Stiffened joint: $V_{\text{wp,add,Rd}} = (4M_{\text{pl,fc,Rd}} + 2n_{\text{c}} M_{\text{pl,fb,Rd}}) / z_{\text{b}}$
	n_{c} = 1 (one-sided) or 2 (double-sided), $M_{\text{pl,fb,Rd}} = 0.25 b_{\text{fb}} t_{\text{fb}}^2 f_{\text{y,b}}$, $M_{\text{pl,fc,Rd}} = 0.25 b_{\text{fc}} t_{\text{fc}}^2 f_{\text{y,c}}$	

	Stiffness: $k_{\mathrm{CWS}} = 0.38 A_{\mathrm{CWS}} / (\beta z_{\mathrm{b}})$
CWT CWC	**CWT Resistance:** $M_{\mathrm{CWT,Rd}} = z_{\mathrm{b}}\, \omega b_{\mathrm{eff,CWT}} t_{\mathrm{wc}} f_{\mathrm{y,c}} / \gamma_{\mathrm{M0}}$ **CWC Resistance**: $M_{\mathrm{CWC,Rd}} = z_{\mathrm{b}} \min\left\{ \rho \omega k_{wc}\, b_{\mathrm{eff,CWC}} t_{\mathrm{wc}} f_{\mathrm{y,c}} / \gamma_{\mathrm{M1}}; \omega k_{wc}\, b_{\mathrm{eff,CWC}} t_{\mathrm{wc}} f_{\mathrm{y,c}} / \gamma_{\mathrm{M0}} \right\}$ Internal: $b_{\mathrm{eff,CWT}} = t_{\mathrm{fb}} + 2\sqrt{2} a_{\mathrm{b}} + 5(t_{\mathrm{fc}} + r_{\mathrm{c}})$. Roof: $b_{\mathrm{eff,CWT}} = t_{\mathrm{fb}} + \sqrt{2} a_{\mathrm{b}} + 2.5(t_{\mathrm{fc}} + r_{\mathrm{c}})$ $b_{\mathrm{eff,CWC}} = t_{\mathrm{fb}} + 2\sqrt{2} a_{\mathrm{b}} + 5(t_{\mathrm{fc}} + r_{\mathrm{c}})$, $k_{\mathrm{wc}} = \begin{cases} \sigma_{\mathrm{com,Ed}} \le 0.7 f_{\mathrm{y,c}} & \rightarrow k_{\mathrm{wc}} = 1 \\ \sigma_{\mathrm{com,Ed}} > 0.7 f_{\mathrm{y,c}} & \rightarrow k_{\mathrm{wc}} = 1.7 - \sigma_{\mathrm{com,Ed}} / f_{\mathrm{y,c}} \end{cases}$ $\left.\begin{array}{ll} 0 \le \beta \le 0.5, & \rightarrow \omega = 1, \\ 0.5 < \beta < 1, & \rightarrow \omega = \omega_1 + 2(1-\beta)(1-\omega_1), \\ \beta = 1, & \rightarrow \omega = \omega_1, \\ 1 < \beta < 2, & \rightarrow \omega = \omega_1 + (\beta - 1)(\omega_2 - \omega_1), \\ \beta = 2, & \rightarrow \omega = \omega_2. \end{array}\right\}$ with $\begin{cases} \omega_1 = \dfrac{1}{\sqrt{1 + 1.3 (b_{\mathrm{eff,CWT}} t_{\mathrm{wc}} / A_{\mathrm{CWS}})^2}} \\ \omega_2 = \dfrac{1}{\sqrt{1 + 5.2 (b_{\mathrm{eff,CWT}} t_{\mathrm{wc}} / A_{\mathrm{CWS}})^2}}, \end{cases}$
	$\bar{\lambda}_p = 0.932 \sqrt{\dfrac{b_{\mathrm{eff,CWC}}\, d_{\mathrm{wc}}\, f_{\mathrm{y,wc}}}{E t_{\mathrm{wc}}^2}}$ $\begin{cases} \bar{\lambda}_{\mathrm{p}} \le 0.72 & \rightarrow \rho = 1 \\ \bar{\lambda}_{\mathrm{p}} > 0.72 & \rightarrow \rho = (\bar{\lambda}_{\mathrm{p}} - 0.2) / \bar{\lambda}_{\mathrm{p}}^2 \end{cases}$	$\bar{\lambda}_p = 0.932 \sqrt{\dfrac{\omega k_{\mathrm{wc}} b_{\mathrm{eff,CWC}}\, d_{\mathrm{wc}}\, f_{\mathrm{y,wc}}}{E t_{\mathrm{wc}}^2}}$ $\begin{cases} \bar{\lambda}_{\mathrm{p}} \le 0.673 & \rightarrow \rho = 1 \\ \bar{\lambda}_{\mathrm{p}} > 0.673 & \rightarrow \rho = (\bar{\lambda}_{\mathrm{p}} - 0.22) / \bar{\lambda}_{\mathrm{p}}^2 \end{cases}$
	Stiffness: $k_{\mathrm{CWC}} = 0.7 b_{\mathrm{eff,CWC}} t_{\mathrm{wc}} / d_{\mathrm{wc}}$, $k_{\mathrm{CWT}} = 0.7 b_{\mathrm{eff,CWT}} t_{\mathrm{wc}} / d_{\mathrm{wc}}$	

FprEC3-1-8 (FprEN 1993-1-8:2023)

The previous equations can be used for $M_{R,FFprEN}$, $S_{j,ini,FFprEN}$, and $S_{j,sec,FFprEN}$, just replacing the EN components by those obtained with the FprEC3-1-8 expressions ($M_{CWS,R,FFprEN}$, $M_{CWC,R,FFprEN}$, $M_{CWT,R,FFprEN}$, $M_{CFB,R,FFprEN}$, $k_{CWS,FFprEN}$, $k_{CWC,FFprEN}$, $k_{CWT,FFprEN}$):

For internal story configuration (I):

$$M_{\mathrm{R,prEN}} = \min\left\{ M_{\mathrm{CWS,R,prEN}} \left(\frac{1}{z_{\mathrm{b}}} - \frac{1}{L_{\mathrm{c}}} \right); M_{\mathrm{CWC,R,prEN}}; M_{\mathrm{CWT,R,prEN}}; M_{\mathrm{CFB,prEN,R}} \right\} \tag{58}$$

For roof configuration (R):

$$M_{\mathrm{R,prEN}} = \min\left\{ M_{\mathrm{CWS,R,prEN}}; M_{\mathrm{CWC,R,prEN}}; M_{\mathrm{CWT,R,prEN}}; M_{\mathrm{CFB,prEN,R}} \right\} \tag{59}$$

The component $M_{\mathrm{CFB,FFprEN,R}}$ is calculated as in EC3-1-8. Joint initial stiffness:

$$S_{\mathrm{j,ini,prEN}} = E\, z_{\mathrm{b}}^2 \left(k_{\mathrm{CWS,prEN}}^{-1} + k_{\mathrm{CWC,prEN}}^{-1} + k_{\mathrm{CWT,prEN}}^{-1} \right)^{-1}, \tag{60}$$

The joint secant stiffness $S_{j,sec,FFprEN}$ is 1/3 of the previous value.

3.2 CBFEM models

Besides the FE shell models, the steel connections are also modelled with the latest version (23) of IDEA StatiCa software, which is based on the so-called Component-Based Finite Element Method (CBFEM). In this chapter, the modelling assumptions, and the main model properties (e.g., geometry, mesh, loading, boundary conditions, etc.) considered are described, as well as the type of analysis used and the data extraction procedure.

3.2.1 Modelling and analysis using Python script

As the number of models and corresponding analyses for a statistically relevant amount of information is significant, in-house tailored Python scripts are developed for fast-track modelling, analysis, and result generation. Namely, the models are first created using the Python script that allows for parametric geometry definition with the so-called IDEA Open Model (IOM), and subsequently, the loading application and the model analysis are carried out using IDEA API.

3.2.2 Model definition

The Python script used to generate the IDEA Open Model (IOM) extracts all the geometrical and material information from an Excel file, as schematically shown in Figure 3.2 a). Geometry is defined using the member and operation tools, setting the column as a bearing member, and concretizing the joint between the beam and the column with a "cut of member" operation. For all the models, full-penetration butt welds are considered, hence eliminating their influence on joint resistance. Once the IDEA Open Model geometry is created, IDEA API is called to generate an IDEA Connection file, Figure 3.1(b).

3.2.3 Material properties

For both columns and beams, the material properties are selected from IDEA StatiCa libraries. The materials adopted are S275 for columns and S235, S275, S355, S460, and S690 for beams. The material model adopted is elastoplastic (for engineering stress and strain) with a nominal yielding plateau slope $E/1000$; it is worth mentioning that EN 1993-1-5 (CEN, 2006) in its annex C contemplates this material model, indicating "$E/10000$ or a similarly small value" for the post-yield tangent stiffness.

3.2.4 Load application

Like FEM models, the loads applied in IDEA are obtained from equilibrium equations using the option 'Loads in Equilibrium', leading to single support at the bottom of the column. This

is achieved using IDEA API, as presented in Figure 3.1. The applied bending moment and the shear forces are adapted to be equal to the corresponding joint resistance values, calculated from EN 1993-1-8:2010.

3.2.5 Mesh

Two different meshes are considered:

- ***'default'***: with 12 finite elements along the longest member plate (web or flange), with a minimal size of the element of 8 mm and a maximum size of 50 mm.
- ***'refined'***: with 24 FE along the longest cross-section plate, whereas the minimum and the maximum size are kept at 4 mm and 25 mm, respectively. The mesh is controlled using the setup options as shown in Figure 3.3.

3.2.6 Joint configurations

The joint configurations are those included in the numerical study, described in the following sections of this report. For every combination of column and beam one joint was generated as presented in Figure 3.4.

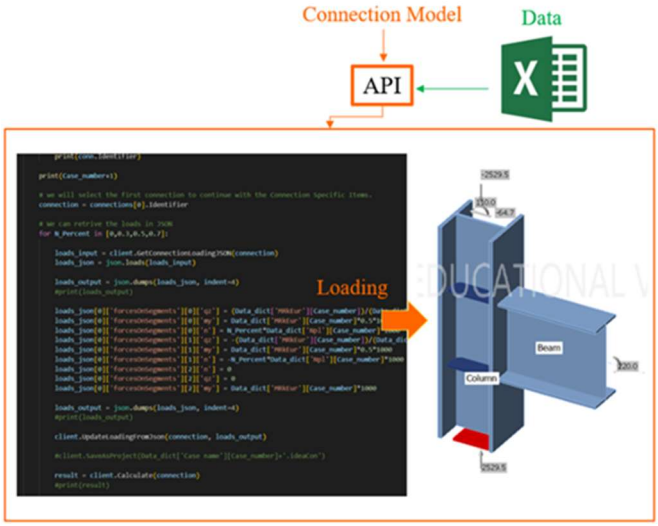

Figure 3.1 API Python Scripting - Loading of the joint.

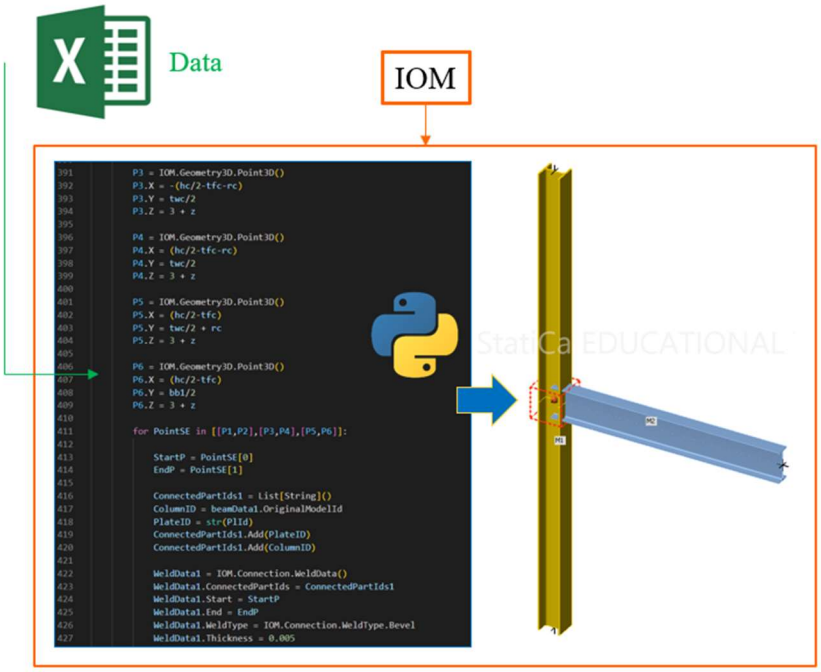

(a)

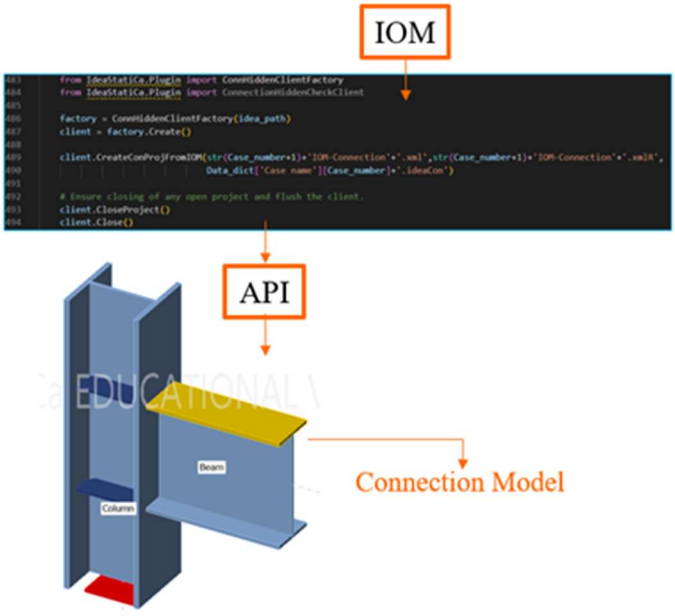

(b)

Figure 3.2 Python Scripting: a) IOM model; b) API - Connection Model Generation.

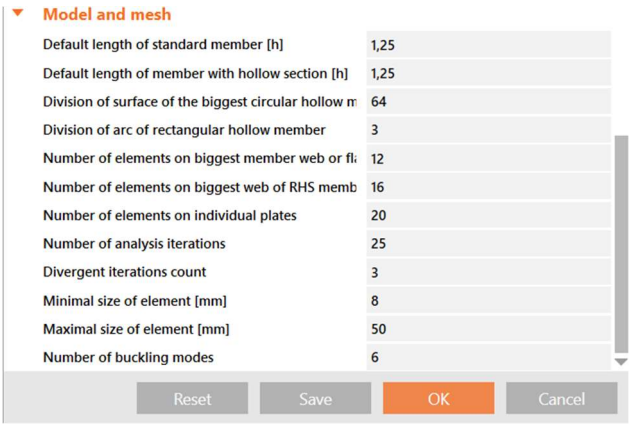

Figure 3.3 Mesh control in IDEA StatiCa.

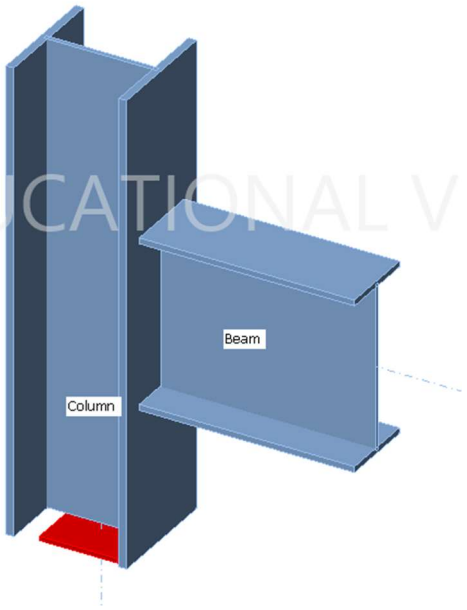

Figure 3.4 IDEA Connection one-sided unstiffened

3.2.7 Type of analysis

For all models, two types of analysis are used:

- i) Design Resistance (DR), and
- ii) Stress-Strain (SS).

Both options are available in the software. No buckling analysis is performed.

The Design Resistance analysis returns the so-called *Applied Load Factor* (*ALF*) which represents the factor by which the applied load must be multiplied to obtain the joint design resistance. In this case, the design resistance is equal to the characteristic value, as no safety factors are considered. Once the moment resistance is obtained for each model, Stress-Strain Analysis is carried out, which gives a graphical interpretation of the Von Mises stress distribution (i.e. equivalent stress). For all the analyses the stopping criterion is defined by the program, corresponding to 5% of the maximum equivalent plastic strain achieved at any point of the connection. An example is shown in Figure 3.5, where the stress distribution, the strain distribution, and the deformed shapes are presented for two different mesh sizes.

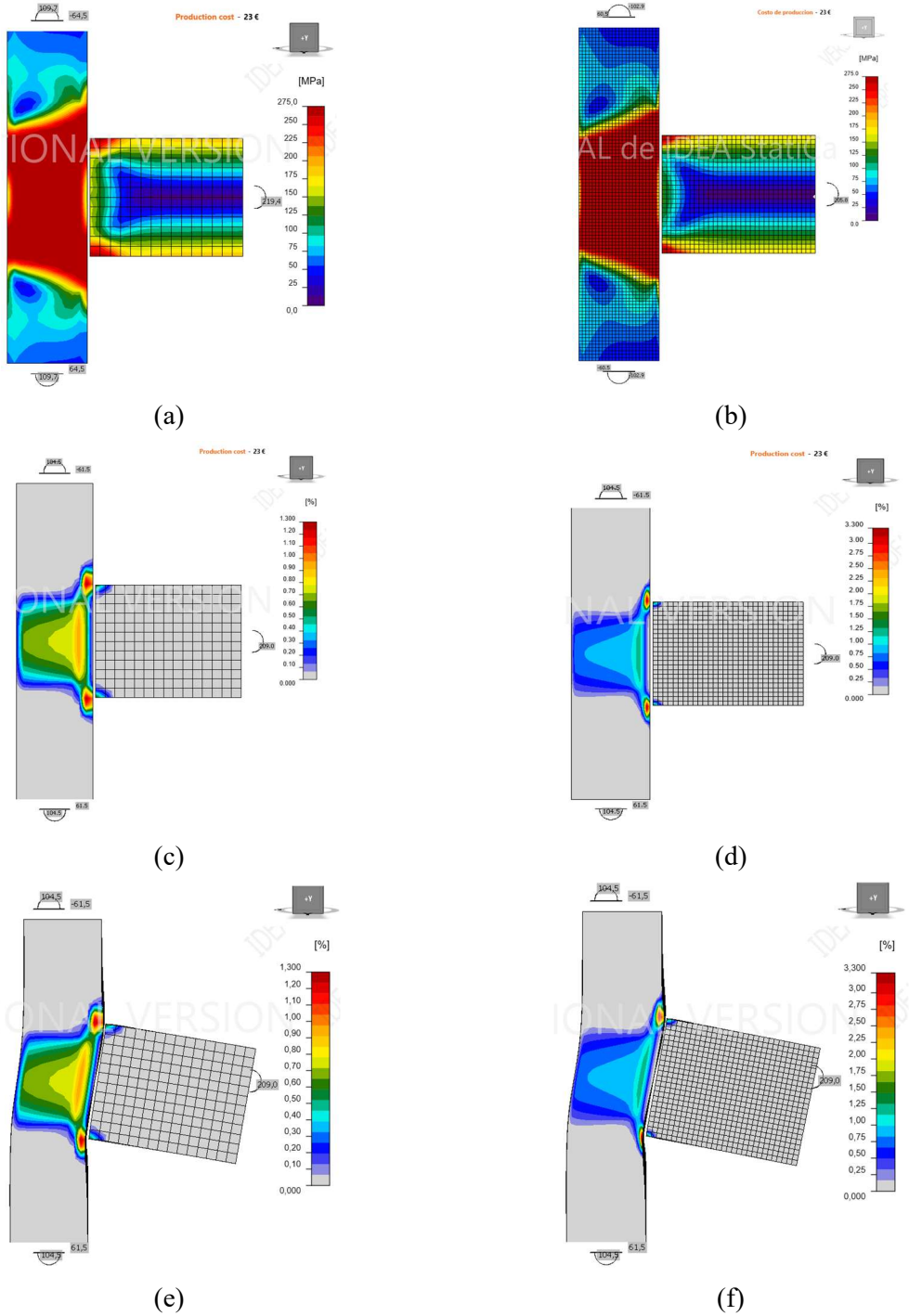

(a) (b)

(c) (d)

(e) (f)

Figure 3.5 Von Mises Stress distribution.

a) 'default' mesh; b) 'refined' mesh; Plastic Stress distribution: c) 'default' mesh; d) 'refined' mesh; Deformed shape: e) 'default' mesh; f) 'refined' mesh.

3.2.8 Geometrically non-linear analysis (GMNA)

For open sections, IDEA StatiCa version 23.0 does not implement by default geometrically non-linear analysis. Therefore, is not possible to create and run IS models with the API using this option.

However, it is possible to use the GMNA analysis by activating the developer version by adding the line *<add key="UserMode" value="16" />* to the file "IdeaConnection.exe.config", as shown in Figure 3.6, and selecting the option "GMNA for each connection" in Code setup, as shown in Figure 3.7.

```
<?xml version="1.0" encoding="utf-8"?>
<configuration>
  <appSettings>
  <add key="UserMode" value="16" />
  </appSettings>
  <startup>
    <supportedRuntime version="v4.0" sku=".NETFramework,Version=v4.8" />
  </startup>
  <runtime>
    <assemblyBinding xmlns="urn:schemas-microsoft-com:asm.v1">
      <dependentAssembly>
        <assemblyIdentity name="CommonServiceLocator" publicKeyToken="489b6accfaf20ef0" culture="neutral"
        <bindingRedirect oldVersion="0.0.0.0-2.0.5.0" newVersion="2.0.5.0" />
```

Figure 3.6 Developer version activation

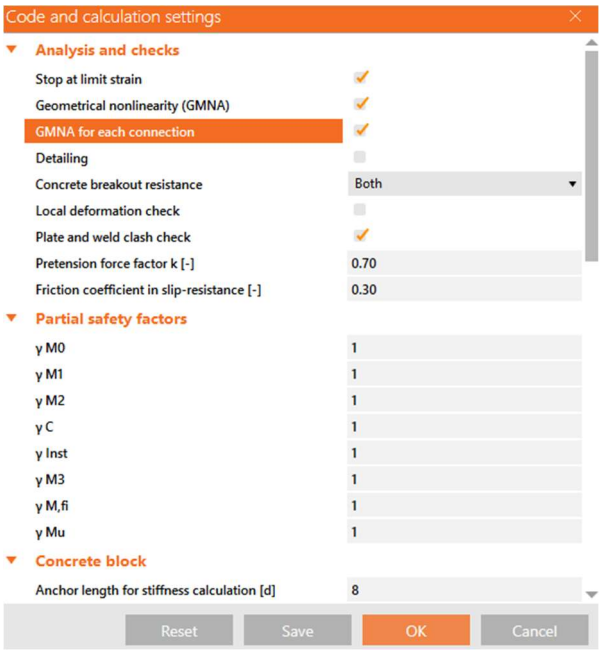

Figure 3.7 GMNA activation in IDEA StatiCa 23.0 Developer version.

3.2.9 Results extraction in case of axially loaded columns

In those cases where, besides bending moment, an additional axial force is applied at the column, it is important to highlight that in the Design Resistance analysis, the obtained Applied Load Factor ALF (i.e., load multiplier) corresponds to all applied loads in the connection (and not only bending moment). The consequence is that the final level of axial force cannot be controlled. Therefore, another approach to obtain the moment resistance was used, namely, for a given axial force acting on the column, the objective is to maintain the force constant while increasing only the applied bending moment. To do so, in the Python script, an iterative procedure is introduced with the steps illustrated in Figure 3.8, as follows:

i) Analyse the connection to obtain the first ALF.
ii) Multiply only the moment acting on the connection by ALF and maintain the same axial force.
iii) Analyse again the connection to obtain a new ALF and store the product of the old and the new ALF as Load Factor (LF).
iv) Repeat 2 to 3 until the new ALF is not equal to 1.0.

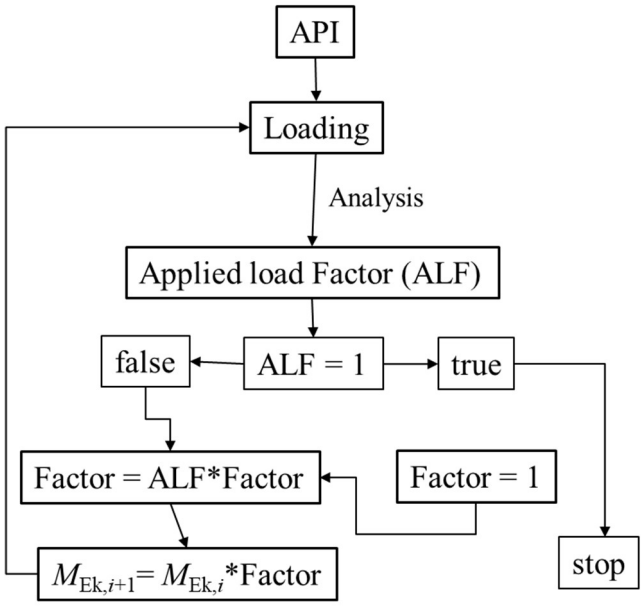

Figure 3.8 Algorithm implemented to obtain the real moment resistance.

3.2.10 Mesh size and Richardson extrapolation

FEM results are dependent on the mesh size. Generally, a coarser mesh has a spurious stiffening effect, which results in higher values of moment resistance and stiffness. Therefore, the mesh size is a variable of interest in the predicted response. In this study, two meshes are considered for each model:

i) the default IDEA StatiCa (v23) mesh, referred to as ISdef,
ii) a refined mesh, half the size of the former, therefore with 4 times the number of planar elements, referred to as ISref.

Values of moment resistance are obtained with both meshes. In addition, a third value is obtained using the Richardson extrapolation. A brief explanation follows (for simplicity, this is given for a unidimensional case, but the concept is directly applicable to multidimensional cases).

In the FE method, the displacement u is approximated by shape functions which are polynomials of order n. The n^{th} degree Taylor approximation $u_{\text{approx},n}$ to the displacement u at a point of coordinate x is given by:

$$u_{\text{approx},n}(x) = u(x_i) + \frac{u'(x_i)}{1!}(x - x_i) + \ldots + \frac{u^{n)}(x_i)}{n!}(x - x_i)^n, \tag{61}$$

where $x_i \leq x$. The exact value of displacement can be expressed as:

$$\begin{aligned} u(x) &= u(x_i) + \frac{u'(x_i)}{1!}(x - x_i) + \ldots + \frac{u^{n)}(x_i)}{n!}(x - x_i)^n + \frac{u^{n+1)}(x_0)}{(n+1)!}(x - x_i)^{n+1} = \\ &= u_{\text{approx},n}(x) + \frac{u^{n+1)}(x_0)}{(n+1)!}(x - x_i)^{n+1}, \end{aligned} \tag{62}$$

where $x_0 \leq x_i \leq x$. Therefore, the error e is:

$$e = u(x) - u_{\text{approx},n}(x) = \frac{u^{n+1)}(x_0)}{(n+1)!}(x - x_i)^{n+1} \approx \lambda(x - x_i)^{n+1}, \tag{63}$$

If a FEM mesh 1 of size s is used, the error e_1 for that mesh is of the order:

$$e_1 \approx \lambda(s)^{n+1}, \tag{64}$$

If a second mesh 2 is used, in which the size of the elements is s/d, the error is:

$$e_2 \approx \lambda(s/d)^{n+1}, \tag{65}$$

Therefore:

$$u - u_{approx}^{(1)} \approx \lambda(s)^{n+1}, \tag{66}$$

$$u - u_{approx}^{(2)} \approx \lambda(s/d)^{n+1}, \tag{67}$$

where u is the exact value of displacement, $u_{approx}^{(1)}$ is the approximation obtained with mesh 1, $u_{approx}^{(2)}$ and is the approximation obtained with mesh 2. Dividing both expressions:

$$\frac{u - u_{approx}^{(1)}}{u - u_{approx}^{(2)}} \approx \frac{\approx \lambda(s)^{n+1}}{\lambda(s/d)^{n+1}} = d^{n+1}, \tag{68}$$

whereupon:

$$u \approx \frac{u_{approx}^{(1)} - u_{approx}^{(2)} d^{n+1}}{1 - d^{n+1}}. \tag{69}$$

The previous expression allows for an estimate of any variable from the values obtained using two meshes. For this study, mesh 1 is the default IDEA StatiCa mesh (ISdef), and mesh 2 is the refined mesh (ISref), with halved element size, therefore $d = 2$. Eq. 69 can be rewritten in the following form:

$$M_{\mathrm{R,ISrich}} = \frac{4M_{\mathrm{R,ISref}}^{(2)} - M_{\mathrm{R,ISdef}}^{(1)}}{3}, \tag{70}$$

where $M_{\mathrm{R,ISdef}}$ is the moment resistance obtained with IDEA StatiCa using the default mesh, $M_{\mathrm{R,ISref}}$ is the moment resistance obtained with the refined mesh, and $M_{\mathrm{R,ISrich}}$ is the moment resistance estimated with the Richardson extrapolation.

3.3 Abaqus finite element shell models

The shell models created by IDEA StatiCa® and the code calculations are evaluated against virtually identical *shell* models built up in ABAQUS software. The most relevant features of the shell models (e.g. type of analysis, geometry, boundary and loading conditions, material properties, finite element (FE) type and size, imperfections, etc.) are described in the following paragraphs.

3.3.1 Geometry

Sophisticated numerical models were developed using the commercial FE software Abaqus© (Simulia, 2021). Both column and beam were simulated using extrusion shell elements. For each column, three different sections were considered. The first section, 'A', neglects the contribution of a thicker web-to-flange connection present in hot-rolled column profiles, defined by a radius *r*, see Figure 3.9 a) and therefore, does not have any change in CWP thickness along the web. The second section, 'B', tries to consider the contribution of the radius *r* by increasing the thickness of the web near the column web-to-flange connection, see Figure 3.9 b). Finally, the third section 'C' tries to consider the contribution of the radius *r* by adding two extra inclined shell elements in the column web-to-flange connection, see Figure 3.9 c).

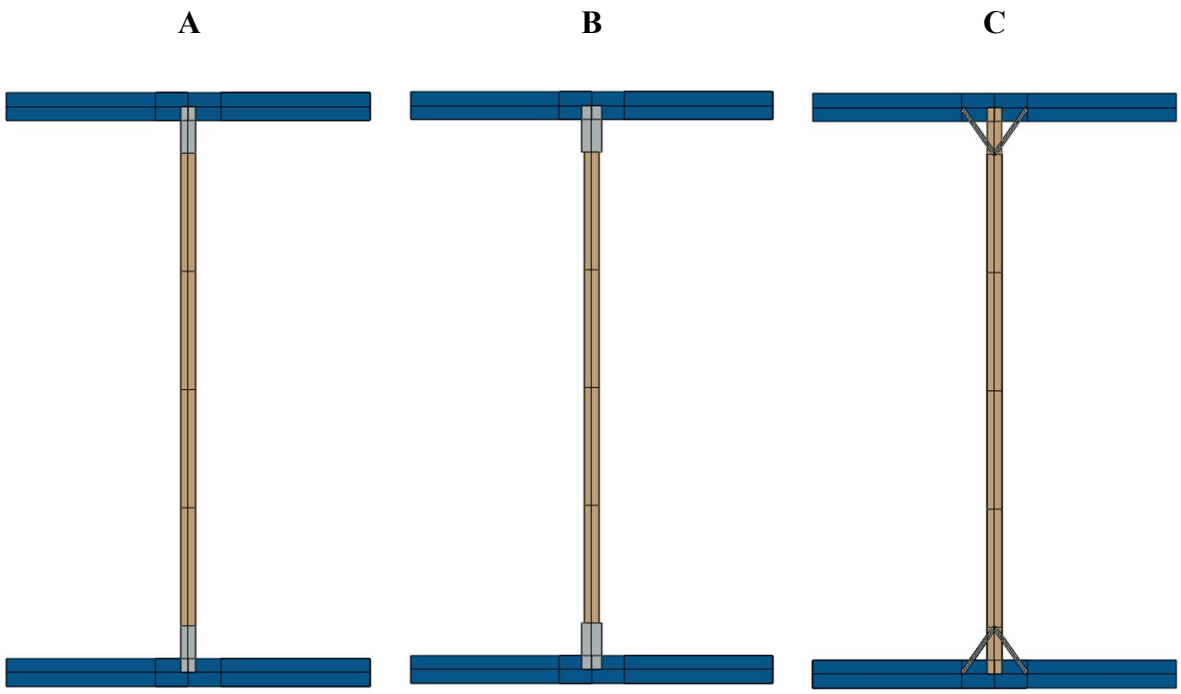

Figure 3.9 Shell FEM sections. a) Section 'A', neglecting radius; b) Section 'B', increase in web thickness; c) Section 'C', inclined elements.

Section 'A'

As previously referred, this section neglects the contribution of the column radius for resistance and stiffness and therefore has the same thickness along the column web. This geometry was considered to have a point of comparison for sections 'B' and 'C' and therefore, try to characterize the contribution of *r*. Also, it may be the simplest geometry possible and so may be common in day-to-day engineering practices.

Section 'B'

This section attempts to consider that the contribution of the column radius *r* is restricted to its effects on stress distribution in the root radius area. Therefore, an increase of thickness in the root-radius zone of the section is considered, see Figure 3.10.

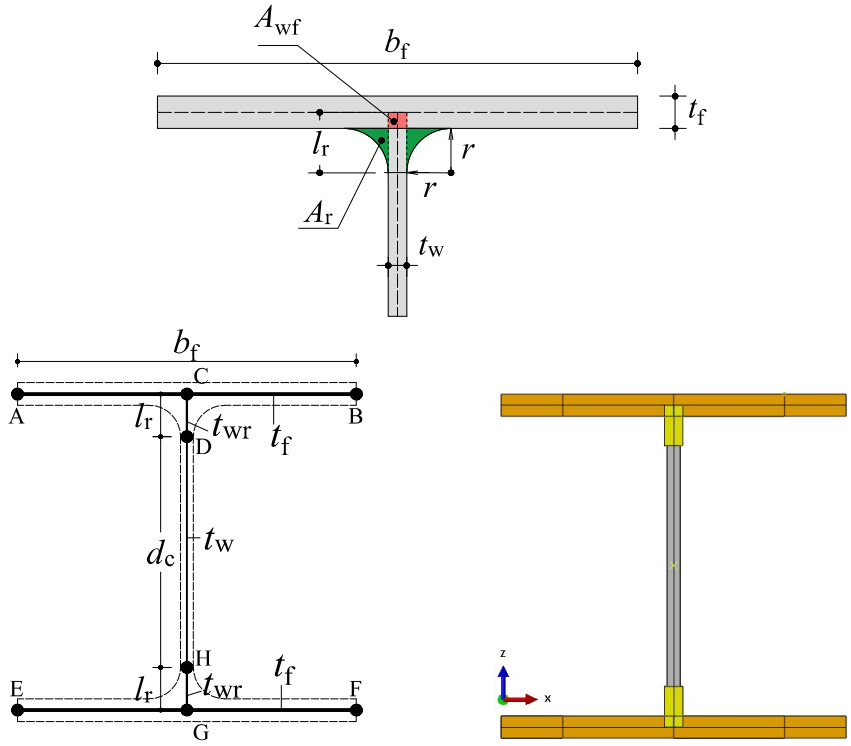

Figure 3.10 Radius modelling by web thickness increase.

The cross-section is divided into three parts.

i) **flanges AB and EF** – with the thickness t_f and the width b_f
ii) **mid-web DH** – with the thickness t_w and the width dc
iii) **web corners CD and GH** – with the thickness t_{wr} and the width l_r

Where t_{wr} is the corrected thickness of the web corners, obtained as:

$$t_{wr} = t_w + \frac{2A_r - A_{wf}}{l_r}, \tag{71}$$

Where A_r and A_{wf} are the areas indicated in Figure 3.10, obtained as:

$$A_r = r^2\left[1 - \frac{\pi}{4}\right] \approx 0.214r^2, \tag{72}$$

$$A_{wf} = \frac{t_f t_w}{2}, \tag{73}$$

And l_r is the length of the web corners, obtained as:

$$l_r = \frac{2r + t_f}{2}, \tag{74}$$

Section 'C'

This section attempts to consider that the contribution of the column radius *r* is related to the stress distribution in both column web and flanges and tries to avoid stress concentrations in the column web-to-flange connection zone, see Figure 3.11. Furthermore, as may be seen later in 'model validation', Jordão (2008) considered inclined elements to simulate fillet welds in beam-column welded connections for shell finite element models to consider the deformation in the 'block' of the connection. Then, the use of a similar solution for the column radius seems to be a reasonable approach.

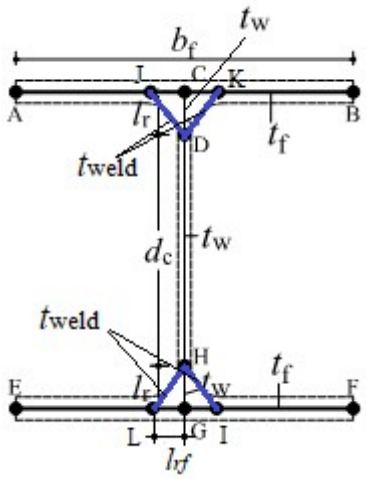

Figure 3.11 Section 'C'

Beyond the same cross-section divisions established in section 'B' adds 4 extra inclined elements: **Welds LH, IH, JD, and KD**. These elements have a thickness t_{weld} obtained as:

$$t_{weld} = \frac{A_r}{\sqrt{l_r^2 + l_{rf}^2}}, \tag{75}$$

$$l_{rf} = \frac{2r + t_w}{2} \tag{76}$$

3.3.2 Type of analysis

For this study, two types of analyses are performed: i) Linear elastic bifurcation (or eigenvalue) analysis (LBA) and ii) Geometrical and materially nonlinear analysis with imperfections included (GMNIA).

First, to generate the eigenmodes, the LBA is performed for each model, using the Lanczos algorithm available in Abaqus®. Subsequently, the extracted eigenmodes are used as the shapes of the initial geometrical imperfections in a GMNIA, in which the ultimate resistance of the joint is obtained, and its elastoplastic behaviour examined. For that purpose, the General static method from the software's library is used, which gives non-linear static equilibrium solutions. When GMNIA is performed, it is necessary to carefully define the arc-length parameters to avoid numerical issues and to fully grasp the spread of yielding of material in the post-critical regime.

The analysis is stopped automatically when the plastic strain at any point of the column exceeds 10%, whereas the ultimate moment resistance of a joint is determined by the value that is reached when the plastic strain reaches 5% to maintain coherence with the IS models.

3.3.3 Imperfections

Owing to the lack of information on the 'real' material and geometrical imperfections, the initial imperfections are modelled as the equivalent imperfections, following the recommendations from Annex C.5 of EN 1993-1-5 for flat plates. According to the standard, for the panels and subpanels, the shape of the initial imperfections should have a form of a critical eigenmode, with an amplitude equal to a minimum between a/200 and b/200. In the case of unstiffened web panels, the value of $d_c/200$ is adopted. The imperfection amplitudes for different column cross-sections belonging to the scope of the study cases in Chapter 4 may be seen in Table 3.2.

Table 3.2 Equivalent initial imperfection amplitudes (in mm).

	Columns	h_c	b_c	t_{wc}	t_{fc}	r_c	d_c	**imp**
C01	HE500A	490	300	12	23	27	390	**1.95**
C02	UC203x203x46	203.2	203.6	7.2	11	10.2	160.8	**0.80**
C03	HE280B	280	280	10.5	18	24	196	**0.98**
C04	HE140M	160	146	13	22	12	92	**0.46**
C05	UC305x305x240	352.5	318.4	23	37.7	15.2	246.7	**1.23**
C06	HE600x399	648	315	30	54	27	486	**2.43**
C07	HE800B	800	300	17.5	33	30	674	**3.37**

3.3.4 Applied material model

The material used in numerical models is steel grade S275 for columns, whereas for the beam different steel grades are considered (S235, S275, S355, S460, S690).

The theoretical elastic-perfectly plastic (EPPL) material law was selected, considering the converted true properties, as depicted in Figure 3.12. The Poisson's ratio υ and the Young's modulus of steel E were taken as 0.3 and 210 GPa, respectively.

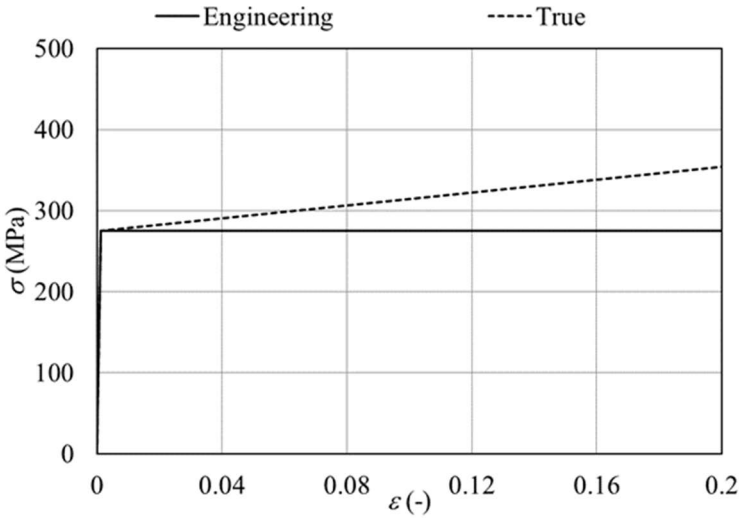

Figure 3.12 Elastic-perfectly plastic (EPPL) material law.

3.3.5 Loading and support conditions

The boundary conditions and the loads applied in the GMNIA analysis are presented in Figure 3.13 a) In the LBA analysis, whose purpose is to determine a critical imperfection shape of the web panel under study, additional displacement constraints are attributed (see Figure 3.13 b)), so that the global torsional eigenmodes, as well as the modes related to the buckling of the beam, are eliminated. In this Figure, the notations U1, U2, and U3 refer to the translations in X, Y, and Z direction respectively, whereas U4, U5, and U6 correspond to the respective rotations. The physical contact between the beam and column face is modelled using *tie constraint* line by line, see Figure 3.14.

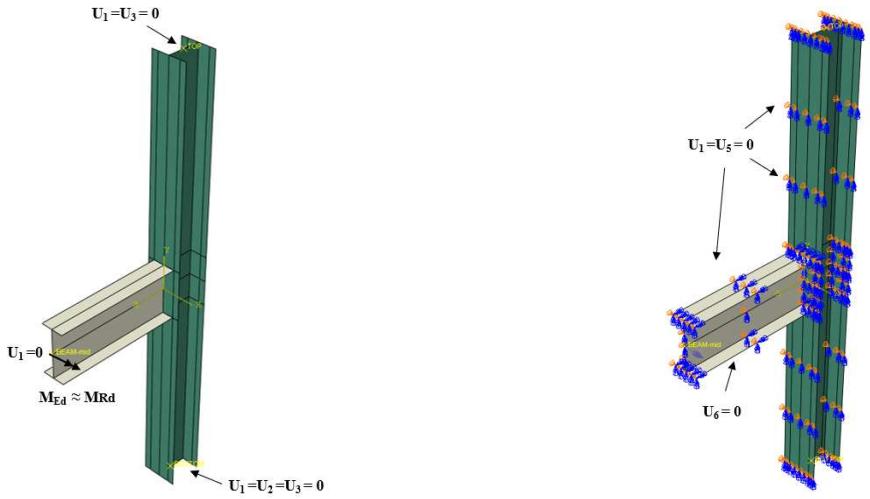

Figure 3.13 Loading and boundary conditions: a) GMNIA; b) LBA.

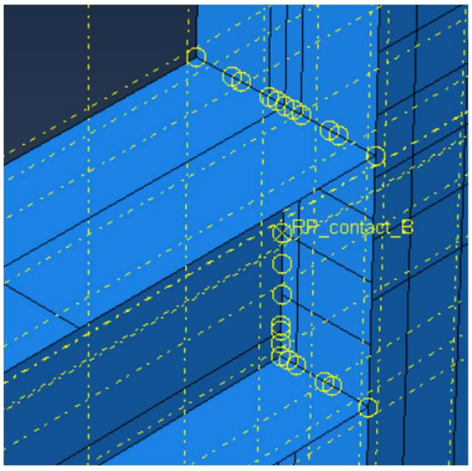

Figure 3.14 *Tie constraint* line by line

Regarding the loading, a concentrated bending moment is applied at the end of the beam with a magnitude slightly higher than the expected moment resistance of the connection, so that the analysis never stops before the ultimate resistance is reached. In addition, in some cases belonging to the scope of the study in Chapter 4, an axial force is applied on the top of the column, ($N_{Ed} = 0.5N_{pl}$), where N_{pl} is the plastic axial resistance of the column ($N_{pl} = A\,f_y$).

3.3.6 Finite element type and size

A linear four-node shell element with reduced integration (S4R) is used for the model discretization. S4R was chosen because it is the general-purpose conventional shell element provided by Abaqus® according to the ABAQUS Analysis User's Manual provided by

Washington University in St. Louis. (2009). Therefore, it seems to be educated for this study and may be expected to be the most widespread shell element used in common engineering practices.

The size of the finite elements is determined based on a convergence study using section 'A' (for the model E1.2 from Jordão (2008), see chapter 3.3.7 validation), in which besides the moment resistance of the joint, the moment at which 5% plastic strain occurs is monitored. Some of the results are presented in Figure 3.15 in which moment-rotation curves for three different mesh sizes are compared (15x15mm^2, 10x10mm^2, and 5x5mm^2).

All three mesh configurations lead to a similar failure mode, see Figure 3.15, however, it may be noticed that the increased FE leads to an increase in bending resistance and a delayed occurrence of the 5% plastic strain. However, as may be seen in Table 3.3 the difference in moment resistance based on the 5% plastic strain criterion is smaller than 5% between meshes, which may be considered small in this study, so then, a 10 mm mesh could be considered sufficient to achieve numerical convergence with acceptable CPU time consumption.

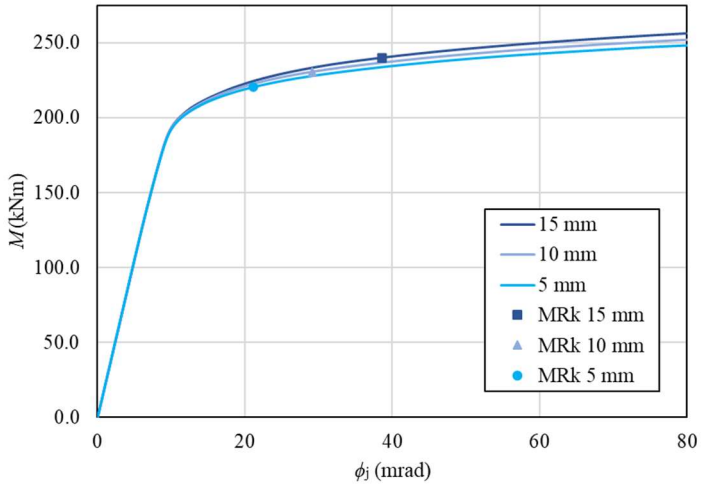

Figure 3.15 Mesh sensitivity analysis moment-rotation curves.

Table 3.3 Moment-resistance difference between meshes.

15 mm	10 mm	5 mm	15 to 10	15 to 5	10 to 5
	M_{Rk} (kNm)			ΔM_{Rk} (%)	
239.9	230.5	220.3	3.9	8.2	4.4

Additionally, as may be seen in Figure 3.15, almost no difference may be found for initial stiffness between meshes. These conclusions coincide with the ones referred by Jordão (2008) about the influence of FE increment in shell FEM.

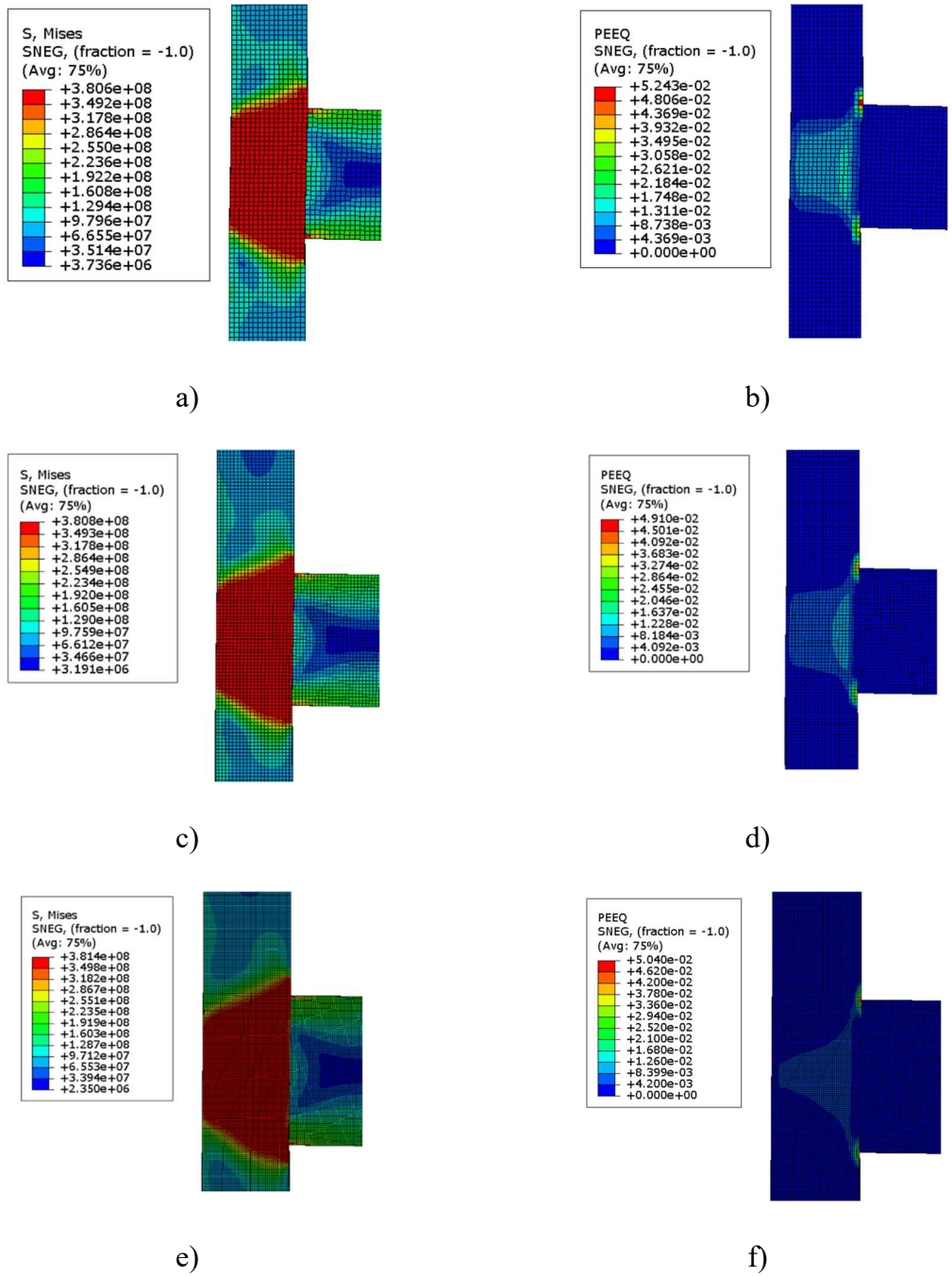

Figure 3.16 Failure modes for model E2 from Jordão (2008). a) Von Mises stress 15 mm mesh; b) Plastic equivalent strain 15 mm Mesh; c) Von Mises stress 10 mm mesh; d) Plastic equivalent strain 10 mm Mesh; e) Von Mises stress 5 mm mesh; f) Plastic equivalent strain 5 mm Mesh.

3.3.7 Model validation

The FE models were validated against experimental data, namely two welded joints from Jordão (2008). The experiments consisted of one-sided welded joints submitted to negative bending

moment and without axial load applied in the column. The geometrical properties of the joints for validation may be seen in Table 3.4.

Table 3.4 Geometry of Jordão (2008) joints E1.1 and E1.2 selected for validation.

Author	Test	Member	h (mm)	b (mm)	t_w (mm)	t_f (mm)	r (mm)	L (mm)	a_f (mm)	a_w (mm)
Jordão (2008)	S355 E1.1	Col HEB240	245.4	242.3	10.4	16.5	21	3000	-	-
		Beam IPE400	404.3	179.5	8.8	12.8	21	1300	16.0	-
	S355 E1.2	Col HEB240	246.0	241.4	10.6	16.8	21	3000	-	-
		Beam IPE400	406.8	179.1	9.1	13.1	21	1300	16.0	5.0

The measured material properties for tests S355 E1.1 and S355 E1.2 are reported in (Jordão, 2008). Figure 3.17 presents the true properties of the above-mentioned experimental tests.

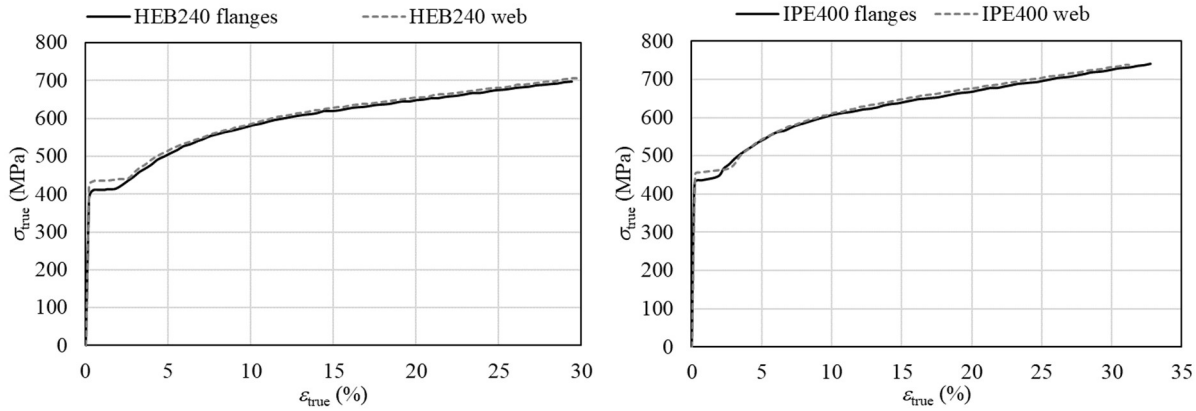

Figure 3.17 Material properties for tests from Jordão.

The models considered in Chapter 4 for the scope of the study use full blend welds to simplify the analysis avoiding the consideration of the welds for moment resistance among other magnitudes. Therefore, a line-to-line *tie constraint* could be considered adequate to represent the welds in a shell model. However, models E1.1 and E1.2 from Jordão (2008) use fillet welds for the connection, and therefore, a 'block' deformation in the contact area between the beam and the column appears and may have a non-neglective effect on the joint behaviour. So then, through the same logic used for section type 'C', inclined elements were included to simulate the welds, see Figure 3.18. The thickness of such elements was calculated due to equations. 75 and 76 considering that A_r is equal to the lateral area of the weld, see Figure 3.19.

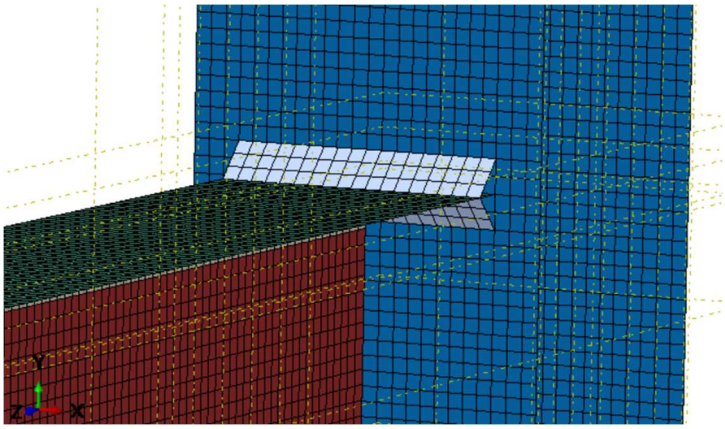

Figure 3.18 Use of inclined elements to simulate fillet welds.

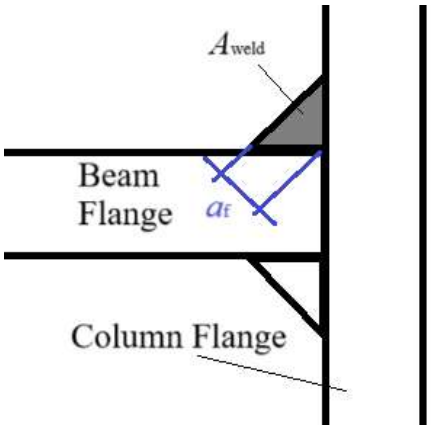

Figure 3.19 Weld lateral area.

It is important to highlight that the fillet welds between the beam web and the column flange were not modelized since model E1.1 does not have that weld and, for model E1.2, the thickness of the weld was 5 mm, therefore, it was considered that the 'block' effect may be neglected.

The use of inclined elements to simulate the welds in shell FEM was also the solution adopted by Jordão (2008).

The initial imperfections were considered as referred to in 3.3.3, For all validation models, the deformed shapes resultant of the buckling analysis may be seen in Figure 3.20 and the eigenvalues are presented in Table 3.5.

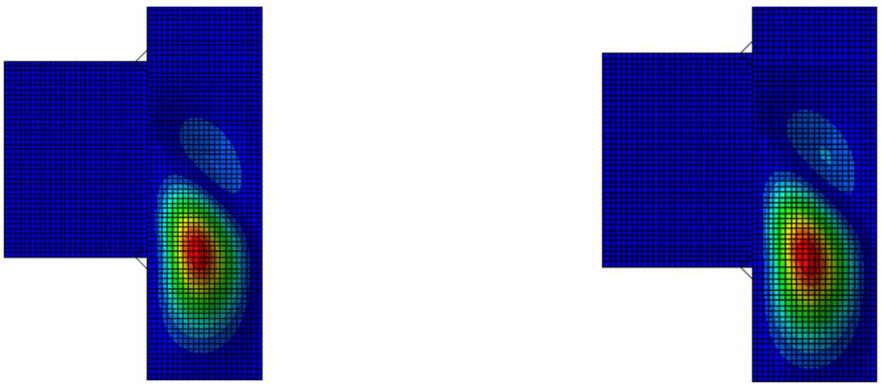

a) b)

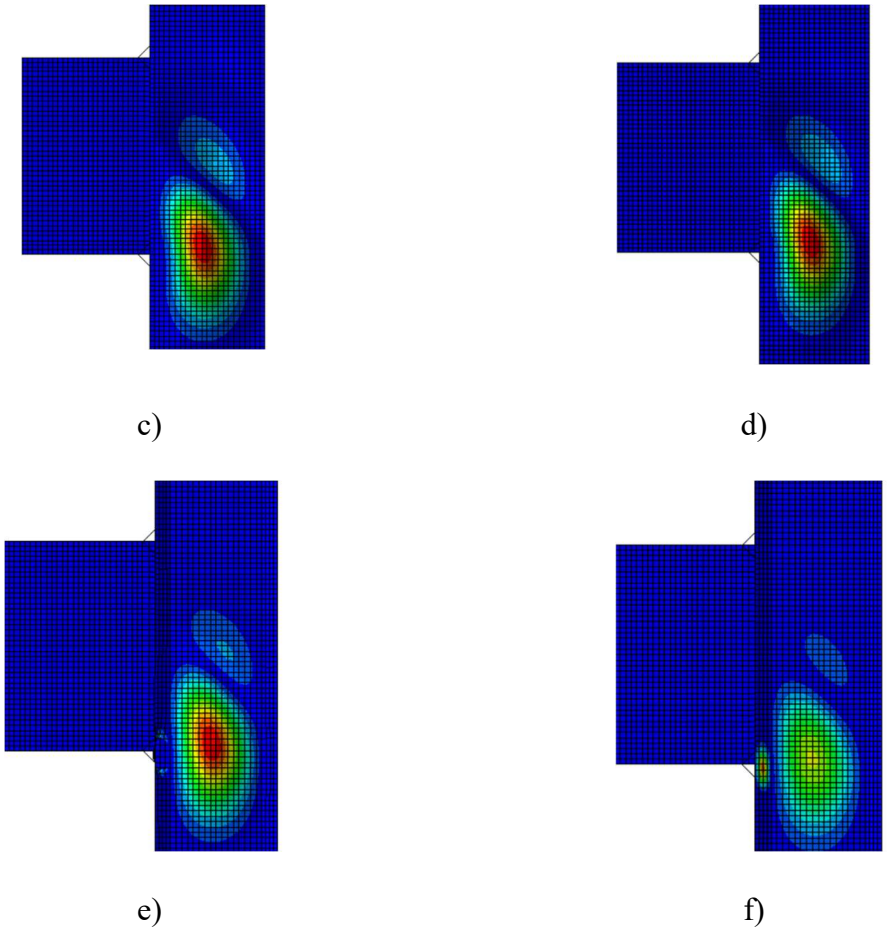

Figure 3.20 Initial geometric imperfections for FE shell models. a) E1.1 section ‘A’; b) E1.2 section ‘A’; c) E1.1 section ‘B’; d) E1.2 section ‘B’; e) E1.1 section ‘C’; f) E1.2 section ‘C’

Table 3.5 Eigenvalues

Eigenvalues					
Section 'A'		**Section 'B'**		**Section 'C'**	
E1.1	E1.2	E1.1	E1.2	E1.1	E1.2
5.3	5.7	6.7	7.1	6.9	7.1

As may be seen in Table 3.5, despite a similar buckle deformed shape, the eigenvalues for models with section ‘A’ are smaller than the values for sections ‘B’ and ‘C’. Therefore, it seems to be that neglecting the effect of the column radius leads to a more susceptible joint to buckling phenomena.

The load-deflection curves that correlate the displacement on the tip of the beam (*d*) and the applied moment were obtained for each model and compared with the experimental data, see

Figure 3.21. The max moment achieved for each joint was also obtained, see Figure 3.21, Table 3.6 and Table 3.7.

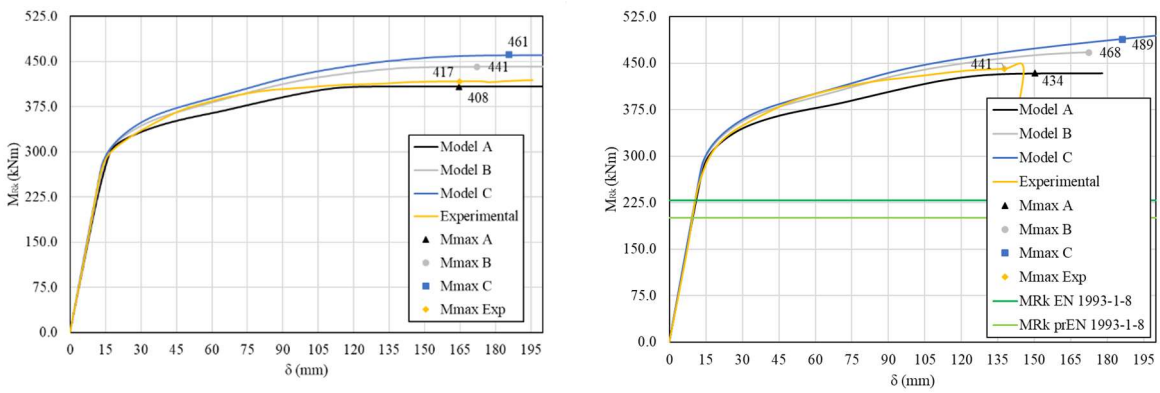

a) b)

Figure 3.21 Moment-displacement curves. a) model E1.1; b) model E1.2.

Table 3.6 Maximum moment for E1.1

M_{max} (kNm)				ΔM_{max} (%)			
A	**B**	**C**	**Exp**	**A-Exp**	**B-Exp**	**C-Exp**	**B-C**
408	441	461	417	-2.1	5.9	10.6	4.5

Table 3.7 Maximum moment for E1.2

M_{max} (kNm)				ΔM_{max} (%)			
A	**B**	**C**	**Exp**	**A-Exp**	**B-Exp**	**C-Exp**	**B-C**
434	468	489	441	-1.6	6.0	10.8	4.5

As may be seen in Figure 3.21 results in terms of initial stiffness, resistance, and deformation seem to be similar between the FE models and the experimental data. Despite a difference between 6 and 11% in the maximum moment achieved the overall behaviour of the joint sems to be well captured, given the uncertainties from the experimental test.

In addition, the major differences between the numerical and experimental results for models C and B are achieved at beam displacements higher than 75 mm, which may be considered a highly deformed joint shape. Calculating by linear interpolation the moment predicted by the models at the higher deformation for experimental data (maximum experimental moment) the difference for model E1.2 (in model E1.2 the beam is welded to the column along his entire

section, including the web of the beam. The joints analysed for parametric study in chapter 4 have the same type of connection) are smaller, below 6%.

Table 3.8 Moment at the experimental test maximum beam displacement.

M_{maxExp} (kNm)				ΔM_{maxExp} (%)			
A	**B**	**C**	**Exp**	**A-Exp**	**B-Exp**	**C-Exp**	**B-C**
433	458	467	441	-1.9	3.8	5.9	2.0

Finally, the true deformed shape of test E1.1 and E1.2 seem to be like the deformed shape of the numerical models, see Figure 3.22 and Figure 3.23.

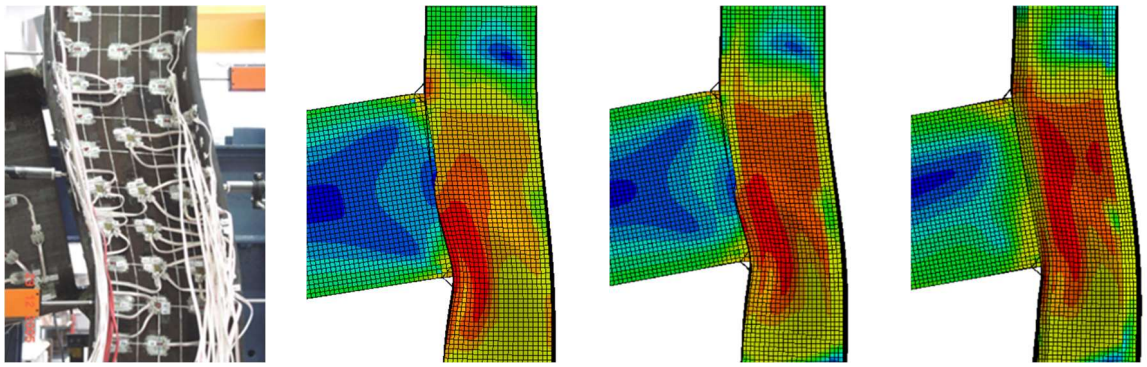

a) b) c) d)

Figure 3.22 Deformed shapes. a) Experimental test E1.1 from Jordão (2008); b) Model A; c) Model B; d) Model C.

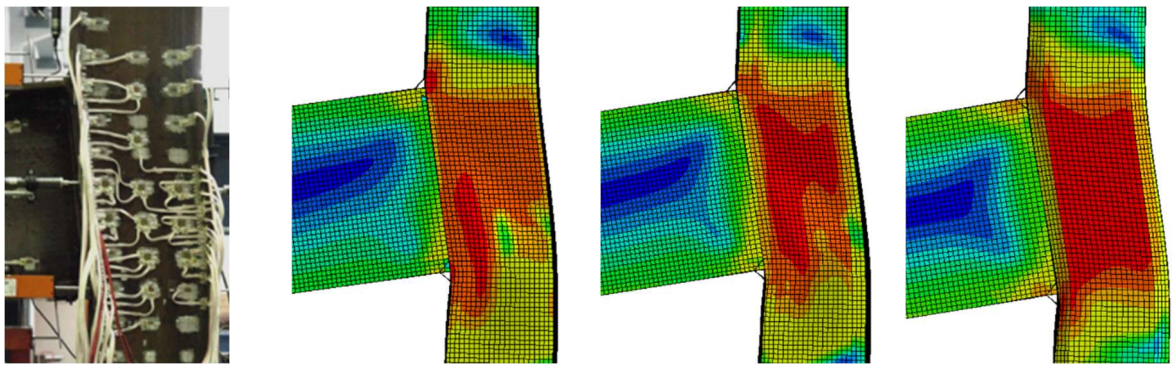

a) b) c) d)

Figure 3.23 Deformed shapes. a) Experimental test E1.2 from Jordão (2008); b) Model A; c) Model B; d) Model C.

3.3.8 Python scripting

In a similar way to the one used for CBFEM models, all Abaqus® FEM models were created, run, monitoring and their results were saved using Python scripts due to the amount of data to be processed for the parametric study. Five scripts were created respectively for:

- Create the model geometry and the buckling analysis *Abaqus_API_SHELL_Joints_Step01_Model_Generator*.
- Running the buckling analysis *Abaqus_API_SHELL_Joints_Step02_Buckle_Run*.
- Creating the static general analysis introducing the imperfection from the buckle analysis ODB file *Abaqus_API_SHELL_Joints_Step03_Static_Analysis_Creation*.
- Run the static general analysis and monitor the plastic strain on the CWP until it reaches the strain limit (10%) *Abaqus_API_SHELL_Joints_Step04_Static_Run.*
- Read the static analysis ODB file and save the data relatively the average displacement of the beam top and bottom, plastic strain in every division of the column, and the applied moment *Abaqus_API_SHELL_Joints_Step05_Results_Read*.

All python scripts read all the geometrical and material information from a text file *Case_Data.*

In addition, 5 sets were created dividing the column profile in 5 areas. Following:

- **S2FL** back flanges of the beam.
- **S1FL** front flanges of the beam.
- **S2RR** back column radius area.
- **S1RR** front column radius area.
- **WP** column web panel
- **Beam 1** beam of the join.

This division may be schematically seen in Figure 3.24.

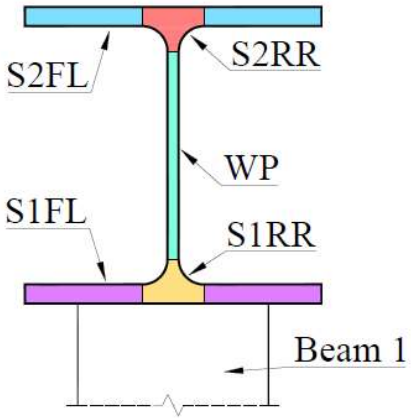

Figure 3.24 Division of the column profile in 5 areas.

4 PARAMETRIC STUDY

In this chapter, a set of different joints is analysed using the 3 methods referred to in Chapter 3. The study is focused on the moment resistance according to the 5% plastic strain criteria and the initial stiffness. In addition, the moment-rotation curve for every model was generated using the FEM results.

4.1 Scope of the study

The study encompasses welded beam-to-column moment-resisting joints between I and H-shaped hot-rolled open-section profiles. Seven different columns were chosen aiming to have a sample that could be representative of the different columns used in common engineering practices, see Table 4.1. This choice was made considering two magnitudes: the shear capacity of the CWP and the column slenderness (see Eq. 77) which may be considered as an important factor due to its influence in the buckling of the web.

Table 4.1 Columns chosen for the parametric study.

	Columns	h_c	b_c	t_{wc}	t_{fc}	r_c	d_c	d_c/t_{wc}	A_{vz}
C01	HE500A	490	300	12	23	27	390	32.50	74.7
C02	UC203x203x46	203.2	203.6	7.2	11	10.2	160.8	22.33	17.0
C03	HE280B	280	280	10.5	18	24	196	18.67	41.1
C04	HE140M	160	146	13	22	12	92	7.08	24.5
C05	UC305x305x240	352.5	318.4	23	37.7	15.2	246.7	10.73	85.85
C06	HE600x399	648	315	30	54	27	486	16.20	213.6
C07	HE800B	800	300	17.5	33	30	674	38.51	161.8

$$\lambda_{wp} = d_c / t_{wc}, \tag{77}$$

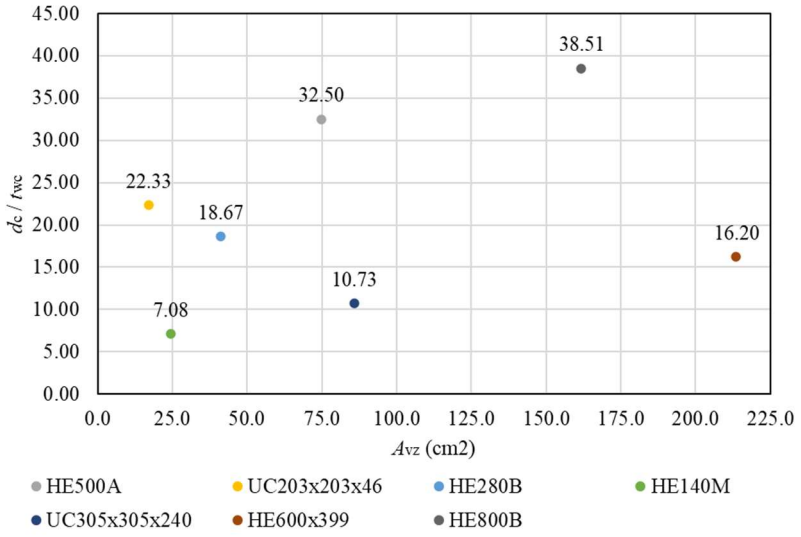

Figure 4.1 Columns slenderness and shear resistance of the CWP.

Based on the 7 columns, two sets of 20 one-sided internal joints were created to have a representative sample of joint aspect ratios, namely:

- **SET01** Unstiffened joint without axial force.
- **SET02N50** Unstiffened joint with an axial force of 50% of the axial plastic resistance of the column.

The geometrical characteristics of the joints may be seen in Table 4.2.

Table 4.2 Joints configuration and geometrical characteristics

nº	Column	Beam	*f*yc (MPa)	*f*yb (MPa)	zb1/*d*c	dc/twc	Lc (m)	Lb (m)
1	HE500A	HE400B	S275	S275	0.964	32.5	3.40	1.00
2	HE500A	HE600A	S275	S275	1.449	32.5	3.59	1.48
3	HE500A	HE800B	S275	S235	1.967	32.5	3.80	2.00
4	UC203x203x46	HE160A	S275	S235	0.887	22.4	3.15	0.38
5	UC203x203x46	IPE240	S275	S275	1.428	22.4	3.24	0.60
6	UC203x203x46	IPE330	S275	S235	1.976	22.4	3.33	0.83
7	HE280B	HE200B	S275	S275	0.944	18.7	3.20	0.50
8	HE280B	IPE300	S275	S355	1.476	18.7	3.30	0.75
9	HE280B	IPE400	S275	S275	1.972	18.7	3.40	1.00
10	HE140M	HE100B	S275	S460	0.978	7.1	3.10	0.25
11	HE140M	HE140B	S275	S355	1.391	7.1	3.14	0.35
12	HE140M	IPE200	S275	S460	2.082	7.1	3.20	0.50
13	UC305x305x240	HE260B	S275	S355	1.023	10.3	3.26	0.65
14	UC305x305x240	HE360B	S275	S275	1.423	10.3	3.36	0.90
15	UC305x305x240	IPE500	S275	S460	2.041	10.3	3.50	1.25
16	HE600x399	HE450M	S275	S355	0.901	16.2	4.48	1.20
17	HE600x399	HE700M	S275	S275	1.391	16.2	4.72	1.79
18	HE600x399	HE1000M	S275	S275	1.992	16.2	5.01	2.52
19	HE800B	HE700B	S275	S275	0.991	38.5	4.70	1.75
20	HE800B	HE1000B	S275	S275	1.430	38.5	5.00	2.50

The name for each model was created based on:

0001-S-I-fy275-HE500A-AR103-N00

The first two numbers represent the number of the set, and the second two numbers represent the number of the joint, I belong to ‘internal’ followed by the yield strength of the steel of the column, the name of the profile of the column, the aspect ratio ‘AR’ and the axial force applied (referred in the percentage of the column plastic resistance 0 or 50%). The names of the models may be seen in Table 4.3.

Table 4.3 Names attributed to the models.

nº	SET01	SET02N50
1	0001-S-I-fy275-HE500A-AR103-N00	0201-S-I-fy275-HE500A-AR103-N50
2	0002-S-I-fy275-HE500A-AR151-N00	0202-S-I-fy275-HE500A-AR151-N50
3	0003-S-I-fy275-HE500A-AR205-N00	0203-S-I-fy275-HE500A-AR205-N50
4	0004-S-I-fy275-UC203x203x46-AR094-N00	0204-S-I-fy275-UC203x203x46-AR094-N50
5	0005-S-I-fy275-UC203x203x46-AR149-N00	0205-S-I-fy275-UC203x203x46-AR149-N50
6	0006-S-I-fy275-UC203x203x46-AR205-N00	0206-S-I-fy275-UC203x203x46-AR205-N50
7	0007-S-I-fy275-HE280B-AR102-N00	0207-S-I-fy275-HE280B-AR102-N50
8	0008-S-I-fy275-HE280B-AR153-N00	0208-S-I-fy275-HE280B-AR153-N50
9	0009-S-I-fy275-HE280B-AR204-N00	0209-S-I-fy275-HE280B-AR204-N50
10	0010-S-I-fy275-HE140M-AR109-N00	0210-S-I-fy275-HE140M-AR109-N50
11	0011-S-I-fy275-HE140M-AR152-N00	0211-S-I-fy275-HE140M-AR152-N50
12	0012-S-I-fy275-HE140M-AR217-N00	0212-S-I-fy275-HE140M-AR217-N50
13	0013-S-I-fy275-UC305x305x240-AR110-N00	0213-S-I-fy275-UC305x305x240-AR110-N50
14	0014-S-I-fy275-UC305x305x240-AR152-N00	0214-S-I-fy275-UC305x305x240-AR152-N50
15	0015-S-I-fy275-UC305x305x240-AR211-N00	0215-S-I-fy275-UC305x305x240-AR211-N50
16	0016-S-I-fy275-HE600x399-AR098-N00	0216-S-I-fy275-HE600x399-AR098-N50
17	0017-S-I-fy275-HE600x399-AR147-N00	0217-S-I-fy275-HE600x399-AR147-N50
18	0018-S-I-fy275-HE600x399-AR207-N00	0218-S-I-fy275-HE600x399-AR207-N50
19	0019-S-I-fy275-HE800B-AR104-N00	0219-S-I-fy275-HE800B-AR104-N50
20	0020-S-I-fy275-HE800B-AR148-N00	0220-S-I-fy275-HE800B-AR148-N50

4.2 Results presentation

Through the FEM, three main outputs are generated for each model: the buckling shape, Von Mises stress distribution, and plastic equivalent strain. Considering as an example case 1 from SET01 and SET02N50 these results are presented in Figures 4.2 and 4.3 considering model C.

Through the FEM, three main outputs are generated for each model: the buckling shape, Von Mises stress distribution, and plastic equivalent strain. Considering as an example case 1 from SET01 and SET02N50 these results are presented in Figures 4.2 and 4.3 considering model C.

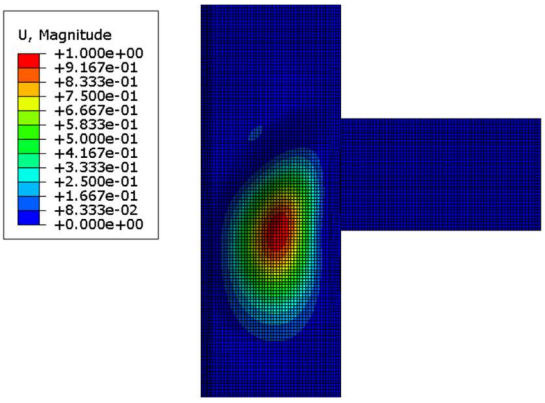

Figure 4.2 Buckling deformed shape for case nº1 of SET01 Model C.

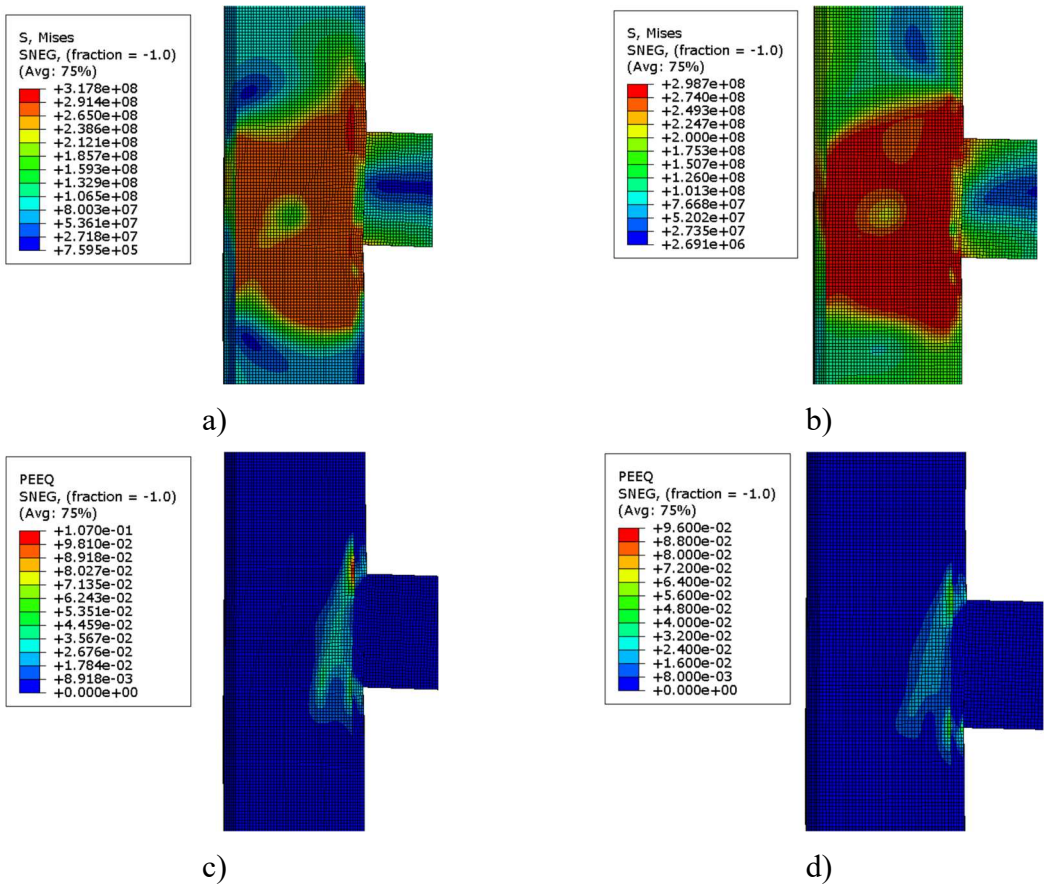

Figure 4.3 Case 1. a) Von Mises stress distribution SET01; b) Von Mises stress distribution SET02N50; c) Plastic equivalent strain SET01; d) Plastic equivalent strain SET02N50.

The moment-rotation and plastic strain-rotation curves were also generated for every case, see Figure 4.4. For every moment rotation curve additionally the secant and tangent stiffness is found as fractions of the initial stiffness and the element of the column where the 5% plastic strain was reached. Also, in the plastic-strain-rotation curve, 5 different curves are represented belonging to the divisions of the column profile following the division shown in Figure 3.24.

For case nº1 the 5% plastic strain was reached at the CWP, see Figure 4.4 c). Specifically, the highly plastified zone may be the connection between the top of the beam and the flange of the column, see Figure 4.3 c), which seems to indicate a CWT failure mode. On the other hand, both EN 1993-1-8 and FprEN 1993-1-8 indicate a CWC failure mode. However, for a better comparison, a more comprehensive study should be conducted to characterize the failure mode in the shell FEM which exceeds the objective of this study.

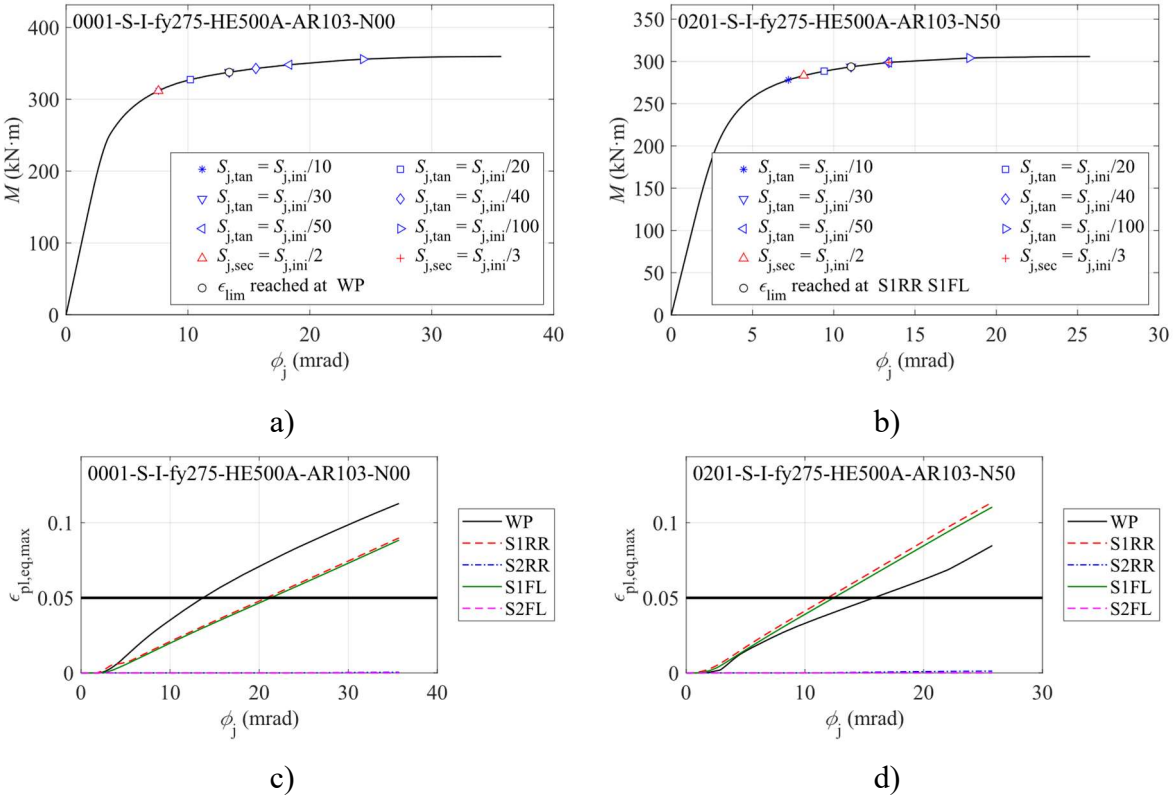

Figure 4.4 Case 1. a) Moment-rotation curve SET01; b) Moment-rotation curve SET02N50 c) Plastic strain-rotation curve SET01; b) Plastic strain-rotation curve SET02N50

4.3 Detailed Results

In this chapter, the results for moment resistance and initial stiffness are going to be presented in following the order:

- Moment-resistance comparison between shell FEM A, B, and C.
- Resume tables for moment-resistance including the results from all 3 methods for SET01 and SET02N50 and graphical comparison of the results.
- Initial Stiffness comparison between shell FEM A, B, and C.
- Resume tables for initial stiffness including the results from FEM and CM for SET01 and SET02N50.

4.3.1 Moment-resistance comparison between shell FEM A, B, and C.

The results for moment-resistance for all three shell FEM for SET01 and SET02N50 are presented and compared in Tables 4.4 and 4.5 respectively.

The moment resistances obtained for models A, B and C were compared between them. The statistical information such as mean, standard deviation, covariance, and maximum and minimum can be seen in Tables 4.6 and 4.7.

Table 4.4 Comparison between the moment resistance for SET01 by all shell FEM.

	M_R (kN·m)			$M_{R,i}$ / $M_{R,j}$		
	A	B	C	B/A	C/A	C/B
nº	[1]	[2]	[3]	[2]/[1]	[3]/[1]	[3]/[2]
1	296.3	332.5	337.7	1.12	1.14	1.02
2	492.6	531.6	539.3	1.08	1.09	1.01
3	719.9	762.7	773.4	1.06	1.07	1.01
4	32.3	33.5	36.3	1.03	1.12	1.08
5	53.2	55.1	58.7	1.03	1.10	1.07
6	75.8	77.0	82.2	1.02	1.08	1.07
7	93.0	109.1	111.1	1.17	1.19	1.02
8	146.5	168.3	171.4	1.15	1.17	1.02
9	197.5	222.6	222.6	1.13	1.13	1.00
10	49.0	41.8	49.8	0.85	1.02	1.19
11	61.8	55.2	63.8	0.89	1.03	1.16
12	85.7	78.2	87.2	0.91	1.02	1.12
13	399.9	335.2	406.7	0.84	1.02	1.21
14	540.4	460.6	553.2	0.85	1.02	1.20
15	759.9	661.8	780.9	0.87	1.03	1.18
16	1286.6	1001.8	1329.2	0.78	1.03	1.33
17	2071.6	1707.8	2172.7	0.82	1.05	1.27
18	3082.2	2677.1	3169.1	0.87	1.03	1.18
19	1058.6	1162.3	1179.6	1.10	1.11	1.01
20	1761.8	1937.3	1912.3	1.10	1.09	0.99

Table 4.5 Comparison between the moment resistance for SET02N50 by all shell FEM.

	M_R (kN·m)			$M_{R,i}$ / $M_{R,j}$		
	A	B	C	B/A	C/A	C/B
nº	[1]	[2]	[3]	[2]/[1]	[3]/[1]	[3]/[2]
1.00	262.6	288.5	293.7	1.10	1.12	1.02
2.00	442.0	473.1	480.9	1.07	1.09	1.02
3.00	650.3	693.1	693.1	1.07	1.07	1.00
4.00	28.1	28.7	30.7	1.02	1.09	1.07
5.00	48.2	49.1	51.2	1.02	1.06	1.04
6.00	68.7	70.0	72.5	1.02	1.05	1.04
7.00	79.9	88.0	90.0	1.10	1.13	1.02
8.00	126.4	138.8	141.9	1.10	1.12	1.02
9.00	174.5	187.1	191.3	1.07	1.10	1.02
10.00	37.6	33.3	39.0	0.89	1.04	1.17

11.00	49.6	44.5	51.6	0.90	1.04	1.16
12.00	69.1	63.1	71.9	0.91	1.04	1.14
13.00	325.0	284.2	338.6	0.87	1.04	1.19
14.00	446.0	397.2	465.5	0.89	1.04	1.17
15.00	640.8	570.8	668.8	0.89	1.04	1.17
16.00	1067.3	883.9	1093.5	0.83	1.02	1.24
17.00	1768.5	1525.9	1808.9	0.86	1.02	1.19
18.00	2648.1	2300.8	2706.0	0.87	1.02	1.18
19.00	963.5	998.1	1032.7	1.04	1.07	1.03
20.00	1573.7	1623.9	1674.0	1.03	1.06	1.03

Table 4.4.6 Statistics SET01 FEM moment resistance comparison.

	$M_{R,i}$ / $M_{R,j}$		
	B/A	**C/A**	**C/B**
Mean	0.984	1.078	1.107
Std	0.128	0.055	0.102
CoV	13.0%	5.1%	9.2%
Max	1.173	1.195	1.327
Min	0.779	1.016	0.987

Table 4.4.7 Statistics SET02N50 FEM moment resistance comparison.

	$M_{R,i}$ / $M_{R,j}$		
	B/A	**C/A**	**C/B**
Mean	0.977	1.064	1.096
Std	0.095	0.033	0.079
CoV	9.8%	3.1%	7.2%
Max	1.101	1.126	1.237
Min	0.828	1.022	1.000

4.3.2 Moment-resistance SET01 and SET02N50

The results corresponding to the moment resistance provided by both EN 1993-1-8 (CEN, 2005b), FprEN 1993-1-8 (CEN, 2023), IDEA StatiCa® default and refined meshes and Richardsson Extrapolation can be seen in Tables 4.8, 4.9 and 4.10 compared to the results of shell FEM with sections 'A', 'B' and 'C' respectively. As general tendency may be highlighted that CM results seem to be more conservative and CBFEM results seem to be less conservative compared with shell FEM without axial force (SET01).

Table 4.8 Moment resistance FEM section 'A', CM and CBFEM.

	M_R (kN·m)						M_R / $M_{R,FEM}$				
	FEM	**EN**	**FprEN**	**IS def**	**IS ref**	**IS rich**	**EN**	**FprEn**	**IS def**	**IS ref**	**IS rich**
n°	**[1]**	**[2]**	**[3]**	**[4]**	**[5]**	**[6]**	**[2]/[1]**	**[3]/[1]**	**[4]/[1]**	**[5]/[1]**	**[6]/[1]**
1	296.3	258.7	251.2	384.1	347.0	334.7	0.87	0.85	1.30	1.17	1.13
2	492.6	389.4	378.1	597.3	553.7	539.2	0.79	0.77	1.21	1.12	1.09
3	719.9	535.2	520.3	851.6	804.2	788.4	0.74	0.72	1.18	1.12	1.10
4	32.3	28.2	27.2	36.8	33.6	32.5	0.87	0.84	1.14	1.04	1.01
5	53.2	45.7	44.0	60.1	55.7	54.2	0.86	0.83	1.13	1.05	1.02
6	75.8	63.9	61.5	83.6	78.7	77.1	0.84	0.81	1.10	1.04	1.02
7	93.0	100.5	88.6	109.9	101.3	98.4	1.08	0.95	1.18	1.09	1.06

8	146.5	155.1	137.1	162.3	151.4	147.8	1.06	0.94	1.11	1.03	1.01
9	197.5	209.0	184.5	219.4	205.8	201.2	1.06	0.93	1.11	1.04	1.02
10	49.0	27.4	27.4	47.6	45.3	44.5	0.56	0.56	0.97	0.92	0.91
11	61.8	46.6	50.9	65.6	62.0	60.9	0.75	0.82	1.06	1.00	0.99
12	85.7	57.7	57.7	84.9	82.1	81.2	0.67	0.67	0.99	0.96	0.95
13	399.9	338.2	333.6	435.2	402.4	391.4	0.85	0.83	1.09	1.01	0.98
14	540.4	487.4	468.0	600.3	561.0	547.9	0.90	0.87	1.11	1.04	1.01
15	759.9	579.5	579.5	828.0	798.8	789.1	0.76	0.76	1.09	1.05	1.04
16	1286.6	1309.5	1266.1	1602.8	1514.1	1484.6	1.02	0.98	1.25	1.18	1.15
17	2071.6	2021.1	1954.0	2426.4	2331.6	2300.0	0.98	0.94	1.17	1.13	1.11
18	3082.2	2894.1	2798.1	3542.3	3429.2	3391.5	0.94	0.91	1.15	1.11	1.10
19	1058.6	864.2	850.6	1357.0	1255.7	1222.0	0.82	0.80	1.28	1.19	1.15
20	1761.8	1253.9	1235.1	2158.5	2047.5	2010.5	0.71	0.70	1.23	1.16	1.14

Table 4.9 SET01 Moment resistance FEM section ‘B’, CM and CBFEM.

	M_R (kN·m)						M_R / $M_{R,FEM}$				
	FEM	**EN**	**FprEN**	**IS def**	**IS ref**	**IS rich**	**EN**	**FprEn**	**IS def**	**IS ref**	**IS rich**
nº	**[1]**	**[2]**	**[3]**	**[4]**	**[5]**	**[6]**	**[2]/[1]**	**[3]/[1]**	**[4]/[1]**	**[5]/[1]**	**[6]/[1]**
1	332.5	258.7	251.2	384.1	347.0	334.7	0.78	0.76	1.16	1.04	1.01
2	531.6	389.4	378.1	597.3	553.7	539.2	0.73	0.71	1.12	1.04	1.01
3	762.7	535.2	520.3	851.6	804.2	788.4	0.70	0.68	1.12	1.05	1.03
4	33.5	28.2	27.2	36.8	33.6	32.5	0.84	0.81	1.10	1.00	0.97
5	55.1	45.7	44.0	60.1	55.7	54.2	0.83	0.80	1.09	1.01	0.98
6	77.0	63.9	61.5	83.6	78.7	77.1	0.83	0.80	1.08	1.02	1.00
7	109.1	100.5	88.6	109.9	101.3	98.4	0.92	0.81	1.01	0.93	0.90
8	168.3	155.1	137.1	162.3	151.4	147.8	0.92	0.81	0.96	0.90	0.88
9	222.6	209.0	184.5	219.4	205.8	201.2	0.94	0.83	0.99	0.92	0.90
10	41.8	27.4	27.4	47.6	45.3	44.5	0.65	0.65	1.14	1.08	1.06
11	55.2	46.6	50.9	65.6	62.0	60.9	0.84	0.92	1.19	1.12	1.10
12	78.2	57.7	57.7	84.9	82.1	81.2	0.74	0.74	1.09	1.05	1.04
13	335.2	338.2	333.6	435.2	402.4	391.4	1.01	1.00	1.30	1.20	1.17
14	460.6	487.4	468.0	600.3	561.0	547.9	1.06	1.02	1.30	1.22	1.19
15	661.8	579.5	579.5	828.0	798.8	789.1	0.88	0.88	1.25	1.21	1.19
16	1001.8	1309.5	1266.1	1602.8	1514.1	1484.6	1.31	1.26	1.60	1.51	1.48
17	1707.8	2021.1	1954.0	2426.4	2331.6	2300.0	1.18	1.14	1.42	1.37	1.35
18	2677.1	2894.1	2798.1	3542.3	3429.2	3391.5	1.08	1.05	1.32	1.28	1.27
19	1162.3	864.2	850.6	1357.0	1255.7	1222.0	0.74	0.73	1.17	1.08	1.05
20	1937.3	1253.9	1235.1	2158.5	2047.5	2010.5	0.65	0.64	1.11	1.06	1.04

Table 4.10 SET01 Moment resistance FEM section 'C', CM and CBFEM.

	M_R (kN·m)						M_R / $M_{R,FEM}$				
	FEM	EN	FprEn	IS def	IS ref	IS rich	EN	FprEn	IS def	IS ref	IS rich
nº	[1]	[2]	[3]	[4]	[5]	[6]	[2]/[1]	[3]/[1]	[4]/[1]	[5]/[1]	[6]/[1]
1	337.7	258.7	251.2	384.1	347.0	334.7	0.77	0.74	1.14	1.03	0.99
2	539.3	389.4	378.1	597.3	553.7	539.2	0.72	0.70	1.11	1.03	1.00
3	773.4	535.2	520.3	851.6	804.2	788.4	0.69	0.67	1.10	1.04	1.02
4	36.3	28.2	27.2	36.8	33.6	32.5	0.78	0.75	1.01	0.93	0.90
5	58.7	45.7	44.0	60.1	55.7	54.2	0.78	0.75	1.02	0.95	0.92
6	82.2	63.9	61.5	83.6	78.7	77.1	0.78	0.75	1.02	0.96	0.94
7	111.1	100.5	88.6	109.9	101.3	98.4	0.90	0.80	0.99	0.91	0.89
8	171.4	155.1	137.1	162.3	151.4	147.8	0.90	0.80	0.95	0.88	0.86
9	222.6	209.0	184.5	219.4	205.8	201.2	0.94	0.83	0.99	0.92	0.90
10	49.8	27.4	27.4	47.6	45.3	44.5	0.55	0.55	0.96	0.91	0.89
11	63.8	46.6	50.9	65.6	62.0	60.9	0.73	0.80	1.03	0.97	0.95
12	87.2	57.7	57.7	84.9	82.1	81.2	0.66	0.66	0.97	0.94	0.93
13	406.7	338.2	333.6	435.2	402.4	391.4	0.83	0.82	1.07	0.99	0.96
14	553.2	487.4	468.0	600.3	561.0	547.9	0.88	0.85	1.09	1.01	0.99
15	780.9	579.5	579.5	828.0	798.8	789.1	0.74	0.74	1.06	1.02	1.01
16	1329.2	1309.5	1266.1	1602.8	1514.1	1484.6	0.99	0.95	1.21	1.14	1.12
17	2172.7	2021.1	1954.0	2426.4	2331.6	2300.0	0.93	0.90	1.12	1.07	1.06
18	3169.1	2894.1	2798.1	3542.3	3429.2	3391.5	0.91	0.88	1.12	1.08	1.07
19	1179.6	864.2	850.6	1357.0	1255.7	1222.0	0.73	0.72	1.15	1.06	1.04
20	1912.3	1253.9	1235.1	2158.5	2047.5	2010.5	0.66	0.65	1.13	1.07	1.05

Table 4.4.11 SET01 Statistics FEM section 'A', CM and CBFEM.

	M_R / $M_{R,FEM}$				
	EN	prEN	IS def	IS ref	IS rich
Mean	0.857	0.825	1.142	1.072	1.049
Std	0.138	0.107	0.086	0.073	0.071
CoV	16.1%	13.0%	7.5%	6.8%	6.7%
Max	1.081	0.984	1.296	1.186	1.154
Min	0.559	0.559	0.972	0.924	0.908

Table 4.4.12 SET01 Statistics FEM section 'B', CM and CBFEM.

	M_R / $M_{R,FEM}$				
	EN	prEN	IS def	IS ref	IS rich
Mean	0.882	0.852	1.176	1.105	1.082
Std	0.176	0.166	0.154	0.153	0.153
CoV	19.9%	19.5%	13.1%	13.8%	14.2%
Max	1.307	1.264	1.600	1.511	1.482
Min	0.647	0.638	0.965	0.900	0.878

Table 4.4.13 SET01 Statistics FEM section 'C', CM and CBFEM.

	$M_R / M_{R,FEM}$				
	EN	**prEN**	**IS def**	**IS ref**	**IS rich**
Mean	0.794	0.765	1.061	0.996	0.975
Std	0.114	0.095	0.072	0.070	0.071
CoV	14.4%	12.4%	6.8%	7.0%	7.3%
Max	0.985	0.953	1.206	1.139	1.117
Min	0.550	0.550	0.947	0.884	0.863

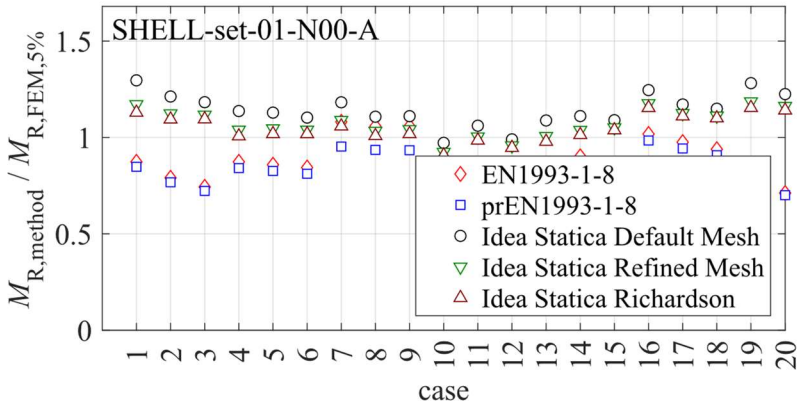

Figure 4.5 SET01 Moment resistance FEM section 'A', CM and CBFEM.

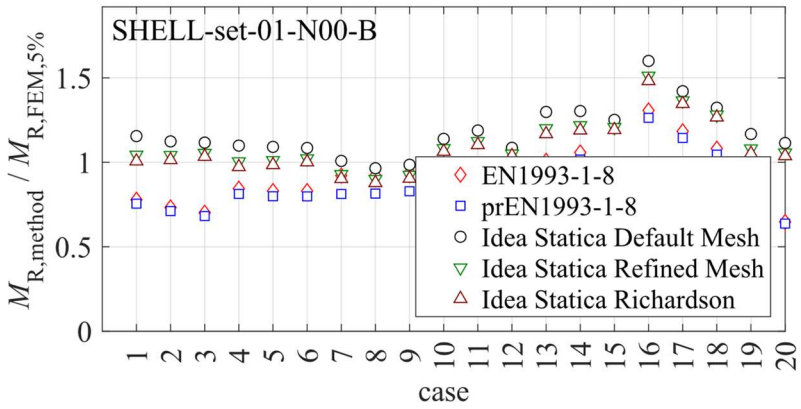

Figure 4.6 SET01 Moment resistance FEM section 'B', CM and CBFEM.

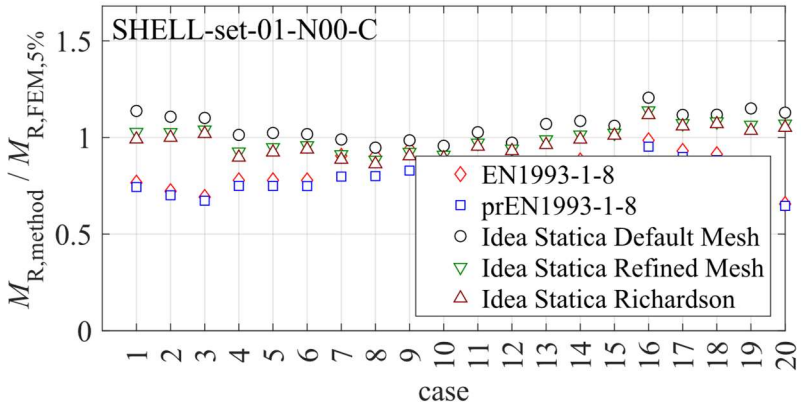

Figure 4.7 SET01 Moment resistance FEM section 'C', CM and CBFEM.

The results comparison between shell FEM, the CM and CBFEM in presence of axial force equal to 50% of the column axial plastic resistance ($N_{pl,Rk}$) (SET02) may be seen in Tables 4.14, 4.16 and 4.18. In general terms, the tendencies observed for SET01 seem to be the similar. However, points out CM results that are unconservative compared to shell FEM. Statistics may be seen in Tables 4.15, 4.17 and 4.19.

Table 4.14 SET02N50 Moment resistance FEM section 'A', CM and CBFEM.

	M_R (kN·m)						M_R / $M_{R,FEM}$				
	FEM	EN	FprEn	IS def	IS ref	IS rich	EN	FprEn	IS def	IS ref	IS rich
nº	[1]	[2]	[3]	[4]	[5]	[6]	[2]/[1]	[3]/[1]	[4]/[1]	[5]/[1]	[6]/[1]
1	262.6	258.7	251.2	354.2	316.0	303.3	0.99	0.96	1.35	1.20	1.15
2	442.0	389.4	378.1	554.2	505.9	489.8	0.88	0.86	1.25	1.14	1.11
3	650.3	535.2	520.3	796.6	740.0	721.2	0.82	0.80	1.22	1.14	1.11
4	28.1	28.2	27.2	34.4	30.9	29.8	1.01	0.97	1.22	1.10	1.06
5	48.2	45.7	44.0	56.0	51.1	49.5	0.95	0.91	1.16	1.06	1.03
6	68.7	63.9	61.5	78.4	73.1	71.3	0.93	0.89	1.14	1.06	1.04
7	79.9	100.5	88.6	100.5	91.8	88.8	1.26	1.11	1.26	1.15	1.11
8	126.4	155.1	137.1	150.6	138.8	134.8	1.23	1.08	1.19	1.10	1.07
9	174.5	209.0	184.5	202.5	189.1	184.6	1.20	1.06	1.16	1.08	1.06
10	37.6	27.4	27.4	45.0	42.1	41.1	0.73	0.73	1.20	1.12	1.10
11	49.6	46.6	50.9	59.9	57.7	57.0	0.94	1.03	1.21	1.16	1.15
12	69.1	57.7	57.7	78.9	76.6	75.8	0.83	0.83	1.14	1.11	1.10
13	325.0	338.2	333.6	409.0	376.3	365.5	1.04	1.03	1.26	1.16	1.12
14	446.0	487.4	468.0	560.2	529.7	519.6	1.09	1.05	1.26	1.19	1.17
15	640.8	579.5	579.5	761.3	731.6	721.6	0.90	0.90	1.19	1.14	1.13
16	1067.3	1309.5	1266.1	1434.4	1347.3	1318.2	1.23	1.19	1.34	1.26	1.24
17	1768.5	2021.1	1954.0	2197.1	2089.8	2054.1	1.14	1.10	1.24	1.18	1.16
18	2648.1	2894.1	2798.1	3209.1	3076.9	3032.9	1.09	1.06	1.21	1.16	1.15
19	963.5	864.2	850.6	1247.6	1148.7	1115.8	0.90	0.88	1.29	1.19	1.16
20	1573.7	1253.9	1235.1	1987.7	1848.7	1802.3	0.80	0.78	1.26	1.17	1.15

Table 4.4.15 SET02N50 Statistics FEM section 'A', CM and CBFEM.

	$M_R / M_{R,FEM}$				
	EN	**prEN**	**IS def**	**IS ref**	**IS rich**
Mean	0.998	0.961	1.229	1.145	1.117
Std	0.157	0.125	0.059	0.050	0.051
CoV	15.7%	13.0%	4.8%	4.4%	4.6%
Max	1.258	1.186	1.349	1.262	1.235
Min	0.729	0.729	1.141	1.060	1.027

Table 4.16 SET02N50 Moment resistance FEM section 'B', CM and CBFEM.

	M_R (kN·m)						$M_R / M_{R,FEM}$				
	FEM	**EN**	**FprEn**	**IS def**	**IS ref**	**IS rich**	**EN**	**FprEn**	**IS def**	**IS ref**	**IS rich**
n°	**[1]**	**[2]**	**[3]**	**[4]**	**[5]**	**[6]**	**[2]/[1]**	**[3]/[1]**	**[4]/[1]**	**[5]/[1]**	**[6]/[1]**
1	288.5	258.7	251.2	354.2	316.0	303.3	0.90	0.87	1.23	1.10	1.05
2	473.1	389.4	378.1	554.2	505.9	489.8	0.82	0.80	1.17	1.07	1.04
3	693.1	535.2	520.3	796.6	740.0	721.2	0.77	0.75	1.15	1.07	1.04
4	28.7	28.2	27.2	34.4	30.9	29.8	0.99	0.95	1.20	1.08	1.04
5	49.1	45.7	44.0	56.0	51.1	49.5	0.93	0.90	1.14	1.04	1.01
6	70.0	63.9	61.5	78.4	73.1	71.3	0.91	0.88	1.12	1.04	1.02
7	88.0	100.5	88.6	100.5	91.8	88.8	1.14	1.01	1.14	1.04	1.01
8	138.8	155.1	137.1	150.6	138.8	134.8	1.12	0.99	1.09	1.00	0.97
9	187.1	209.0	184.5	202.5	189.1	184.6	1.12	0.99	1.08	1.01	0.99
10	33.3	27.4	27.4	45.0	42.1	41.1	0.82	0.82	1.35	1.27	1.24
11	44.5	46.6	50.9	59.9	57.7	57.0	1.05	1.14	1.35	1.30	1.28
12	63.1	57.7	57.7	78.9	76.6	75.8	0.91	0.91	1.25	1.21	1.20
13	284.2	338.2	333.6	409.0	376.3	365.5	1.19	1.17	1.44	1.32	1.29
14	397.2	487.4	468.0	560.2	529.7	519.6	1.23	1.18	1.41	1.33	1.31
15	570.8	579.5	579.5	761.3	731.6	721.6	1.02	1.02	1.33	1.28	1.26
16	883.9	1309.5	1266.1	1434.4	1347.3	1318.2	1.48	1.43	1.62	1.52	1.49
17	1525.9	2021.1	1954.0	2197.1	2089.8	2054.1	1.32	1.28	1.44	1.37	1.35
18	2300.8	2894.1	2798.1	3209.1	3076.9	3032.9	1.26	1.22	1.39	1.34	1.32
19	998.1	864.2	850.6	1247.6	1148.7	1115.8	0.87	0.85	1.25	1.15	1.12
20	1623.9	1253.9	1235.1	1987.7	1848.7	1802.3	0.77	0.76	1.22	1.14	1.11

Table 4.4.17 SET02N50 Statistics FEM section 'B', CM and CBFEM.

	$M_R / M_{R,FEM}$				
	EN	**prEN**	**IS def**	**IS ref**	**IS rich**
Mean	1.031	0.996	1.269	1.184	1.156
Std	0.197	0.186	0.144	0.148	0.151
CoV	19.1%	18.7%	11.3%	12.5%	13.0%
Max	1.481	1.432	1.623	1.524	1.491
Min	0.772	0.751	1.082	1.000	0.971

Table 4.18 SET02N50 Moment resistance FEM section 'C', CM and CBFEM.

	M_R (kN·m)						M_R / $M_{R,FEM}$				
	FEM	EN	FprEn	IS def	IS ref	IS rich	EN	FprEn	IS def	IS ref	IS rich
nº	[1]	[2]	[3]	[4]	[5]	[6]	[2]/[1]	[3]/[1]	[4]/[1]	[5]/[1]	[6]/[1]
1	293.7	258.7	251.2	354.2	316.0	303.3	0.88	0.86	1.21	1.08	1.03
2	480.9	389.4	378.1	554.2	505.9	489.8	0.81	0.79	1.15	1.05	1.02
3	693.1	535.2	520.3	796.6	740.0	721.2	0.77	0.75	1.15	1.07	1.04
4	30.7	28.2	27.2	34.4	30.9	29.8	0.92	0.89	1.12	1.01	0.97
5	51.2	45.7	44.0	56.0	51.1	49.5	0.89	0.86	1.09	1.00	0.97
6	72.5	63.9	61.5	78.4	73.1	71.3	0.88	0.85	1.08	1.01	0.98
7	90.0	100.5	88.6	100.5	91.8	88.8	1.12	0.99	1.12	1.02	0.99
8	141.9	155.1	137.1	150.6	138.8	134.8	1.09	0.97	1.06	0.98	0.95
9	191.3	209.0	184.5	202.5	189.1	184.6	1.09	0.96	1.06	0.99	0.97
10	39.0	27.4	27.4	45.0	42.1	41.1	0.70	0.70	1.16	1.08	1.06
11	51.6	46.6	50.9	59.9	57.7	57.0	0.90	0.99	1.16	1.12	1.10
12	71.9	57.7	57.7	78.9	76.6	75.8	0.80	0.80	1.10	1.07	1.06
13	338.6	338.2	333.6	409.0	376.3	365.5	1.00	0.99	1.21	1.11	1.08
14	465.5	487.4	468.0	560.2	529.7	519.6	1.05	1.01	1.20	1.14	1.12
15	668.8	579.5	579.5	761.3	731.6	721.6	0.87	0.87	1.14	1.09	1.08
16	1093.5	1309.5	1266.1	1434.4	1347.3	1318.2	1.20	1.16	1.31	1.23	1.21
17	1808.9	2021.1	1954.0	2197.1	2089.8	2054.1	1.12	1.08	1.21	1.16	1.14
18	2706.0	2894.1	2798.1	3209.1	3076.9	3032.9	1.07	1.03	1.19	1.14	1.12
19	1032.7	864.2	850.6	1247.6	1148.7	1115.8	0.84	0.82	1.21	1.11	1.08
20	1674.0	1253.9	1235.1	1987.7	1848.7	1802.3	0.75	0.74	1.19	1.10	1.08

Table 4.4.19 SET02N50 Statistics FEM section 'C', CM and CBFEM.

	M_R / $M_{R,FEM}$				
	EN	prEN	IS def	IS ref	IS rich
Mean	0.938	0.904	1.156	1.077	1.051
Std	0.144	0.122	0.062	0.065	0.068
CoV	15.3%	13.5%	5.4%	6.0%	6.5%
Max	1.198	1.158	1.312	1.232	1.206
Min	0.702	0.702	1.059	0.978	0.950

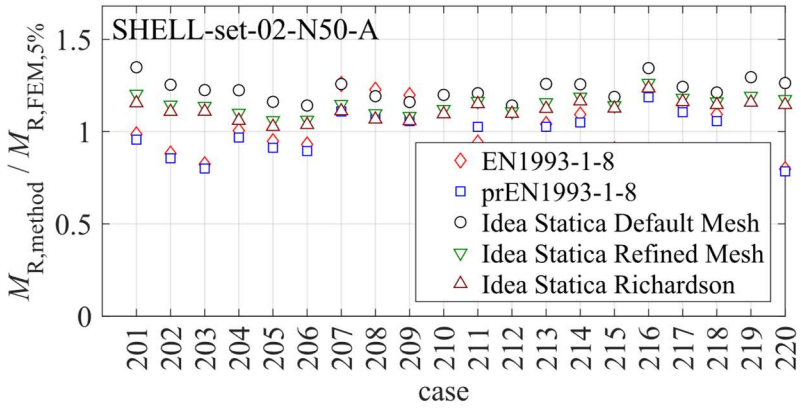

Figure 4.8 SET02N50 Moment resistance FEM section 'A', CM and CBFEM.

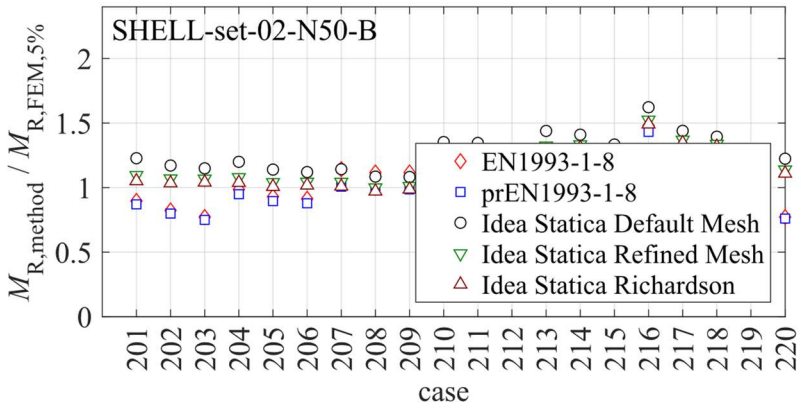

Figure 4.9 SET02N50 Moment resistance FEM section 'B', CM and CBFEM.

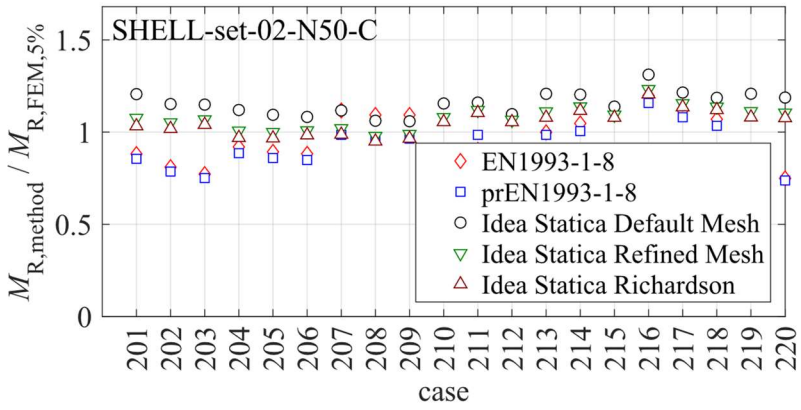

Figure 4.10 SET02N50 Moment resistance FEM section 'C', CM and CBFEM.

Independently of the application of axial moment or not, and so for both SET01 and SET02N50, Tables 4.20 to 4.22 present the statistical information about moment resistance considering different methods.

Table 4.4.20 All cases statistics FEM section 'A', CM and CBFEM.

	$M_R / M_{R,FEM}$				
	EN	**prEN**	**IS def**	**IS ref**	**IS rich**
Mean	0.927	0.893	1.185	1.109	1.083
Std	0.162	0.134	0.085	0.072	0.070
CoV	17.5%	15.0%	7.1%	6.5%	6.4%
Max	1.258	1.186	1.349	1.262	1.235
Min	0.559	0.559	0.972	0.924	0.908

Table 4.4.21 All cases statistics FEM section 'B', CM and CBFEM.

	$M_R / M_{R,FEM}$				
	EN	**prEN**	**IS def**	**IS ref**	**IS rich**
Mean	0.956	0.924	1.223	1.145	1.119
Std	0.199	0.189	0.154	0.154	0.155
CoV	20.8%	20.5%	12.6%	13.5%	13.8%
Max	1.481	1.432	1.623	1.524	1.491
Min	0.647	0.638	0.965	0.900	0.878

Table 4.4.22 All cases statistics FEM section 'C', CM and CBFEM.

	$M_R / M_{R,FEM}$				
	EN	**prEN**	**IS def**	**IS ref**	**IS rich**
Mean	0.866	0.835	1.108	1.037	1.013
Std	0.147	0.129	0.082	0.078	0.079
CoV	17.0%	15.4%	7.4%	7.6%	7.8%
Max	1.198	1.158	1.312	1.232	1.206
Min	0.550	0.550	0.947	0.884	0.863

4.3.3 Initial stiffness SET01 and SET02N50

The calculation of initial stiffness was only developed for shell FEM models and CM. The results a respective statistical information is presented hereafter. Tables 4.23 and 4.24 compare the initial stiffness results for sections models 'A', 'B' and 'C' for SET01 and SET02 respectively. In addition, Tables 4.25 and 4.26 present the statistical information referred to that analysis. As a general tendency may be seen that model section 'C' reports the higher initial stiffness.

Table 4.23 Comparison between the initial stiffness for SET01 by all shell FEM.

	$S_{j,ini}$ (kN·m/mrad)			$S_{j,ini,i}/ S_{j,ini,j}$		
	A	**B**	**C**	**B/A**	**C/A**	**C/B**
n°	**[1]**	**[2]**	**[3]**	**[2]/[1]**	**[3]/[1]**	**[3]/[2]**
1	77.0	81.1	83.6	1.05	1.09	1.03
2	139.4	146.3	150.3	1.05	1.08	1.03
3	208.1	218.0	222.5	1.05	1.07	1.02

4	6.7	6.8	7.1	1.00	1.05	1.04
5	14.2	14.3	14.9	1.00	1.05	1.04
6	21.2	21.2	22.0	1.00	1.04	1.04
7	18.5	20.0	21.0	1.08	1.14	1.05
8	35.8	38.6	40.7	1.08	1.14	1.06
9	51.8	55.7	57.9	1.08	1.12	1.04
10	8.4	7.7	8.9	0.92	1.06	1.15
11	11.8	10.9	12.5	0.93	1.06	1.14
12	20.3	18.5	21.5	0.91	1.06	1.17
13	76.2	71.3	79.7	0.94	1.05	1.12
14	116.5	108.4	121.1	0.93	1.04	1.12
15	191.8	177.5	199.1	0.93	1.04	1.12
16	310.6	289.4	321.7	0.93	1.04	1.11
17	569.0	531.3	587.4	0.93	1.03	1.11
18	867.2	812.3	891.9	0.94	1.03	1.10
19	328.0	333.3	346.9	1.02	1.06	1.04
20	556.0	564.2	583.4	1.01	1.05	1.03

Table 4.24 Comparison between the initial stiffness for SET02N50 by all shell FEM.

	$S_{j,ini}$ (kN·m/mrad)			$S_{j,ini,i}/S_{j,ini,j}$		
	A	**B**	**C**	**B/A**	**C/A**	**C/B**
n°	**[1]**	**[2]**	**[3]**	**[2]/[1]**	**[3]/[1]**	**[3]/[2]**
1	63.1	67.8	70.1	1.07	1.11	1.03
2	115.7	123.5	127.3	1.07	1.10	1.03
3	176.0	186.7	191.2	1.06	1.09	1.02
4	5.9	6.0	6.2	1.01	1.05	1.05
5	12.4	12.5	13.0	1.00	1.05	1.04
6	18.5	18.6	19.3	1.00	1.04	1.04
7	16.7	18.1	19.1	1.08	1.14	1.05
8	31.8	34.4	36.3	1.08	1.14	1.05
9	46.4	50.0	52.0	1.08	1.12	1.04
10	7.5	7.0	7.9	0.92	1.06	1.14
11	10.6	9.8	11.2	0.92	1.05	1.15
12	17.4	15.9	18.4	0.92	1.06	1.15
13	70.1	64.9	73.5	0.93	1.05	1.13
14	106.6	99.3	111.8	0.93	1.05	1.13
15	172.8	159.2	179.9	0.92	1.04	1.13
16	280.7	260.5	296.1	0.93	1.05	1.14
17	512.7	477.7	537.3	0.93	1.05	1.12
18	781.5	731.4	813.2	0.94	1.04	1.11
19	241.1	247.8	261.1	1.03	1.08	1.05
20	419.9	430.3	450.1	1.02	1.07	1.05

Table 4.4.25 Statistics SET01 FEM initial stiffness comparison.

	$S_{j,ini,i}/S_{j,ini,j}$		
	B/A	**C/A**	**C/B**
Mean	0.989	1.063	1.077
Std	0.061	0.033	0.047
CoV	6.2%	3.1%	4.4%
Max	1.077	1.137	1.165
Min	0.908	1.028	1.021

Table 4.4.26 Statistics SET02N50 FEM initial stiffness comparison.

	$S_{j,ini,i}/S_{j,ini,j}$		
	B/A	**C/A**	**C/B**
Mean	0.992	1.072	1.083
Std	0.066	0.033	0.048
CoV	6.7%	3.1%	4.5%
Max	1.082	1.139	1.155
Min	0.915	1.041	1.024

Table 4.27 present the statistical information about the comparison between model sections, for SET01 and SET02 together.

Table 4.4.27 Statistics all cases FEM initial stiffness comparison.

	$S_{j,ini,i}/S_{j,ini,j}$		
	B/A	**C/A**	**C/B**
Mean	0.990	1.067	1.080
Std	0.063	0.033	0.047
CoV	6.3%	3.1%	4.4%
Max	1.082	1.139	1.165
Min	0.908	1.028	1.021

The comparison between the results provided for initial stiffness by the CM and the shell FEM for SET01 may be seen on Tables 4.28 and 4.29 for EN 1993-1-8 (CEN, 2005b) and Tables 4.30 and 4.31 for FprEN 1993-1-8 (CEN, 2023). It may be noticed that, as general tendency the shell FEM seem to present higher initial stiffness values than the CM.

Table 4.28 Comparison between the initial stiffness for SET01 by all shell FEM and CM EN 1993-1-8.

	$S_{j,ini}$ (kN·m/mrad)				$S_{j,ini,FEM}/S_{j,ini,EN}$		
	A	**B**	**C**	**EN**	**A**	**B**	**C**
n°	**[1]**	**[2]**	**[3]**	**[4]**	**[1]/[4]**	**[2]/[4]**	**[3]/[4]**
1	77.0	81.1	83.6	63.0	1.22	1.29	1.33
2	139.4	146.3	150.3	124.9	1.12	1.17	1.20
3	208.1	218.0	222.5	206.5	1.01	1.06	1.08
4	6.7	6.8	7.1	5.5	1.23	1.24	1.29
5	14.2	14.3	14.9	12.2	1.17	1.18	1.23
6	21.2	21.2	22.0	20.4	1.04	1.04	1.08
7	18.5	20.0	21.0	20.2	0.92	0.99	1.04
8	35.8	38.6	40.7	41.2	0.87	0.94	0.99
9	51.8	55.7	57.9	64.5	0.80	0.86	0.90
10	8.4	7.7	8.9	8.1	1.03	0.95	1.09

11	11.8	10.9	12.5	13.8	0.85	0.79	0.90
12	20.3	18.5	21.5	24.1	0.84	0.77	0.89
13	76.2	71.3	79.7	74.2	1.03	0.96	1.07
14	116.5	108.4	121.1	124.3	0.94	0.87	0.97
15	191.8	177.5	199.1	207.7	0.92	0.85	0.96
16	310.6	289.4	321.7	255.0	1.22	1.13	1.26
17	569.0	531.3	587.4	512.4	1.11	1.04	1.15
18	867.2	812.3	891.9	881.3	0.98	0.92	1.01
19	328.0	333.3	346.9	220.1	1.49	1.51	1.58
20	556.0	564.2	583.4	414.9	1.34	1.36	1.41

Table 4.29 Statistics SET01 FEM initial stiffness comparison with CM EN 1993-1-8.

	$S_{j,ini,FEM} / S_{j,ini,EN}$		
	A	**B**	**C**
Mean	1.057	1.046	1.121
Std	0.181	0.198	0.183
CoV	17.1%	18.9%	16.4%
Max	1.490	1.514	1.576
Min	0.802	0.766	0.893

Table 4.30 Comparison between the initial stiffness for SET01 by all shell FEM and CM FprEN 1993-1-8.

	$S_{j,ini}$ (kN·m/mrad)				$S_{j,ini,FEM} / S_{j,ini,FprEn}$		
	A	**B**	**C**	**FprEn**	**A**	**B**	**C**
n^o	**[1]**	**[2]**	**[3]**	**[4]**	**[1]/[4]**	**[2]/[4]**	**[3]/[4]**
1	77.0	81.1	83.6	58.5	1.32	1.39	1.43
2	139.4	146.3	150.3	113.5	1.23	1.29	1.32
3	208.1	218.0	222.5	184.0	1.13	1.18	1.21
4	6.7	6.8	7.1	5.2	1.29	1.29	1.35
5	14.2	14.3	14.9	11.5	1.24	1.25	1.30
6	21.2	21.2	22.0	19.0	1.11	1.12	1.16
7	18.5	20.0	21.0	17.9	1.04	1.12	1.18
8	35.8	38.6	40.7	35.1	1.02	1.10	1.16
9	51.8	55.7	57.9	53.7	0.96	1.04	1.08
10	8.4	7.7	8.9	7.5	1.12	1.03	1.18
11	11.8	10.9	12.5	12.6	0.94	0.87	0.99
12	20.3	18.5	21.5	21.7	0.94	0.85	0.99
13	76.2	71.3	79.7	70.6	1.08	1.01	1.13
14	116.5	108.4	121.1	117.1	0.99	0.93	1.03
15	191.8	177.5	199.1	193.8	0.99	0.92	1.03
16	310.6	289.4	321.7	246.7	1.26	1.17	1.30
17	569.0	531.3	587.4	490.8	1.16	1.08	1.20
18	867.2	812.3	891.9	837.2	1.04	0.97	1.07

19	328.0	333.3	346.9	211.7	1.55	1.57	1.64
20	556.0	564.2	583.4	394.5	1.41	1.43	1.48

Table 4.31 Statistics SET01 FEM initial stiffness comparison with CM FprEN 1993-1-8.

	$S_{j,ini,FEM} / S_{j,ini,prEN}$		
	A	**B**	**C**
Mean	1.141	1.130	1.211
Std	0.166	0.194	0.172
CoV	14.5%	17.2%	14.2%
Max	1.549	1.574	1.639
Min	0.936	0.853	0.989

The results referred to SET02, comparing the CM and shell FEM may be consulted on Tables 4.32 to 4.35.

Table 4.32 Comparison between the initial stiffness for SET02N50 by all shell FEM and CM EN 1993-1-8.

	$S_{j,ini}$ (kN·m)				$S_{j,ini,FEM} / S_{j,ini,EN}$		
	A	**B**	**C**	**EN**	**A**	**B**	**C**
n^o	**[1]**	**[2]**	**[3]**	**[4]**	**[1]/[4]**	**[2]/[4]**	**[3]/[4]**
1	63.1	67.8	70.1	63.0	1.00	1.08	1.11
2	115.7	123.5	127.3	124.9	0.93	0.99	1.02
3	176.0	186.7	191.2	206.5	0.85	0.90	0.93
4	5.9	6.0	6.2	5.5	1.08	1.09	1.14
5	12.4	12.5	13.0	12.2	1.02	1.02	1.07
6	18.5	18.6	19.3	20.4	0.91	0.91	0.95
7	16.7	18.1	19.1	20.2	0.83	0.90	0.94
8	31.8	34.4	36.3	41.2	0.77	0.84	0.88
9	46.4	50.0	52.0	64.5	0.72	0.77	0.81
10	7.5	7.0	7.9	8.1	0.92	0.85	0.98
11	10.6	9.8	11.2	13.8	0.77	0.71	0.81
12	17.4	15.9	18.4	24.1	0.72	0.66	0.76
13	70.1	64.9	73.5	74.2	0.95	0.87	0.99
14	106.6	99.3	111.8	124.3	0.86	0.80	0.90
15	172.8	159.2	179.9	207.7	0.83	0.77	0.87
16	280.7	260.5	296.1	255.0	1.10	1.02	1.16
17	512.7	477.7	537.3	512.4	1.00	0.93	1.05
18	781.5	731.4	813.2	881.3	0.89	0.83	0.92
19	241.1	247.8	261.1	220.1	1.10	1.13	1.19
20	419.9	430.3	450.1	414.9	1.01	1.04	1.09

Table 4.33 Statistics SET02N50 FEM initial stiffness comparison with CM EN 1993-1-8.

	$S_{j,ini,FEM} / S_{j,ini,EN}$		
	A	**B**	**C**
Mean	0.913	0.905	0.978
Std	0.120	0.131	0.123
CoV	13.1%	14.5%	12.6%
Max	1.101	1.126	1.187
Min	0.719	0.661	0.763

Table 4.34 Comparison between the initial stiffness for SET02N50 by all shell FEM and CM FprEN 1993-1-8.

	$S_{j,ini}$ (kN·m)				$S_{j,ini,FEM} / S_{j,ini,FprEn}$		
	A	**B**	**C**	**FprEn**	**A**	**B**	**C**
n^o	**[1]**	**[2]**	**[3]**	**[4]**	**[1]/[4]**	**[2]/[4]**	**[3]/[4]**
1	63.1	67.8	70.1	58.5	1.08	1.16	1.20
2	115.7	123.5	127.3	113.5	1.02	1.09	1.12
3	176.0	186.7	191.2	184.0	0.96	1.01	1.04
4	5.9	6.0	6.2	5.2	1.13	1.14	1.19
5	12.4	12.5	13.0	11.5	1.08	1.09	1.13
6	18.5	18.6	19.3	19.0	0.98	0.98	1.02
7	16.7	18.1	19.1	17.9	0.94	1.02	1.07
8	31.8	34.4	36.3	35.1	0.91	0.98	1.03
9	46.4	50.0	52.0	53.7	0.86	0.93	0.97
10	7.5	7.0	7.9	7.5	1.00	0.92	1.06
11	10.6	9.8	11.2	12.6	0.84	0.77	0.89
12	17.4	15.9	18.4	21.7	0.80	0.74	0.85
13	70.1	64.9	73.5	70.6	0.99	0.92	1.04
14	106.6	99.3	111.8	117.1	0.91	0.85	0.96
15	172.8	159.2	179.9	193.8	0.89	0.82	0.93
16	280.7	260.5	296.1	246.7	1.14	1.06	1.20
17	512.7	477.7	537.3	490.8	1.04	0.97	1.09
18	781.5	731.4	813.2	837.2	0.93	0.87	0.97
19	241.1	247.8	261.1	211.7	1.14	1.17	1.23
20	419.9	430.3	450.1	394.5	1.06	1.09	1.14

Table 4.35 Statistics SET02N50 FEM initial stiffness comparison with CM FprEN 1993-1-8.

	$S_{j,ini,FEM} / S_{j,ini,prEN}$		
	A	**B**	**C**
Mean	0.986	0.979	1.056
Std	0.100	0.126	0.109
CoV	10.2%	12.9%	10.3%
Max	1.139	1.171	1.234
Min	0.804	0.735	0.849

The statistical information of the comparison between CM and shell FEM for all cases is presented on Tables 4.36 and 4.37.

Table 4.36 All cases FEM initial stiffness comparison with CM EN 1993-1-8.

	$S_{j,ini,FEM} / S_{j,ini,EN}$		
	A	**B**	**C**
Mean	0.985	0.976	1.050
Std	0.168	0.180	0.171
CoV	17.0%	18.5%	16.3%
Max	1.490	1.514	1.576
Min	0.719	0.661	0.763

Table 4.37 All cases FEM initial stiffness comparison with CM FprEn 1993-1-8.

	$S_{j,ini,FEM} / S_{j,ini,prEN}$		
	A	**B**	**C**
Mean	1.063	1.055	1.134
Std	0.156	0.179	0.162
CoV	14.7%	17.0%	14.3%
Max	1.549	1.574	1.639
Min	0.804	0.735	0.849

5 DISCUSSION OF RESULTS

In this chapter, the results for moment-resistance and initial stiffness presented in Chapter 4 are going to be discussed.

5.1 Moment-resistance comparison

Between different shell FEM (B or C and A) the higher differences in moment resistance seems to occur for cases 10 to 18 for model B, see Table 4.4 and 4.5. Model B shows systematically lower resistances than model A (with a minimum of 22% lower for SET01). A possible explanation for this can be found in the formulation of section B, where the area resulting from the overlap of web and flange shell elements is considered and discounted. For cases 10 to 18, the column profiles have thick flanges and therefore, the discount of the overlap area leads, in fact, to a decrease and not an increase in web thickness for the root-radius zone compared to the actual web thickness.

On the other hand, for the remaining cases, both models C and B show systematically higher or equal moment resistances than model A. Model C leads to a mean moment resistance increase of 7.8% without axial force and 6.4% with axial force applied on the column, with Std. deviations below 0.06. Model C also presents systematically higher moment resistances than model B for all cases. Namely, a mean 11% increase for SET01 and 9.6 for SET02N50 and maximum values that are 33 and 24% higher respectively, see Tables 4.6 and 4.7 and Figures 5.1 and 5.2.

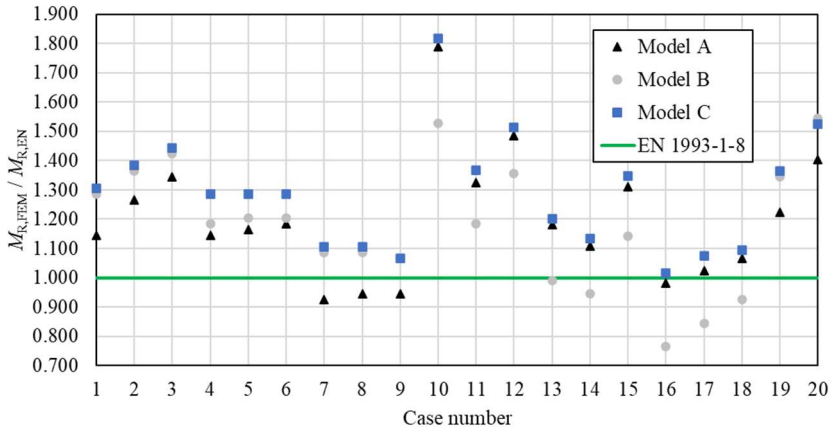

Figure 5.1 Moment-resistance comparison between model A, B, and C and Eurocode EN 1993-1-8 for SET01.

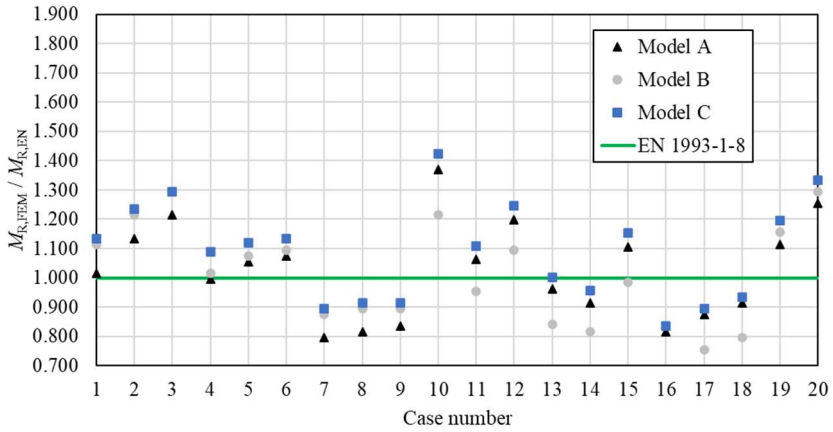

Figure 5.2 Moment-resistance comparison between model A, B, and C and Eurocode EN 1993-1-8 for SET02N50

In general, the covariance and standard deviation of the results may be con considered relatively low, when comparing model C to model A, under 5.1% and 0.06 respectively. The comparisons with model B present higher covariance and standard deviation values. Namely between 13 and 9.8% and between 0.13 and 0.095. This higher dispersion of results may be due to the previously referred situation for cases 10 to 18.

5.1.1 Eurocodes EN 1993-1-8 and FprEN 1993-1-8

Comparing the shell FEM with CM as a general tendency EN 1993-1-8 and FprEN 1993-1-8 may lead to conservative results for SET01 (without axial force). Namely, the mean moment resistance calculated according to EN 1993-1-8 represents 85.7, 88.2, and 79.4% of the moment resistance obtained for models A, B, and C, respectively. The mean moment resistance calculated according to FprEN 1993-1-8 represents 82.5, 85.2, and 76.5% of the moment resistance obtained for models A, B, and C, respectively, see Tables 4.8 to 4.13 and Figures 4.5 to 4.7.

For SET02N50 similar tendencies may be observed when comparing CM with models A and C. Namely, EN-1993-1-8 leads to moment resistances that represent 99.8 and 93.8% of the FEM value, and FprEn-1993-1-8 leads to mean moment resistances that represent 96.1 and 90.4% of the FEM value, see Tables 4.14, 4.15, 4.18 and 4.19 and Figures 4.8 and 4.10. However, compared with model B the CM leads to approximately equal or higher mean moment resistance values. Namely, EN 1993-1-8 103.1% of the FEM value, and FprEN 1993-1-8 leads to 99.6% of the FEM value, see Tables 4.17 and 4.18 and Figure 4.9. Once again, the different main behaviour of model B when compared to models A and C may be due to the effective reduction of thickness that exists for some cases, leading to a smaller profile section and, therefore, smaller axial force resistance.

When considering all sets, and so independently of the application of axial force, for all three models both EN 1993-1-8 and FprEN 1993-1-8 seem to lead to conservative results when compared with FEM. EN 1993-1-8 leads to a mean fraction of the FEM moment resistance between 87 and 96% while the FprEN 1993-1-8 leads to a mean fraction of the FEM moment resistance between 84 and 93%, see Tables 4.20 to 4.22. However, for some specific cases, the CM seems to lead to non-conservative results with a maximum between 25% and 16% higher moment-resistance when compared to models A and C. That fraction increases when comparing CM to model B positioning between 49 and 43%.

5.1.2 CBFEM IDEA StatiCa®

Compared with shell FEM A, CBFEM as a general tendency seems to lead to unconservative results for SET01 (without axial force). Namely, the mean moment resistance calculated is 14, 7.2, and 4.9% higher than the FEM value for default and refined meshes and Richardsons extrapolation respectively, see Tables 4.8 and 4.9. Comparing with shell FEM B a similar conclusion may be obtained, with CBFEM leading to resistances that are 17.6, 10.5, and 8.2% higher than the correspondent FEM value for default and refined meshes and Richardson extrapolation respectively.

However, compared with shell FEM C, only CBFEM moment-resistance values using IDEA StatiCa® default mesh seems to be unconservative for SET01. CBFEM mean moment resistance using that mesh is 6.1% higher than the FEM value while may be considered as approximately the same (only 0.4% lower) using a refined mesh and 2.5% lower considering Richardssons extrapolation results, see Tables 4.12 and 4.13.

On the other hand, compared with shell FEM A, B, and C, CBFEM a general tendency seems to lead to unconservative results for SET02N50 (with axial force). For IS default mesh, the mean moment-resistance is between 27 and 16 % higher than the FEM value. Considering the refined mesh such values decrease to an interval between 18.4 and 7.7% higher than the FEM value and finally, considering the Richardsson extrapolation those values decrease to an interval between 15.6 and 5.1% higher than the FEM value, see Tables 4.14 to 4.19 and Figures 4.8 and 4.9.

Considering all cases (SET01 and SET02N50) CBFEM IDEA StatiCa® lead to moment-resistance mean values that seem to be higher than FEM values between 22.3 and 10.8% when using IS default mesh and between 14.5 and 3.7% when using IS refined mesh, see Tables 4.20 to 4.22.

It is important to highlight that when comparing Richardsson extrapolation IS moment-resistance values with model C mean moment-resistance values obtained with CBFEM and

FEM get closer. Specifically, IS values are only 1.3% higher than C FEM values with a standard deviation of 0.079 and a covariance of 7.8%.

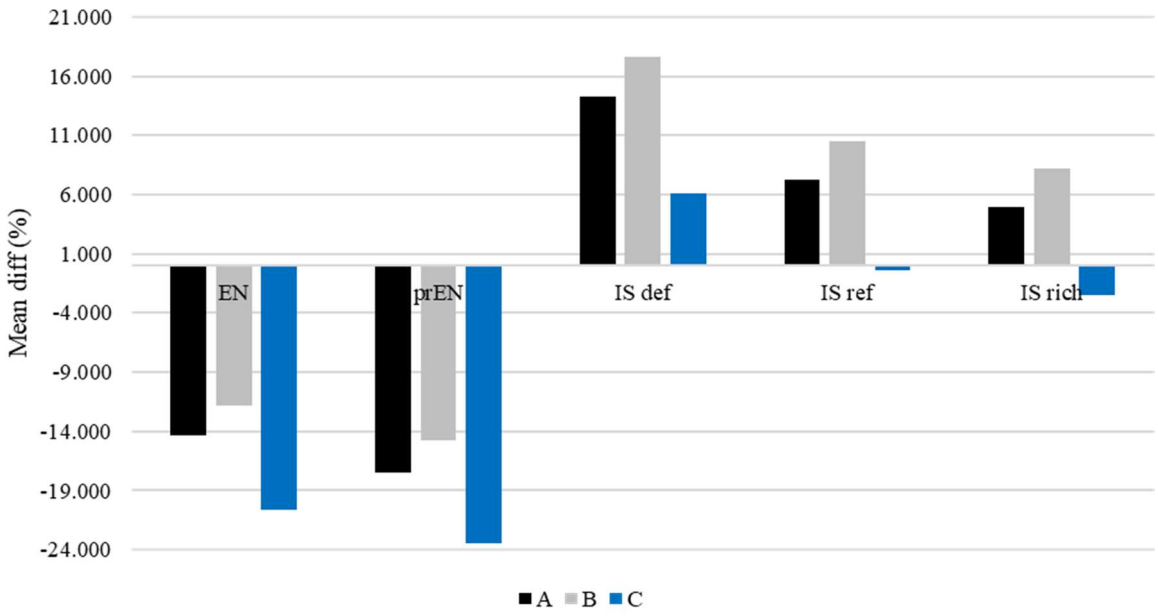

Figure 5.3 Mean difference moment-resistance SET01 models A, B and C.

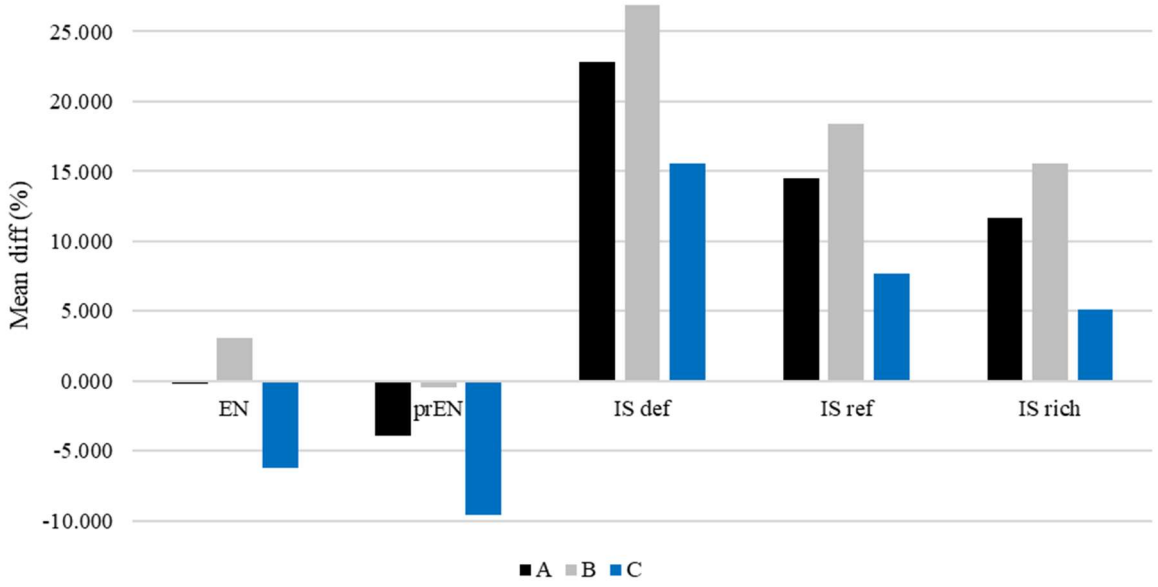

Figure 5.4 Mean difference moment resistance SET02N50 models A, B and C.

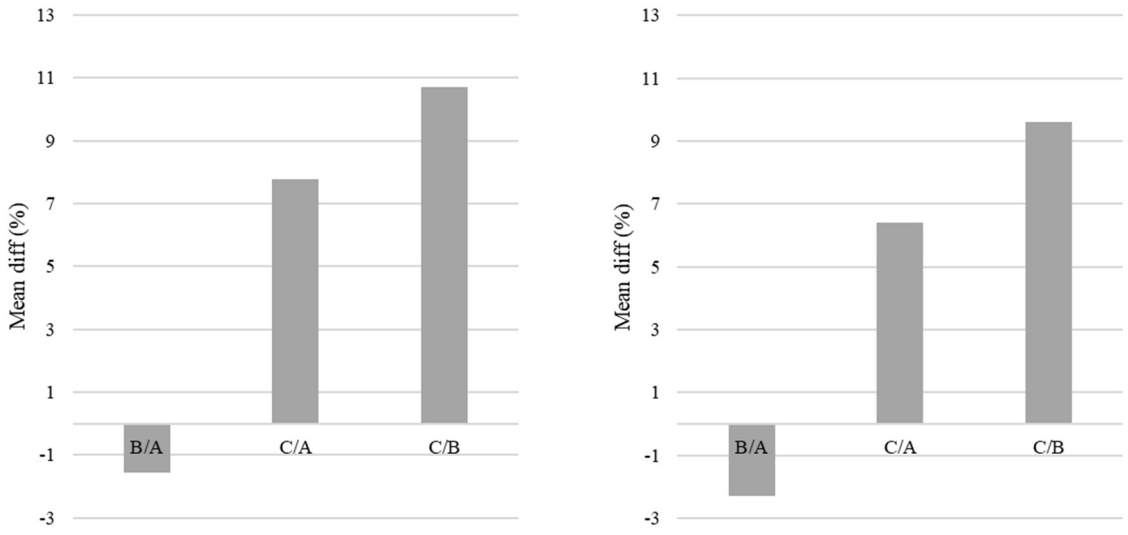

a) b)

Figure 5.5 Mean difference between moment resistance by FEM A, B and C. a) for SET01; b) for SET02N50.

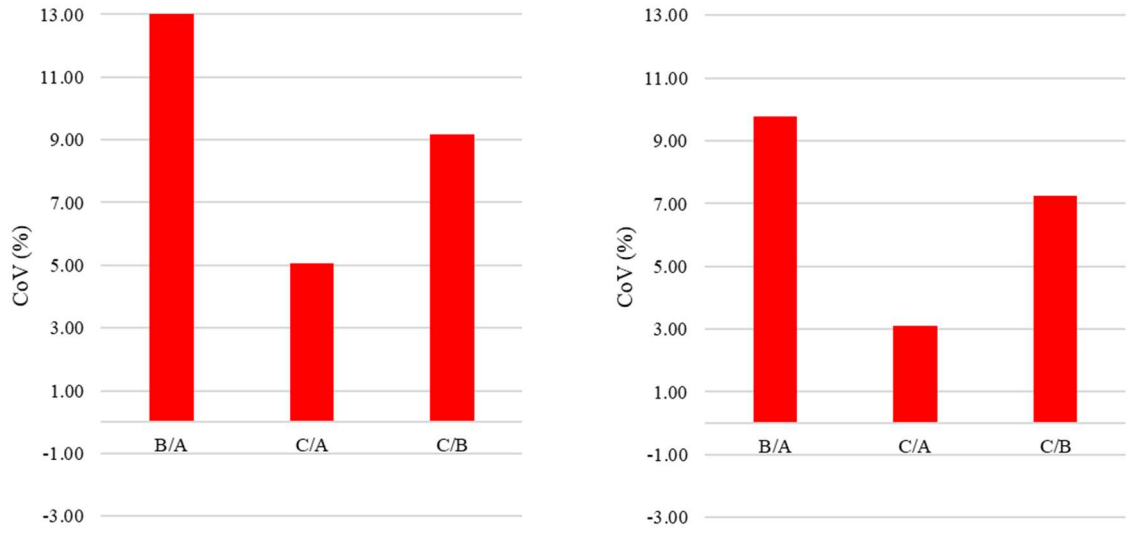

a) b)

Figure 5.6 Covariance between moment-resistance FEM A, B and C. a) for SET01; b) for SET02N50.

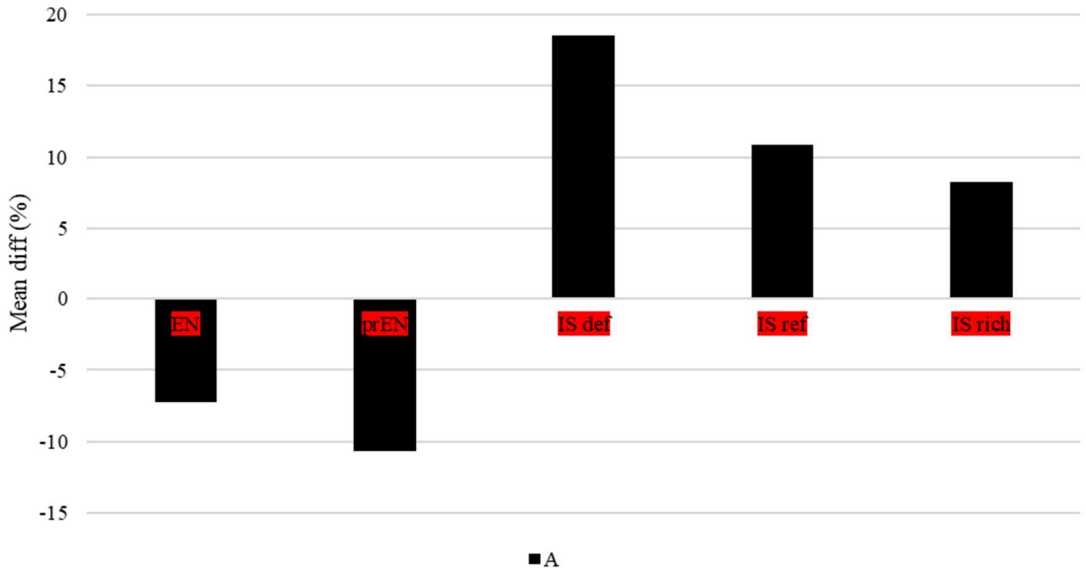

Figure 5.7 Mean difference, all cases, for moment-resistance between CM, CBFEM and FEM A.

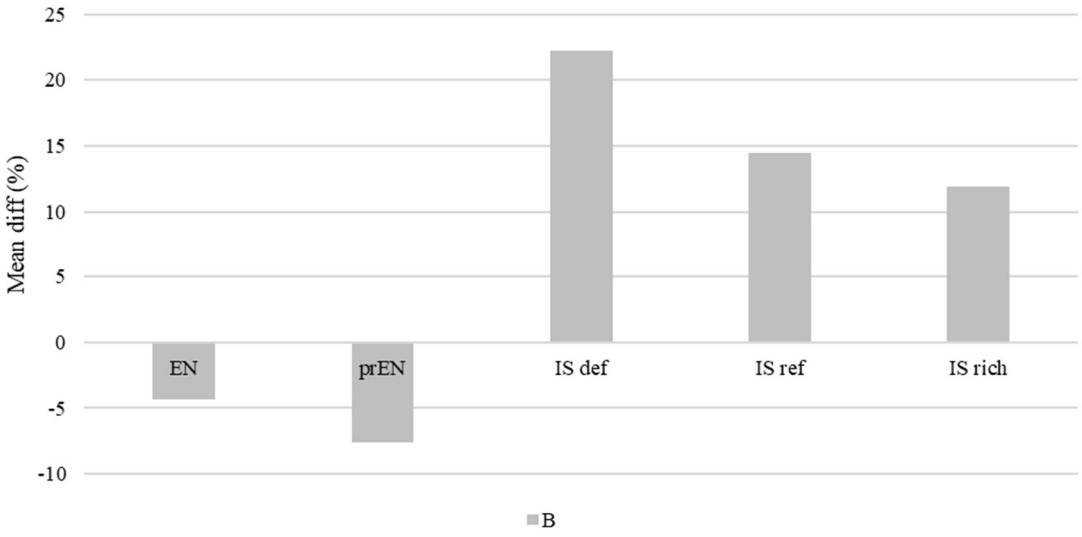

Figure 5.8 Mean difference, all cases, for moment-resistance between CM, CBFEM, and FEM B.

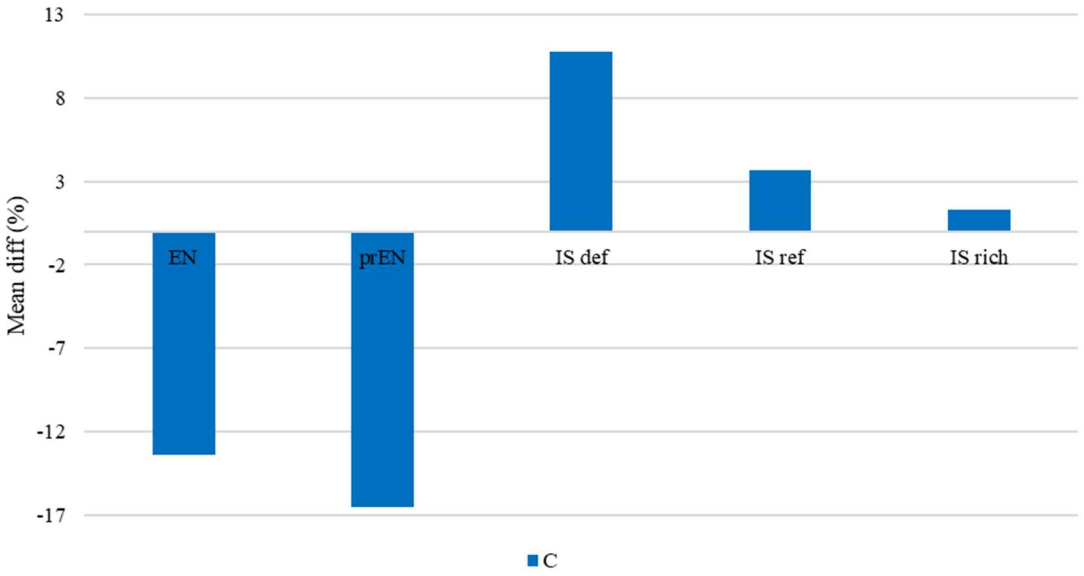

Figure 5.9 Mean difference, all cases, for moment-resistance between CM, CBFEM, and FEM C.

5.2 Initial stiffness comparison

Between different shell FEM (B or C and A) the higher difference in initial stiffness seems to occur for cases 10 to 18 for model B, see Table 4.23 and 4.5. Model B shows systematically lower stiffnesses than model A (with a minimum of 9.2% lower for SET01 and 8.5% for SET02N50). Once more, a possible explanation for this can be found in the formulation of section B as previously referred to in chapter 5.2, see Tables 4.23 and 4.25.

However, the general tendency that seems to be observed is what seems to be a relatively small variation of the mean initial stiffness between models A, B, and C. Model B leads to a mean initial stiffness 1.1% lower than model A for SET01 while Model C leads to a mean initial stiffness 6.3% higher than model A. For SET02N50 those values are 0.8% lower and 7.2% higher, see Tables 4.24 and 4.26.

Considering all cases, models B and C may lead to 1% lower and 6.7% higher mean initial stiffness than model A, with a standard deviation of 0.063 and 0.033 and covariance of 6.3% and 3.1% respectively. Comparing model C with model B's mean initial stiffness model C leads to 8% higher initial stiffness than model B with a standard deviation of 0.047 and a covariance of 4.4%, see Table 4.27.

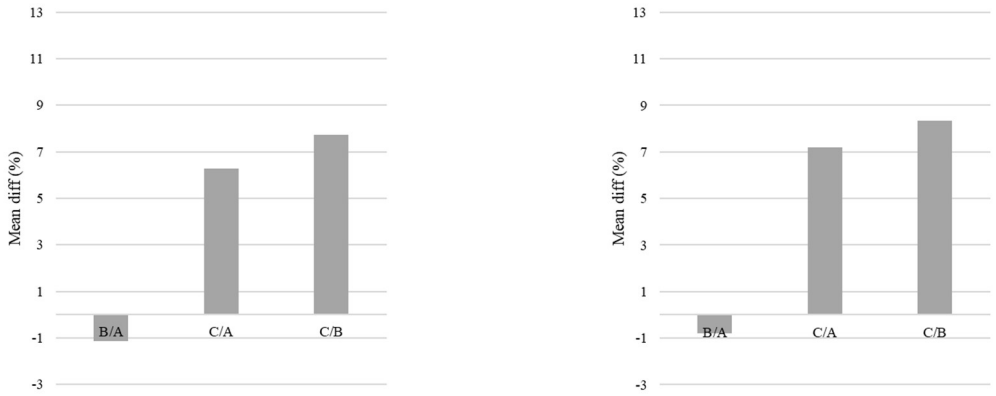

a) b)

Figure 5.10 Comparison between mean initial stiffness by FEM A, B and C. a) SET01; b) SET02N50

5.2.1 Eurocodes EN 1993-1-8 and FprEN 1993-1-8

When compared with EN 1993-1-8, the mean initial stiffness for SET01 is systematically over the FEM obtained value. Specifically, 5.7, 4.6 and 12.1% for models A, B, and C respectively. However, a covariance between 18.9 and 16.4% is observed, see Table 4.29. Such values are even higher when compared to the new European code FprEN 1993-1-8. Specifically, 14, 13, and 21 % for models A, B, and C respectively. Nevertheless, the covariance is lower, between 17.2 and 14.2%.

Should be highlighted that the European codes EN 1993-1-8 and FprEN 1993-1-8 do not consider any change in both stiffness and moment resistance due to the presence of axial force in the column until up to 70% of the column axial plastic strain resistance. However, the FEM does, and when comparing the results for SET02N50 whit EN 1993-1-8 the mean initial stiffness values obtained by FEM turn out to be lower. Namely, 8.7, 9.5, and 2.2% lower for models A, B and C. The covariance of the results also decreases, being between 14.5 and 12.6%, see Table 4.33.

The mean initial values for initial stiffness remain lower compared to the ones obtained by CM FprEN 1993-1-8 for FE models A and B. Nevertheless, the mean initial value obtained by FEM C turns out to be higher at 5.6% compared with CM, see Tables 4.36 and 4.37.

Considering all cases, the mean initial stiffness obtained by FEM C is higher compared with the results from both CM European codes. The mean initial stiffness obtained by FE models A and B turns out to be lower compared with the results from CM EN 1993-18 but higher than the ones obtained by CM FprEN 1993-1-8, see Tables 4.36 and 4.37.

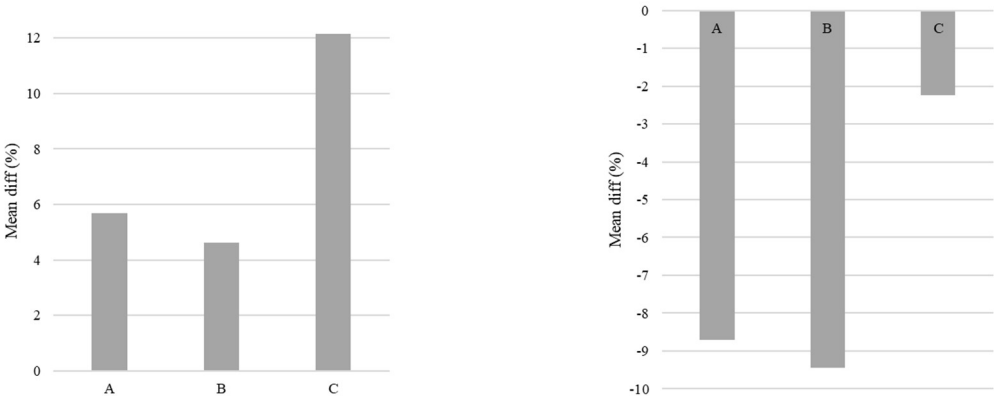

a) b)

Figure 5.11 Mean difference between initial stiffness by EN 1993-1-8 and FEM. a) SET01; b) SET02N50.

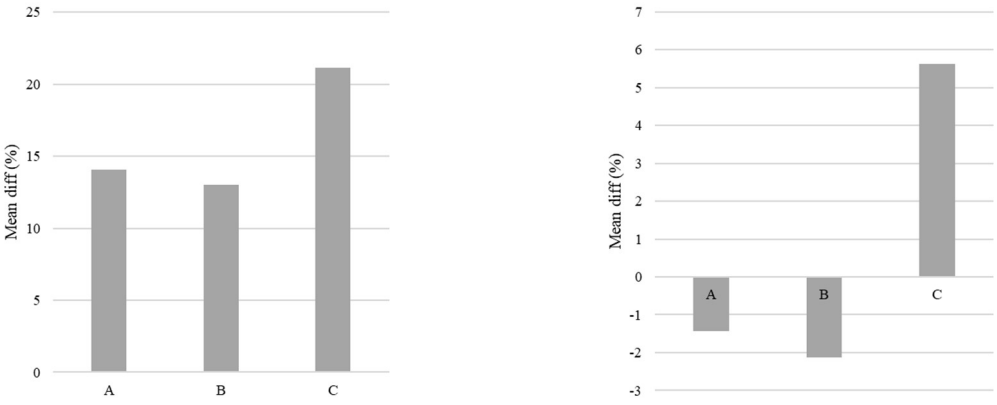

a) b)

Figure 5.12 Mean difference between initial stiffness by FprEN 1993-1-8 and FEM. a) SET01; b) SET02N50.

6 CONCLUSIONS

This study assesses the moment-resistance and initial stiffness of a group of one-sided internal beam-to-column joints considered representative of common steel construction solutions using open hot-rolled profiles. Using shell finite element models, the component method (CM) and a component-based finite element method (CBFEM) through the commercial software IDEA StatiCa® parametric study was carried out and its subsequent results and statistical processing led to the following conclusions and findings:

6.1 Shell finite element models

The use of shell finite element to model on-sided internal beam-to-column joints with hot-rolled open sections may be acceptable, allowing a reasonable reproduction of the overall behaviour of such joints shown on experimental tests. However, it seems to be necessary to validate the models with a more extensive experimental sample to choose one model geometry among others due to non-neglective differences in joint moment-rotation behaviour between different column shear resistance, WP slenderness, and aspect ratios.

The use of a model where the effect of the column radius in FEM overall behaviour is neglected seems to lead to lower bending moment resistance values when compared with models considering its effect by increasing the thickness of the web near the flanges or using inclined elements linking column web and flanges. Therefore, it may indicate that the contribution of the column radius could not be neglected to model the joint's overall behaviour with numerical shell FEM. Furthermore, the calculation of an *equivalent thickness* to use in the column web areas near the column flanges to model the column radius may be carried out carefully when dealing with profiles with thick flanges due to the shell elements overlap that may affect the joint behaviour.

Finally, the consideration of the column radius in shell FEM seems to also have significant effects on the joint initial stiffness and may lead to lower initial stiffness values when neglected. However, it should be noted that the overall stiffness behaviour of the joints may have to be more deeply studied (for example analysing the secant and tangent stiffness at several points) to compare the effect of different geometries when using shell FEM.

6.2 Component method

The component method adopted by the European code EN 1993-1-8 and the new generation European code FprEN 1993-1-8 may lead to more conservative results for moment resistance in one-sided-unstiffened joints without axial force. Nevertheless, in the presence of axial force for some specific cases the CM may lead to less conservative results than FEM (as much as 26% higher). Therefore, a more profound investigation should be performed to estimate the true effects of axial force in column moment resistance and the adequacy of the actual approach used by the codes.

In terms of initial stiffness, the CM may lead to lower values than the shell FEM when no axial force is applied. Nevertheless, in the presence of axial force, the initial stiffness provided by the CM (using both Eurocodes) turns out to be smaller than the initial stiffness provided by the shell FEM.

6.3 CBFEM IDEA StatiCa®

The moment resistance given by the component-based finite element method used by IDEA StatiCa® seems to be highly dependent on the mesh size. The IS default mesh may lead to less conservative results compared to shell FEM among all methods. However, the results improve using a more refined mesh (elements with half the size) and get closer to the theoretical mesh of Richardson extrapolation. Hence, the results provided by the CBFEM may lead to moment-resistance values considerably closer to shell FEM if a sufficiently refined mesh is used.

6.4 Future work proposal

Ultimately, this study may provide a base for the use and/or creation of alternatives to the component method, especially when dealing with non-standard problems related to CWP in shear. It may guide the development of shell FEM and the use of commercial CBFEM for steel beam-to-column joints using open hot-rolled profiles. However, due to the relatively restricted scope of the study (one-sided, unstiffened internal beam-to-column joints), the conclusions and findings presented in this chapter may not be interpreted as definitive. Therefore, future more comprehensive research should be performed to cover a larger scope: two-sided joints, the use of horizontal and/or vertical stiffeners, the consideration of more levels of axial force (for instance 30 and 70% of the axial column plastic resistance), the consideration of an improved model B avoiding the problems verified for columns with thick flanges, and the use of other moment resistance criteria beyond the 5% plastic strain.

7 REFERENCES

American Institute of Steel Construction. (2016). Specification for Structural Steel Buildings. *Specification for Structural Steel Buildings*. AISC.

Atamaz, W. S., & Jaspart, J. P. (1989, October). Étude du comportement jusqu'a la ruine des nœuds complètement soudés. *Étude du comportement jusqu'a la ruine des nœuds complètement soudés*. Université de Liége Institut de Génie Civil MSN.

Bose, B. (1998, January). Design resistance of unstiffened column web subject to transverse compression in beam-to-column joints. *Journal of Constructional Steel Research, 45*, 1-15. doi:10.1016/s0143-974x(97)00065-5

Bose, S. K., McNeice, G. M., & Sherbourne, A. N. (1972a, February). Column webs in steel beam-to-column connexions part I—Formulation and verification. *Computers & Structures, 2*, 253–279. doi:10.1016/0045-7949(72)90030-2

Bose, S. K., McNeice, G. M., & Sherbourne, A. N. (1972b, February). Column webs in steel beam-to-column connexions part II—Design recommendations. *Computers & Structures, 2*, 281–301. doi:10.1016/0045-7949(72)90031-4

Brandonisio, G., De Luca, A., & Mele, E. (2012, April). Shear strength of panel zone in beam-to-column connections. *Journal of Constructional Steel Research, 71*, 129-142. doi:10.1016/j.jcsr.2011.11.004

CBFEM Team. (2021). About CBFEM. *About CBFEM*. Retrieved from https://www.cbfem.com/about-cbfem

CEN. (2002a). *Eurocode – Basis of structural design.* European Committee for Standardization.

CEN. (2002b). *Eurocode 1: Actions on structures - Part 1-1: General actions - Densities, self-weight, imposed loads for buildings.* European Committee for Standardization.

CEN. (2005a). Eurocode 3: Design of steel structures - Part 1-1: General rules and rules for buildings. *Eurocode 3: Design of steel structures - Part 1-1: General rules and rules for buildings*. European Committee for Standardization.

CEN. (2005b). Eurocode 3: Design of steel structures - Part 1-8: Design of joints. *Eurocode 3: Design of steel structures - Part 1-8: Design of joints*. European Committee for Standardization.

CEN. (2006). Eurocode 3: Design of steel structures – Part 1-5: Plated structural elements. *Eurocode 3: Design of steel structures – Part 1-5: Plated structural elements*. European Committee for Standardization.

CEN. (2022). Eurocode 3: Design of steel structures — Part 1-14: Design assisted by finite element analysis. *Eurocode 3: Design of steel structures — Part 1-14: Design assisted by finite element analysis*. European Committee for Standardization.

CEN. (2023). Eurocode 3: Design of steel structures — Part 1-8: Joints. *Eurocode 3: Design of steel structures — Part 1-8: Joints*. European Committee for Standardization.

Corman, A., Jaspart, J.-P., & Demonceau, J.-F. (2019, August). Resistance of the beam-to-column component ”column web panel in shear“. *Steel Construction, 12*, 222-230. doi:10.1002/stco.201900020

Corman, Adrien. (2022). *Characterization of the full non-linear behaviour up to failure of the sheared panel zone under monotonic loading conditions.* Liège: Université de Liège.

El-Khoriby, S., Sakr, M. A., Khalifa, T. M., & Eladly, M. M. (2017, February). Modelling and behaviour of beam-to-column connections under axial force and cyclic bending. *Journal of Constructional Steel Research, 129*, 171-184. doi:10.1016/j.jcsr.2016.11.006

Girão Coelho, A. M. (2001). Infernal Report XVIa. *Infernal Report XVIa*, 1-49. University of Coimbra.

Girão Coelho, A. M., Bijlaard, F. S., & Kolstein, H. (2009, July). Experimental behaviour of high-strength steel web shear panels. *Engineering Structures, 31*, 1543-1555. doi:10.1016/j.engstruct.2009.02.023

Gödrich, L., Wald, F., Kabeláč, J., & Kuříková, M. (2019, June). Design finite element model of a bolted T-stub connection component. *Journal of Constructional Steel Research, 157*, 198-206. doi:10.1016/j.jcsr.2019.02.031

Golea, T., Jaspart, J.-P., & Demonceau, J.-F. (2022). Characterisation of the Behaviour of beam-to-column Steel Joints up to Failure. *Advanced Steel Construction, 18*, 679–686. doi:https://doi.org/10.18057/ijasc.2022.18.3.5

Graham, J. D., Sherbourne, A. N., & Khabbaz, R. N. (1960). *Welded interior beam-to-column connections.* American Institute of Steel Construction.

Hetényi, M. (1952). *Beams on Elastic Foundation: Theory with Applications in the Fields of Civil and Mechanical Engineering* (4th ed.). The University of Michigan Press.

in St. Louis, W. U. (2009). ABAQUS Analysis User's Manual (v6.6) 23.6.1 Shell elements: overview. *ABAQUS Analysis User's Manual (v6.6) 23.6.1 Shell elements: overview*. Retrieved from https://classes.engineering.wustl.edu/2009/spring/mase5513/abaqus/docs/v6.6/books/usb/default.htm?startat=pt06ch22s01alm01.html

Jaspart, J.-P. (1990, April). Shear and Load-Introduction deformability and strength of column web panels in strong axis beam-to-column joints. *Shear and Load-Introduction deformability and strength of column web panels in strong axis beam-to-column joints*. EC3 Formulae. Retrieved March 21, 2023, from https://orbi.uliege.be/handle/2268/192886

Jaspart, J.-P., & Weynand, K. (2016). *Design of joints in steel and composite structures.* Ernst & Sohn, a Wiley branch, Brussels, Belgium. doi:10.1002/9783433604762

Jaspart, J.-P., Corman, A., & Demonceau, J.-F. (2022a, November). Characterization of unstiffened column webs in transverse compression in steel beam-to-column joints. *180*, 109848-109848. doi:10.1016/j.tws.2022.109848

Jaspart, J.-P., Corman, A., & Demonceau, J.-F. (2022b, September). Mechanical Properties of the Component “Column Web in Compression” in Steel Beam-to-column Joints. *ce/papers, 5*, 242-250. doi:10.1002/cepa.1752

Jordão, S. (2008). *Comportamento de juntas soldadas em nó interno com vigas de diferentes alturas e aço de alta resistência (in Portuguese).* Ph.D. dissertation. Retrieved from http://hdl.handle.net/10316/7542

Krawinkler, H. (1987). Shear in Beam-Column Joints in Seismic Design of Steel Frames. *Engineering Journal, American Institute of Steel Construction, 15*, 82-91.

Krawinkler, H., Bertero, V., & Popov, E. (1973). The influence of the elastic plastic deformation of beam-to-column connections on the stiffness, ductility and strength of open frames.

Krawinkler, H., Bertero, V., & Popov, E. P. (1971). *Inelastic behavior of steel beam-to-column subassemblages.* University of California, Berkeley Earthquake Engineering Research

Center. Retrieved from https://www.worldcat.org/pt/title/inelastic-behavior-of-steel-beam-to-column-subassemblages/oclc/809195999

Popov, E. P. (1987, January). Panel zone flexibility in seismic moment joints. *Journal of Constructional Steel Research, 8*, 91-118. doi:10.1016/0143-974x(87)90055-1

Popov, E., & Stephen, R. (1972, February). Cyclic loading of full-size steel connections. *Cyclic loading of full-size steel connections*. Retrieved March 29, 2023, from https://scholarsmine.mst.edu/ccfss-library/112/

Rannacher, R. (1987, January). Richardson Extrapolation with Finite Elements. *Numerical Techniques in Continuum Mechanics, 15*, 90-101. doi:10.1007/978-3-322-85997-6_9

Simões da Silva, L. (2008, September). Towards a consistent design approach for steel joints under generalized loading. *Journal of Constructional Steel Research, 64*, 1059-1075. doi:10.1016/j.jcsr.2008.02.017

Skiadopoulos, A., Elkady, A., & Lignos, D. G. (2021, April). Proposed Panel Zone Model for Seismic Design of Steel Moment-Resisting Frames. *Journal of Structural Engineering, 147*. doi:10.1061/(asce)st.1943-541x.0002935

StatiCa(R), I. D. (2016). Component-based finite element design of steel connections. *Component-based finite element design of steel connections*. Retrieved October 11, 2023, from https://www.ideastatica.com/support-center/cbfem-book-component-based-finite-element-design-of-steel-connections

StatiCa(R), I. D. (n.d.). Why IDEA StatiCa Connection? *Why IDEA StatiCa Connection?* Retrieved October 11, 2023, from https://www.ideastatica.com/support-center/why-idea-statica-connection

Timoshenko, S., & Gere, J. (1985). *Theory of Elastic Stability* (2nd ed.). McGraw-Hill.

Tsai, K., & Popov, E. (1990). Seismic Behavior of Moment-Resisting Steel Frames: Analytical Study. *Journal of Structural Engineering, 116*(2), 3285–3301. doi:https://doi.org/10.1061/(asce)0733-9445

Tsai, K.-C., & Popov, E. P. (1990, December). Seismic Panel Zone Design Effect on Elastic Story Drift in Steel Frames. *Journal of Structural Engineering, 116*, 3285-3301. doi:10.1061/(asce)0733-9445(1990)116:12(3285)